

Science Concept 3: Key Planetary Processes are Manifested in the Diversity of Lunar Crustal Rocks

Science Concept 3: Key planetary processes are manifested in the diversity of crustal rocks

Science Goals:

- a. Determine the extent and composition of the primary feldspathic crust, KREEP layer, and other products of differentiation.
- b. Inventory the variety, age, distribution, and origin of lunar rock types.
- c. Determine the composition of the lower crust and bulk Moon.
- d. Quantify the local and regional complexity of the current lunar crust.
- e. Determine the vertical extent and structure of the megaregolith.

INTRODUCTION

Formation and Evolution of the Moon

The Moon is a unique environment, preserving crucial information about the early history and later evolution of the solar system. The lack of major surficial tectonic processes within the past few billion years or so, as well as the lack of significant quantities of surface water, have allowed for excellent preservation of the lithologies and geomorphological features that formed during the major planetary formation events.

Fundamental discoveries during the Apollo program showed that the Moon is made up of a variety of volcanic and impact rock types that exhibit a particular range of chemical and mineralogical compositions. The key planetary processes conveyed by this diversity include planetary differentiation, volcanism, and impact cratering. Analysis of Apollo, Luna, and lunar meteoritic samples, as well as orbital data from a series of lunar exploration missions, generated geophysical models that strove to tell the story of the Moon. However, such models are restricted in the sense that they are based on information gathered from the samples that have so far been acquired. Figure 3.1 shows that previous sample return missions only covered a very limited area of the Moon (less than 4%). To significantly enhance our knowledge of the Moon and planetary evolution in general we must expand this previously limited dataset and gather a comprehensive sample collection, as well as conduct detailed in-situ geological and geophysical studies.

Each Science Goal within this Science Concept targets a particular aspect of lunar crustal diversity. Science Goals 3a and 3c relate to the vertical stratification of the lunar crust and products of planetary differentiation. The aim of Science Goal 3b is to catalogue the surface products of planetary processes by inventorying and classifying different rock types present on the lunar surface. In Science Goal 3d, the focus is primarily on local and regional crustal complexity, rather than global diversity, thus yielding information about the variety and lateral and vertical distribution of crustal materials on a smaller scale. The information thus obtained could be used to constrain current geophysical and geochemical models. Science Goal 3e investigates the properties of the megaregolith layer, thought to have formed as a result of the Late Heavy Bombardment.

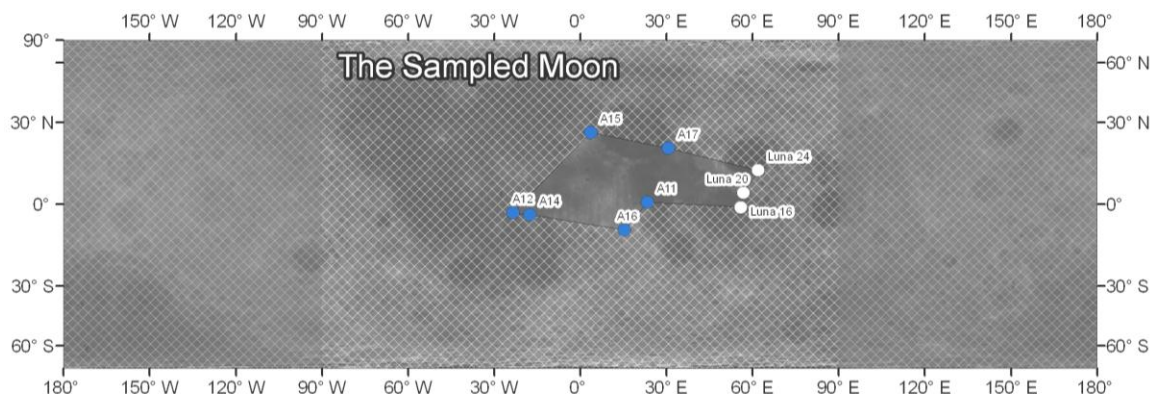


FIGURE 3.1 Direct sampling of the Moon has been limited to a small region on the central nearside, roughly delimited by the polygon which has for apexes the Apollo and Luna landing sites. The area covered by that region is less than 4% of the total surface of the Moon. Though some meteorites may originate from the farside highlands, there is no exact way to determine their precise origin. (Image modified from Warren and Kallemeyn, (1991). World cylindrical equal-area projection, background is LOLA elevation map).

Lunar rock types

The mineralogy of lunar samples (including lunar meteorites) is somewhat limited when compared to terrestrial samples. This is due to the limited range of chemical compositions on the lunar surface and to the lack of significant amount of water and of weathering processes (Mason and Melson, 1970). The major lunar rock types are composed of a combination of four major minerals: plagioclase, pyroxene, olivine, and ilmenite (in lunar basalts). Not all these minerals are necessarily present in a particular rock type, but they can all be considered as major rock forming minerals on the Moon. Figure 3.2 shows the classification for igneous rocks composed of the first three minerals (note that most lunar surface igneous rocks have been

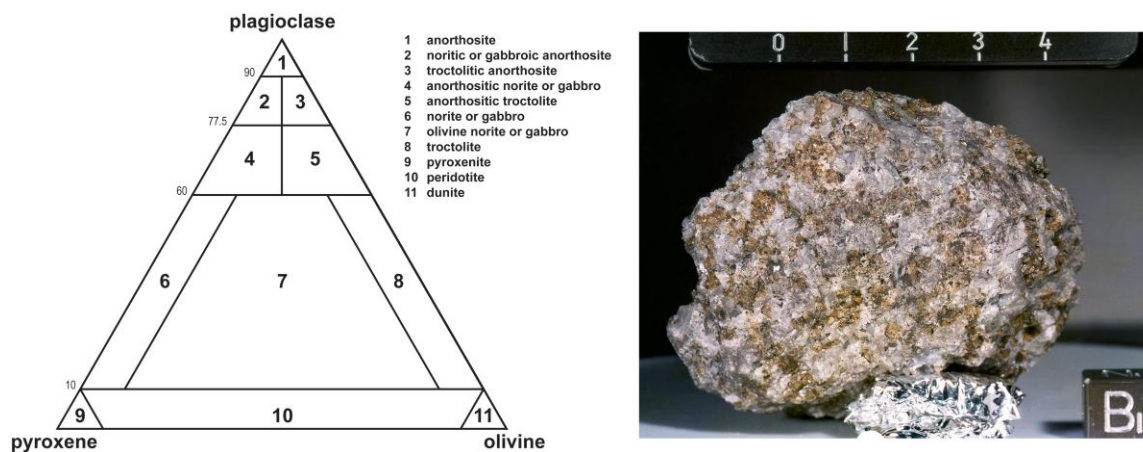


FIGURE 3.2 Left: Ternary diagram showing lunar rocks classification based on the relative content of plagioclase, pyroxene and olive. The values on the left side of the diagram are in % plagioclase. Most of the rock types in this diagram are discussed in this report. Right: Photo of lunar sample 62237, a troctolitic anorthosite (region 3 in ternary diagram). The pale, white crystals are plagioclase (anorthite) and the greenish crystals are olivine.

partly thermally and shocked metamorphosed due to impact cratering but that they still retain their igneous name). A rock with an important component of ilmenite (up to 20%) will be dubbed “Ti-rich” (*e.g.*, Ti-rich basalt).

Plagioclase is a solid solution of the end-members albite ($\text{NaAlSi}_3\text{O}_8$) and anorthite ($\text{Ca}_2\text{Al}_2\text{Si}_2\text{O}_8$). The anorthite component is dominant and the average lunar plagioclase is made up of 90% anorthite (An_{90}). A rock with 90% or more anorthite is called an anorthosite. Anorthosite is thought to be the major component of the lunar upper crust.

Pyroxene ($(\text{Ca,Mg,Fe})_2\text{Si}_2\text{O}_6$) is a silicate mineral generally common in meteorite and lunar basalts. The pyroxene crystals found on the Moon have a wide range of compositions. They are normally classified based on their Ca- (wollastonite), Mg- (enstatite) or Fe-content (ferrosilite). Pyroxenes are further separated into two main groups: orthopyroxenes (low calcium) and clinopyroxenes (medium to high calcium). Different pyroxene-rich rocks can also be classified based on the presence of minor components (*e.g.*, titanium, aluminum, etc.). The proportion of pyroxene in the crust tends to increase with depth.

Olivine is a magnesium iron silicate ($(\text{Mg,Fe})_2\text{SiO}_4$) solid solution. The Fe mole % in the lunar sample olivine ranges from 20% to 50% (with an average of 30%). Olivine is one of the main constituents of the Earth's mantle and is thought to be a major component of the Moon's mantle.

Ilmenite (FeTiO_3) is uncommonly abundant in lunar samples (basalts) when compared to the average terrestrial basalt (a lunar rock can have up to 20% ilmenite, whereas a terrestrial basalt will seldom have more than 5%). It is thought that lunar ilmenite could be a valuable potential resource for oxygen extraction.

A particular rock class, however, is not strictly defined by its mineralogy; the main rock classes are based on the origin and internal structure of the rock. Three main rock classes are found on the Moon: pristine crustal rocks, volcanic rocks, and impact breccia rocks. The pristine crustal rocks form the upper to lower part of the crust. They are thought to have formed during the first 2 Gy of the Moon's evolution. The volcanic rocks were formed through surface volcanism. The most common rock of this class are the dark-colored mare basalts visible from Earth. Impact breccias have been reworked by billions of years of impacts and are composed of broken fragments of all rock types found on the lunar surface. The very top layer of the lunar surface, called the regolith, is composed of fine- to very-fine-grained rock particles created by the constant bombardment of meteorites and micrometeorites of the surface. Table 3.1 presents an overview of the current classification of lunar rock types, along with characteristic mineralogy.

TABLE 3.1 Classification of lunar rocks (adapted from Hiesinger and Head, 2006), with mineralogy. Abbreviations: pl (plagioclase), px (pyroxene), cpx (clinopyroxene), opx (orthopyroxene), ol (olivine), al (albite), ilm (ilmenite).

Rock class: Primordial Magma Ocean Products			
Rock type	Rock type subdivision	Mineralogy	Chemistry
Ferroan Anorthosite (FAN)	anorthosite	pl (90%) + px (+ ol)	low FeO, high Al_2O_3 , low trace elements (Th), high Al_2O_3
Lower Crust urKREEP Mantle	norite	opx + pl	rich in incompatible elements
	troctolite	ol + pl	rich in incompatible elements
	dunite	ol	rich in incompatible elements
	gabbro / gabbronorite	cpx + pl	rich in incompatible elements
Rock class: Serial Magmatism Products			
Rock type	Rock type subdivision	Mineralogy	Chemistry
Mg-suite	norite	opx + pl	rich in incompatible elements
	troctolite	ol + pl	rich in incompatible elements
	dunite	ol	rich in incompatible elements
	gabbro / gabbronorite	cpx + pl	rich in incompatible elements

Alkali-suite	Na-anorthosite to norite, granites (felsites) and quartz monzogabbro	al (90%) + px (+ ol)	high Na (instead of Ca) anorthosite to norite, enriched in incompatible elements. Possible relation to KREEP?
KREEP basalt	basalt	pl (50%), opx (30%), ilm, Si- and K-rich glass	low siderophiles, high Mg, high silica and high incompatible elements, high Th
Basaltic lavas / flows (mare basalts)	High-Ti	pl, px, ilm	high FeO, low Al ₂ O ₃ , high Ti, and high or low K
	Low-Ti	pl, px	high FeO, low Al ₂ O ₃ , low Ti, higher concentration in light REE than heavier REE
	Very-low-Ti	pl, px	high FeO, low Al ₂ O ₃ , very low Ti
Pyroclastic deposits	glass		

Rock class: Impact Rocks

Rock type	Rock type subdivision
Breccia	fragmental breccia
	glassy melt breccia
	impact melt breccia
	clast-poor impact melt
	granulitic breccia and granulite
	dimictic breccias
	regolith breccia
Melt	Impact melt

Lunar chronology and stratigraphy

Craters are some of the most useful features on the lunar surface. They can be useful not only to determine the structure and composition of the Moon's surface, but the density of craters on a particular surface can be used to calculate the relative age of that region. The density of impact craters on the lunar surface generally increases as the surface ages increases. Although the impact rate is thought to have decreased steadily since the formation of the Moon 4.5 Gy ago, radiometric ages of the Apollo impact melt samples have suggested the occurrence of a spike in the impact rate curve between approximately 4.1 to 3.8 Gy ago. During this period, referred to as Late Heavy Bombardment (LHB, also referred to as the lunar cataclysm), a large number of impact craters are believed to have completely reshaped the surface of the Moon. The occurrence and extent of the intense bombardment period can be tested by assessing Science Goal 3e.

The relative ages of various regions of the Moon can also be calculated from observed crater densities. Apollo and Luna samples allowed for radiometric dating of specific regions of the Moon, thus providing a calibration for lunar ages. Relative ages (and approximate absolute ages) of other regions were then established by studying relative densities of impact craters, overlapping ejecta and lava flows, the presence of crater rays (considered younger craters), and crater degradation state (Fig. 1.11). Using the calibration relationship developed from radiometrically dated samples, one can infer absolute ages for these areas, and for the whole surface of the Moon.

The most generally accepted lunar geologic chronology is the one established by Wilhelms (1987). This chronology divides lunar history into five main epochs: the pre-Nectarian (>3.92 Ga), the Nectarian (3.92 to 3.85 Ga), the Imbrian (3.85 to 3.2 Ga), the Eratosthenian (3.2 to 0.8 Ga), and the Copernican (<0.8

Ga) (Fig. 1.9). Only the lower Imbrian time boundary, and earlier ones, are known with any accuracy, because of the Apollo and Luna samples. The later periods are based on relative stratigraphy of surface features and the boundaries are approximate. Figure 3.3 is an interesting summary of radiometric dating of existing lunar samples. It shows the limited range of sampled ages (2.9–4.6 Ga), but it also shows that each rock type comes from a particular period of the Moon’s geologic history.

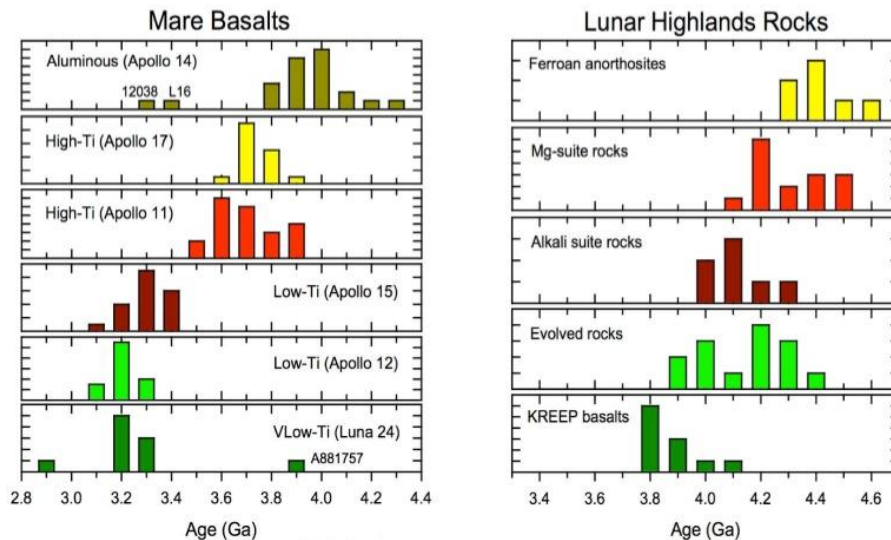


FIGURE 3.3 Histogram of radiometric ages for lunar mare basalts and lunar highlands rocks. These ages were derived with various dating methods and compiled by Nyquist *et al.*, 2001. These data suggest that each lunar rock type correlates with a particular period in the Moon’s geological history (Image from Nyquist *et al.*, 2001). The variations in ages reflect different mechanism and locales of origin.

DATASETS AND METHODS

Available Datasets and Approach

To achieve the objective of determining the global coverage of all possible locations where Science Concept 3 Science Goals can be addressed, either individually or collectively, we needed to:

1. Review the lunar literature, along with databases of Apollo, Luna and lunar meteorite samples, to gather information on the lunar crust composition and its lateral and vertical diversity;
2. Define requirements for landing site targets specific to each of the five goals;
3. Gather, process and geo-reference all available datasets from previous lunar orbital missions (Tables 3.2 and 3.3) into ArcGIS, which is a widely used Geographic Information System software;
4. Map features of interest, and create a database to combine all the features that reveal the diversity of the crust;
5. Pick some case studies to illustrate how the whole of Concept 3 could be achieved at some of the suggested landing sites.

Table 3.2 lists the different datasets used here and classifies them depending on the type of observations they can be used for. Table 3.3 reports the mission of origin, resolution and source for each of those datasets.

TABLE 3.2 Lunar datasets publicly available for different types of observations.

Observations	Datasets available*
Morphologies	Clementine UVVIS, LROC, Lunar Orbiter Photographic Mosaic and individual photographs, USGS geological maps
Mineralogical composition	Clementine UVVIS (multispectral imagery)
Elemental abundances	Clementine UVVIS, Lunar Prospector Neutron spectrometer, Lunar Prospector GRS
Topographic data	LOLA
Other physical properties (gravity, crustal thickness)	Clementine

*Does not include recent Chandrayaan, Change'1, Smart1 datasets, and parts of Kaguya and LRO datasets, which had not been publicly released at the time of writing this report.

TABLE 3.3 List of all the available global maps used to define regions of interest, with their mission of origin, digital resolution, and source. Abbreviations are defined at the bottom of the Table.

Data	Mission	Resolution	Source
Clementine UVVIS global map (5 bands) and derived products (RBG)	Clementine	200 m/px	USGS
Clementine UVVIS 750nm filter albedo map	Clementine	100 m/px	USGS
Lunar Orbiter global mosaic	Lunar Orbiter	~60 m/px	USGS
FeO global distribution map	Clementine	100 m/px	USGS, Lucey <i>et al.</i> , 1998
	Lunar Prospector	0.5 deg = 15 km/px	PDS
TiO global distribution map	Clementine	100 m/px	USGS, Lucey <i>et al.</i> , 2000
	Lunar Prospector	2 deg = 60 km/px	PDS
Th and H global distribution maps	Lunar Prospector	0.5 deg = 15 km/px	PDS
K and Sm global distribution maps	Lunar Prospector	2 deg = 60 km/px	PDS
Al, Ca, Mg, Si, O global distribution maps	Lunar Prospector	5 deg = 150 km/px	PDS
Lunar Impact Crater Database			LPI
Crustal thickness maps	Clementine	1 deg = 30 km/px	Wieczorek <i>et al.</i> , 2006

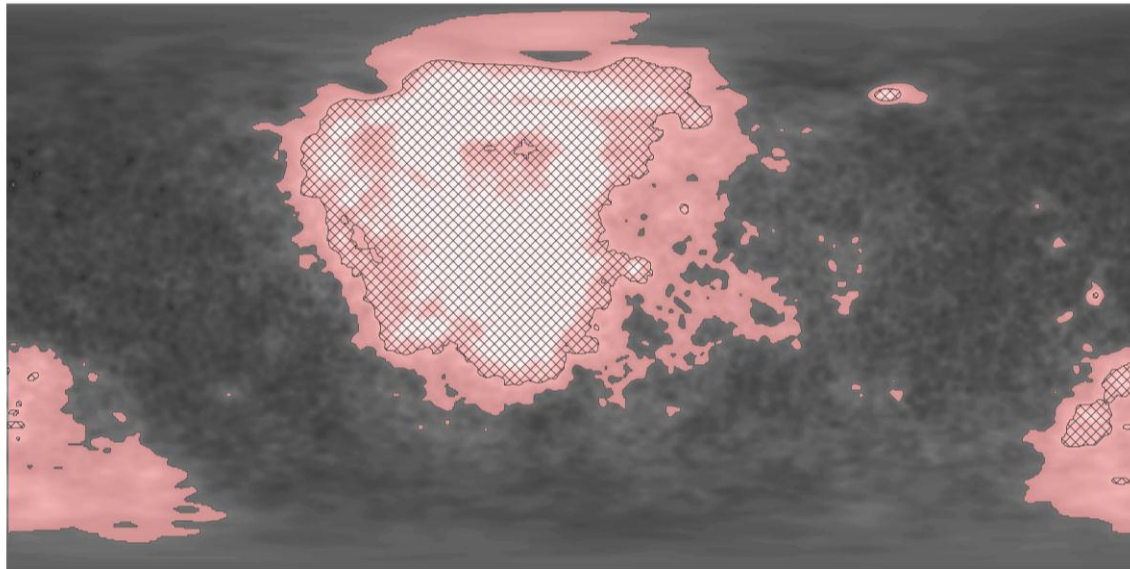
topographic maps	Clementine	Horizontal: ~1.9 km/pixel, Vertical: ~140 m/pixel	USGS
	Selene (Kaguya LALT)	16 ppd= 1.8 km/px	JAXA
	LRO (LOLA)	64 ppd = 470 m/px	MIT
List of abbreviations:			
	USGS	(United States Geological Survey, www.usgs.gov)	
	PDS	(Planetary Data System, NASA, pds.nasa.gov)	
	JAXA	(Japan Aerospace Exploration Agency, www.jaxa.jp)	
	LPI	(Lunar and Planetary Institute, USRA, www.lpi.usra.edu)	

Extensive Mapping of Interesting Features

We mapped different surface units on the Moon and digitized them in the form of shapefiles. These mapped surface units include: mare areas, cryptomare areas, highland areas, highland types (based on Chevrel *et al.*, 2002), basin areas, pyroclastic and other volcanic deposits, massifs, plateaus, sinuous rilles and fresh craters (Copernican and bright-rayed, list provided by S. Werner, of the DLR Berlin). We derived a slope map from LOLA high resolution topography data to help identify scarps. LOLA data were also used to create topographic profiles of regions of interest. We generated contour maps using both Lunar Prospector and Clementine elemental abundance maps, to help locate the main geochemical terranes, and possible regional anomalies. These maps are useful in understanding the lateral heterogeneity of the crust. To assess the vertical structure, we calculated a number of important morphological parameters related to impact cratering like the depth of excavation, maximum depth of melting, stratigraphic uplift, central peak height, apparent/final depth and created maps showing the global variation of these parameters. All of these maps were combined and overlaid to assist in evaluating candidate lunar landing sites.

Analysis of elemental and mineralogical remote sensing data

Thorium: Analysis of Lunar Prospector gamma ray spectrometer data provides estimates of thorium abundance across the surface of the crust. Traces of thorium are found in abundances up to nearly 13 ppm, such as in the Fra Mauro region. Generally, regions containing abundances greater than 2.2 ppm are considered to be enriched in Thorium. Regions containing over 3.5–4.5 ppm are almost entirely located in the mare regions of the nearside (this region is generally labeled the Procellarum KREEP Terrane [PKT] [Haskin *et al.*, 2000; Jolliff *et al.*, 2000]). According to Lawrence *et al.*, (2000), regions containing thorium abundances of over 7 ppm are likely small area regions that may also be of particular concern when discussing local or regional points of interest. Figure 3.4 shows the areas of the lunar crust that are enriched (>2.2 ppm) in thorium. These particular areas are understood to contain elevated levels of KREEP material, and analysis of samples from sites within this range could help to determine the extent and structure of the KREEP layer.



Legend

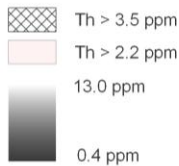
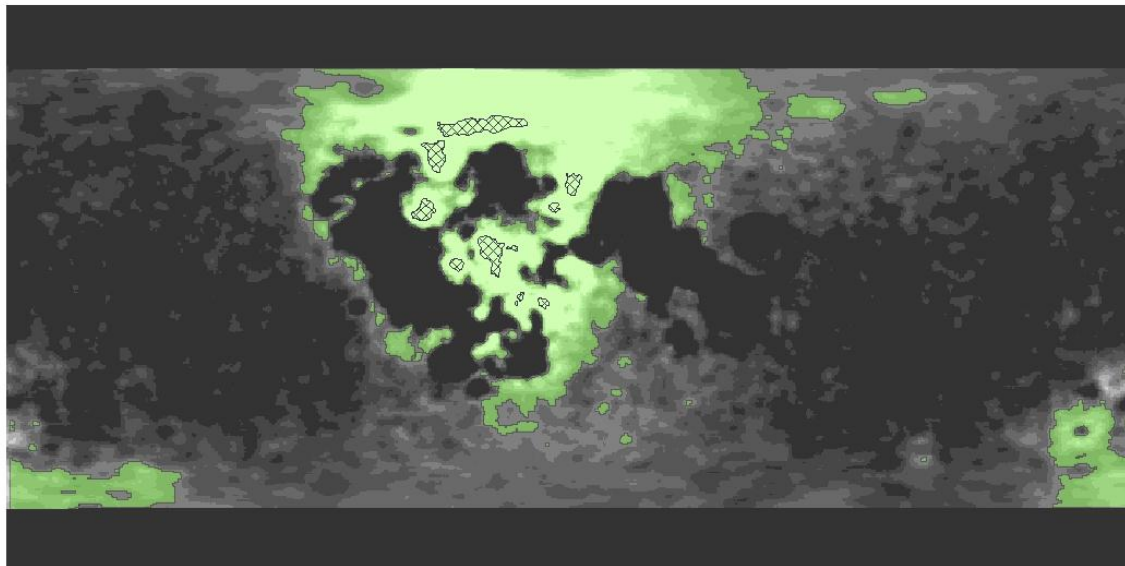


FIGURE 3.4 Lunar Prospector gamma ray spectrometer thorium abundance map. The thorium abundances range from 0.5 ppm to 13 ppm in this map. Outlined in pink contour is the area on the lunar surface containing over 2.2 ppm thorium. Also depicted in cross hatch is thorium abundance greater than 3.5 ppm. Note that the majority of high thorium abundance lies within the nearside mare, with a few exceptions located in the South Pole-Aitken Basin.

Rare Earth Elements (REE): Neutron spectrometer data returned from the Lunar Prospector mission is a good indicator of the rare earth elements samarium (Sm) and gadolinium (Gd). Although these REEs only occur as trace elements, the combined thermal neutron absorption is very large, producing a strong signature in neutron spectroscopy. Respective abundances of Sm and Gd can then be inferred from the neutron spectrometer data, as the ratio of the two elements is nearly constant in samples with high potassium, rare earth elements, and phosphorus (KREEP) ($Gd/Sm = 1.18$). For mare basalts, the Gd/Sm range is slightly broader, with ratios between 1.3–1.6 (Wieczorek *et al.*, 2006). Generally, Sm abundances of 20 ppm and higher are indicative of KREEPy terrane (Wieczorek *et al.*, 2006), although across the whole lunar surface the abundance ranges from nearly 0 ppm to as high as 51 ppm in localized areas on the nearside (Elphic *et al.*, 2000). On the farside highlands, the Sm abundance ranges from zero to highs of about 2 ppm. For the purpose of demonstrating enriched Sm regions, we will highlight values (somewhat arbitrarily) that are more than double the highland values (Fig. 3.5).



Legend

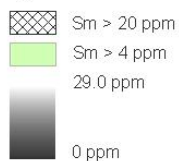
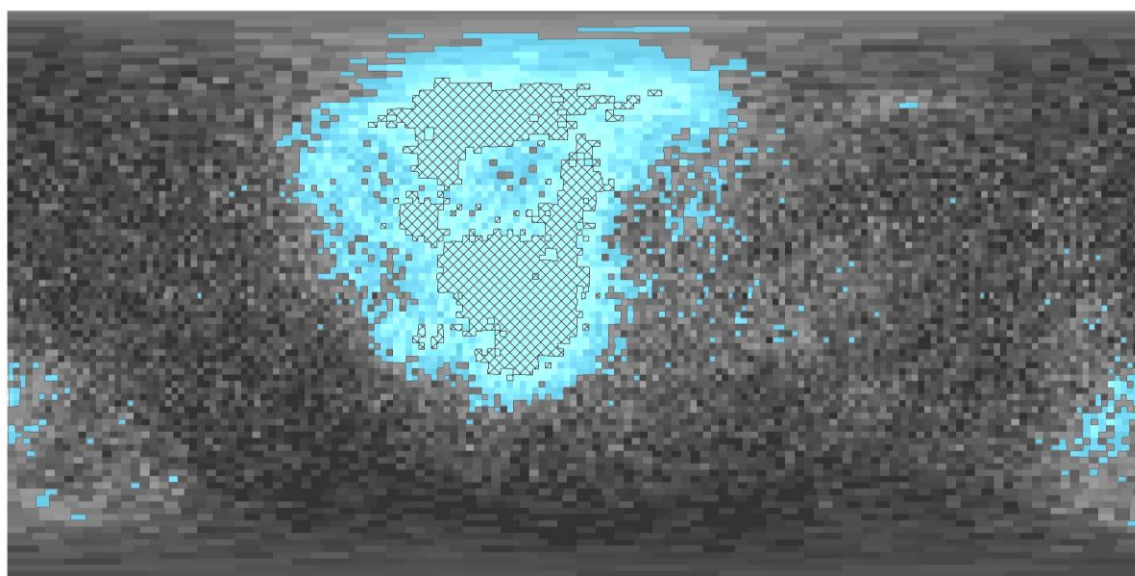


FIGURE 3.5 Global map of lunar surface samarium abundance, adapted from Lunar Prospector neutron spectrometer data. The Sm abundance ranges from 1 to about 29 ppm, although some sources (*e.g.*, Elphic *et al.*, 2000) may locate small regions of up to 51 ppm. Green areas indicate elevated levels of Sm over 4 ppm, while the crosshatched areas represent KREEPy terrane of over 20 ppm Sm.



Legend

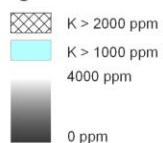


FIGURE 3.6 Global map of lunar potassium abundance from Lunar Prospector. Map ranges from 0 to 4000 ppm, while blue areas indicate regions with greater than 1000 ppm, and crosshatch areas are greater than 2000 ppm. Note that due to the low resolution, the data are less reliable.

Potassium: Potassium is yet another indicator of KREEP-rich material (Fig. 3.6). Using similar methods as the thorium and samarium analyses, we will also assess global potassium maps. Gillis *et al.*,

2004 have used Lunar Prospector data combined with Apollo samples as ground-truth to determine global potassium abundance. These maps suggest an average value of approximately 700 ppm, and a mode of 240 ppm (Gillis *et al.*, 2004). For the purpose of our study, we will label any K abundance greater than 1000 ppm as being enriched, while emphasizing areas of greater than 2000 ppm in crosshatch. These distinctions are somewhat more arbitrary than the contours for thorium and samarium. However, sources such as Snyder *et al.* (1995) do use this designation of 1000 ppm to distinguish alkali-rich rocks, whose formation is thought to be tied with KREEP material. In addition, the lunar prospector potassium data is less reliable due to the lower spatial resolution of 5 degrees per pixel.

Clementine RGB or 'false color' composition: We also analyzed RGB images based on five-band UVVIS data from the Clementine multispectral data set, covering wavelengths from 415 to 1000 nm. As is standard, these RGB images are made using the following ratios to control the spectral channels: red=750/415 nm, green=750/950 nm, blue=415/750 nm (Heather and Dunkin, 2002). The color ratio image product serves to cancel out the dominant brightness variations of the scene (controlled by albedo variations and topographic shading) and enhances color differences related to soil mineralogy and maturity. The lunar highlands, mostly old (~4.5 billion years) gabbroic anorthosite rocks, are dominated by shades of red (old) and blue (younger). The lunar maria (~3.9 to ~1 billion years), mostly iron-rich basaltic materials of variable titanium contents, are portrayed in shades of yellow/orange (iron-rich, lower titanium) and blue (iron-rich, higher titanium). Superimposed on and intermingled with these basic units are materials from basins and craters of various ages, ranging from the dark reds and blues of ancient basins to the bright blue crater rays of younger craters (*e.g.*, McEwen *et al.*, 1994; Pieters *et al.*, 1994). Figure 3.7 shows the RGB Clementine mineral ratio map for the whole lunar surface.

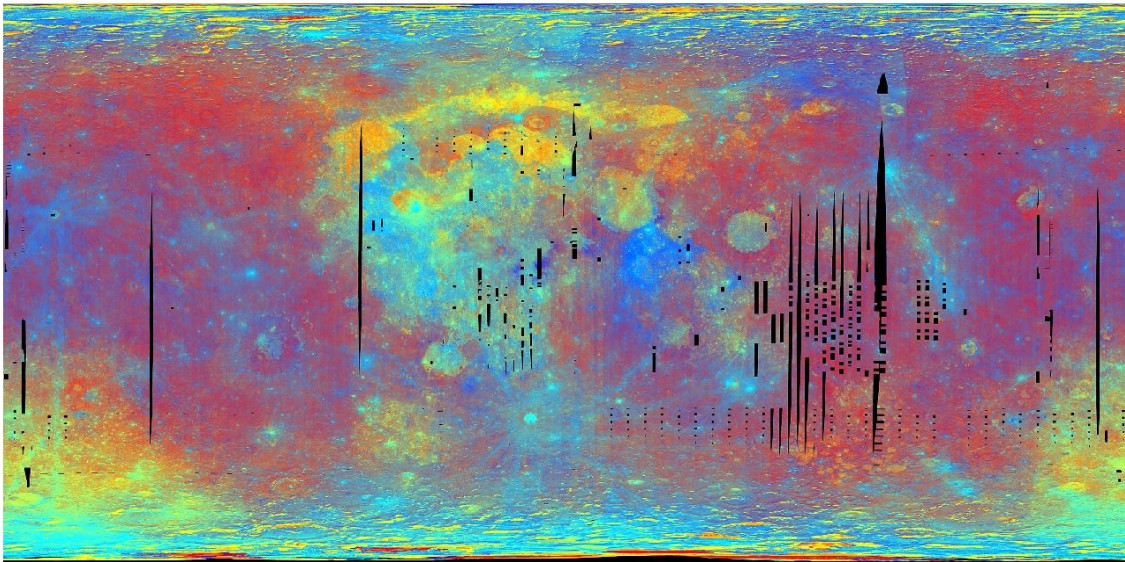


FIGURE 3.7 A multispectral mosaic of the lunar surface. In this image, the red channel is controlled by the Clementine 750/415 nm ratio, green by the 750/950 nm ratio, and blue by the 415/750 nm ratio. Color differences are related to soil mineralogy and maturity. The lunar highlands, mostly old (~4.5 billion years) gabbroic anorthosite rocks, are dominated by shades of red (old) and blue (younger). The lunar maria (~3.9 to ~1 billion years), mostly iron-rich basaltic materials of variable titanium contents, are portrayed in shades of yellow/orange (iron-rich, lower titanium) and blue (iron-rich, higher titanium). Superimposed on and intermingled with these basic units are materials from basins and craters of various ages, ranging from the dark reds and blues of ancient basins to the bright blue crater rays of younger craters (*e.g.*, McEwen *et al.*, 1994; Pieters *et al.*, 1994).

Limitations and sources of error in using remote sensing spectroscopic data

While remote sensing and especially spectroscopic data is an invaluable resource for lunar studies, the analysis is subject to strong limitations and assumptions. Resolution may vary from instrument to

instrument. For example, the Lunar Prospector thorium maps cover an area of half a degree per pixel. Since the surface of the moon covers an area of approximately thirty kilometers per degree, each thorium map pixel covers an area of about 15×15 kilometers square on the lunar surface, setting a minimum resolution of at least features of 15 km. Smaller features will not be resolved, and therefore cannot be accurately analyzed. Spectral or elemental composition for a given pixel will only be an average of the composition on the 15×15 km area. As technology and imagery progresses, resolution becomes less of an issue. Recent remote sensing data from the Lunar Reconnaissance Orbiter Camera has provided data imagery with a resolution of 0.5 meters per pixel. Figure 3.8 compares a low-resolution (200m/pixel) Clementine true color image of Copernicus crater (diameter 93 km) with a high-resolution image, taken by the wide-angle camera (WAC) onboard the Lunar Reconnaissance Orbiter.

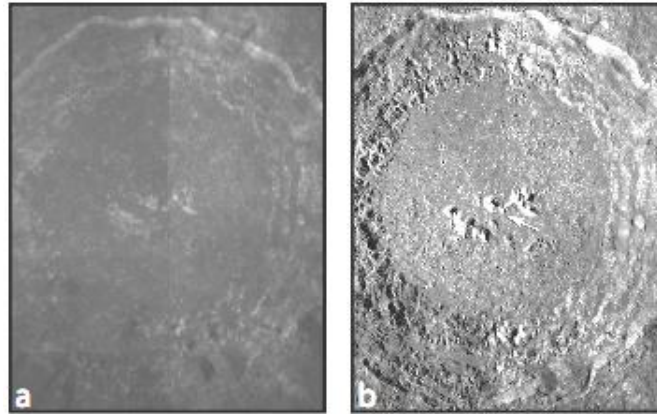


FIGURE 3.8 This figure demonstrates the significance of obtaining higher-resolution datasets. The left image shows a low resolution (200m/px) Clementine true color image of Copernicus crater, while the right image is a higher resolution (67m/px) LROC WAC image (M119985095ME) of the same terrain.

Another important limitation of remote sensing data is the probing depth. Depending on the instrument used, the returned data will sample only to a specific depth of the lunar surface. Clementine UVVIS data represents reflected sunlight at specific wavelengths, therefore only revealing the characteristics of the top few microns of the lunar surface (Ostrach and Robinson, 2010). Though we may infer that in any region the regolith will be composed mainly of underlying material, such assumptions are likely to have a large error. Similarly, the Lunar Prospector neutron and gamma ray spectrometers probe to depths of approximately 50 cm and 20 cm, respectively (Feldman *et al.*, 1999). While this may still be a surficial signature, the deeper probing depth offers more valuable insight into crustal composition below, although the possibility of vertical heterogeneities cannot be ignored. It has been speculated that such differences in data gathering technique may account for discrepancies in measured titanium values between the Clementine UVVIS analysis and results from the Lunar Prospector neutron spectrometer (Ostrach and Robinson, 2010; Gillis *et al.*, 2004).

Some remote sensing techniques also encounter geographic limitations when mapping the polar regions of the Moon, as well as the far side of the Moon. Spatial resolution at the poles becomes an issue for Clementine spectral reflectance data, limiting the accuracy of data greater than about ± 70 degrees (Chevrel *et al.*, 2002). In addition, due to a lack of cartographic control on the lunar farside, some Clementine data may be inaccurate or offset by as much as 2 km (Cook *et al.*, 2002), thereby introducing error in our crustal thickness and image analysis modeling.

Using impact craters as natural drills to sample material from deeper layers

Large impact craters and impact basins have the capacity to excavate or uplift material from the lower crust and upper mantle. Figures 3.9 and 3.10 illustrate different stages of an impact event, for simple and complex craters, as well as for basins. Small craters are simple, bowl-shaped depressions. Complex craters (with diameters ~ 16 – 20 km on the Moon) display broad flat shallow floors, terraced walls, and central peaks. Larger craters or basins (generally >200 km) can have multiple central rings, referred as peak rings,

instead of a central peak. The transition between a central peak to peak rings and their precise origin is still unclear.

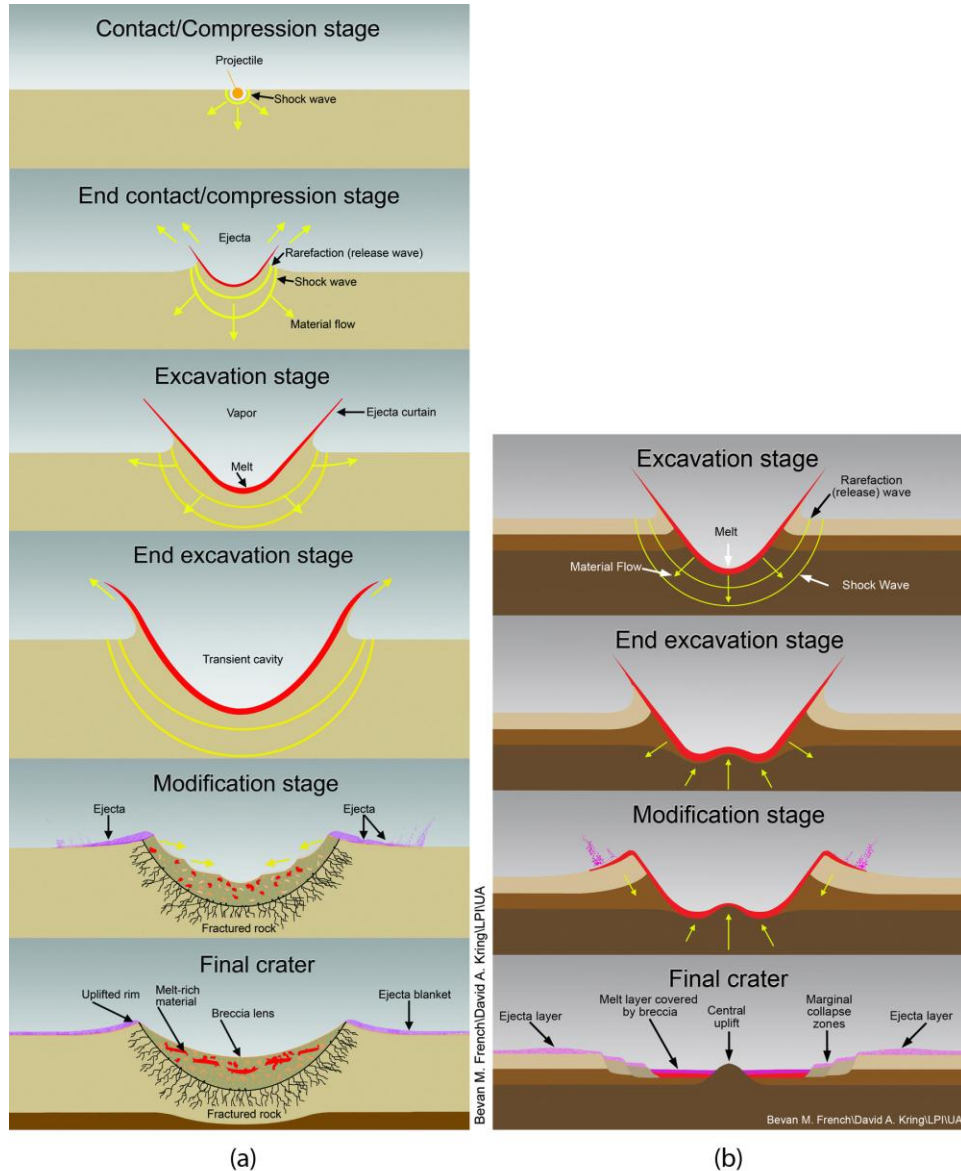


FIGURE 3.9 Difference in the formation mechanism of a simple (a) and a complex (b) crater.

Calculations of relevant morphological parameters

Excavation depth: Depth of excavation refers to the depth of origin of ejecta excavated from a crater. Target material deeper than the maximum depth of excavation is displaced downward beneath the crater floor and does not emerge in the ejecta to be deposited on the target's surface. Strata below the depth of excavation are thus pushed downward (Melosh, 1989).

As a rule of thumb, depth of excavation (D_e) is generally equal to one third of the transient crater depth (D_{td}), or one tenth of the transient crater diameter (D_{tc}) (Melosh, 1989, page 78; Croft, 1980):

$$D_e = (D_{td})/3 = (D_{tc})/10 ; \quad (3.1)$$

For simple craters, the transient crater diameter (D_{tc}) can be calculated using equation 3.2, where D represents the final diameter of the crater. For complex craters, we utilize equation 3.3 to find the transient diameter (also the same as Equation 6 on page 893 of Cintala and Grieve, 1998). Here, D_{sc} is the transition diameter from simple to complex craters (approximately 16–20 km for the Moon).

$$D_{tc} = 0.84D \text{ for simple craters; all parameters in km} \quad (3.2)$$

$$D = D_{sc}^{-0.18} D_{tc}^{1.18} \text{ for complex craters; all parameters in cm} \quad (3.3)$$

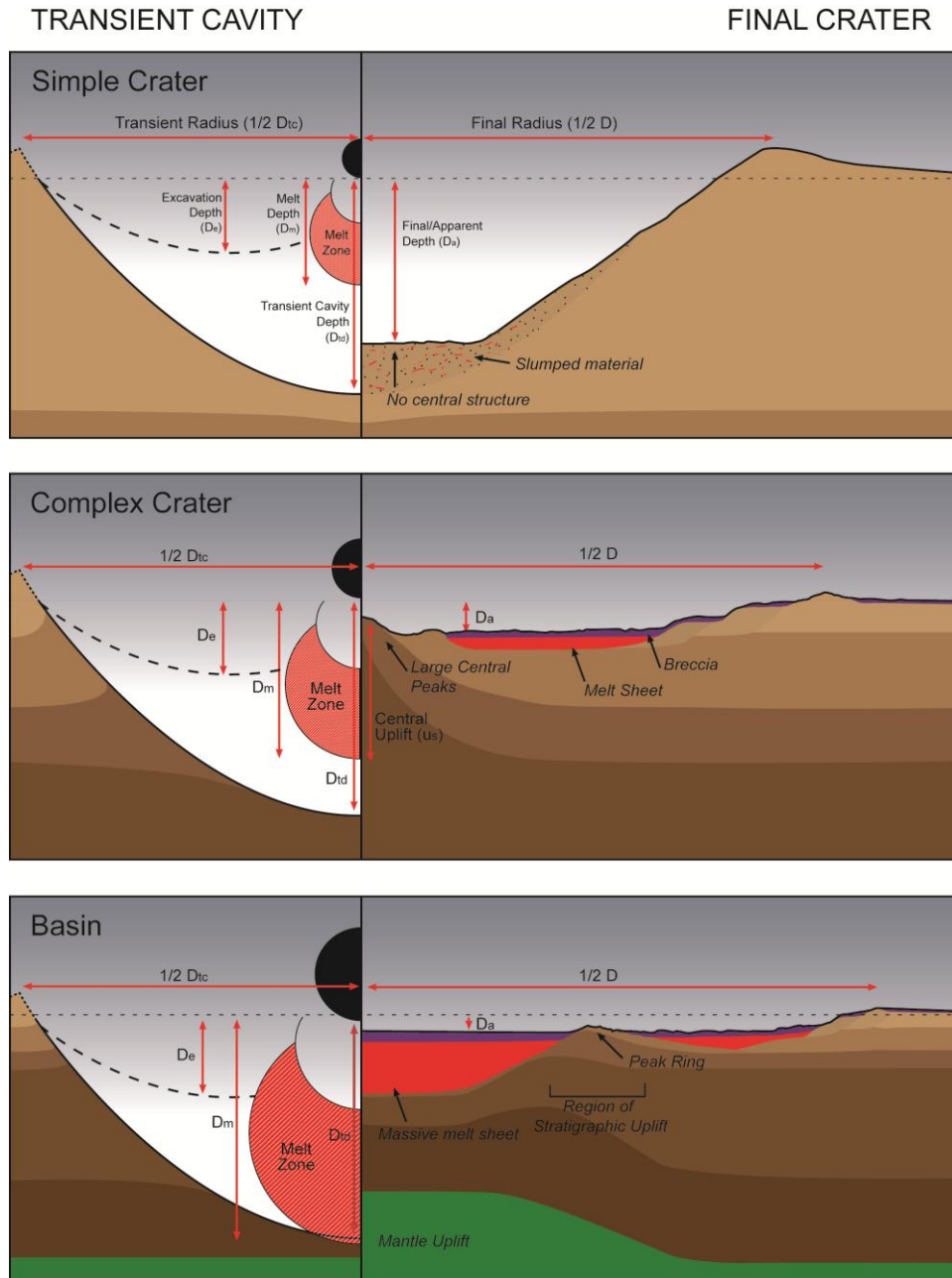


FIGURE 3.10 Diagram comparing the relative sizes of melt zone, transient cavity depth, and excavation depth to final crater diameter and depth for different crater morphologies. Note that the comparative sizes of morphologies are not to scale. In addition, subsurface structure for basins is approximate, as the exact formation process is still unknown. Images based on Figs. 12, 14, 15 of Cintala and Grieve (1998).

Depth of melting: For complex craters on the Moon (greater than 16–20 km in diameter), the depth of melting (D_m) is given by equation 3.4, where D is the final rim diameter of the crater in kilometers:

$$D_m = 0.109D^{1.08}; \text{ all parameters in km} \quad (3.4)$$

This expression for the depth of melting is derived through curve-fitting of Fig. 22 on page 1343 of Cintala and Grieve (1998). This equation has also been used in Cahill *et al.*, (2009) and Tompkins and Pieters (1999) for calculating the melt depth. Depth of melting is a function of both the impactor type and the impactor velocity; the calculations in Cintala and Grieve (1998) specify impacts of chondritic projectiles into anorthosite at 16.1 km/s. As concluded in this paper, the minimum depth of origin for a central peak coincides with the maximum depth of melting. We are using this assumption for inferring the composition of crater central peaks.

Stratigraphic uplift: The stratigraphic uplift (u_s) for lunar impact craters is given by equation 3.5 (from Eq. 12 on page 908 of Cintala and Grieve [1998], based on empirical analysis of lunar crater datasets):

$$u_s = 0.022D^{1.45}; \text{ all parameters in km} \quad (3.5)$$

Lunar crustal thickness: Lunar crustal thickness has been estimated from gravity and topography measurements taken by instruments onboard the Clementine, Lunar Prospector, and more recently, Kaguya missions. We use crustal thickness values of Wieczorek *et al.*, (2006), based on crustal thickness models using Clementine topography of Smith *et al.*, (1997; GLTM2C) and the Lunar Prospector LP150Q gravity model of Konopliv *et al.*, (2001). The thickness of the mare basalts within the large basins is based on the model of Solomon and Head (1980), modified by the maximum basalt thicknesses of Williams and Zuber (1999).

There are three crustal thickness models derived by Wieczorek *et al.*, 2006. The first two models describe the lunar crust as a traditional single layer, with the second model taking into account a first order gravitational attraction of the surface topography (*i.e.* the Bouguer correction). This attraction was set to zero before inverting for the relief along the crust-mantle interface. The third model is a dual-layered model in which the upper crust is allowed to vary in thickness, but the lower crust is constrained to have a constant thickness of 25 km. Although we have done our calculations using all three crustal thickness models, we have only used results from the models 1 and 3 in our final interpretations and conclusions since they are more reliable and consistent with each other. Figure 3.11 demonstrates sample data from our calculations, demonstrating the similar results from models 1 and 3, and the large variance of model 2. Figure 3.12 shows the global crustal thickness maps based on models 1 and 3 from Wieczorek *et al.*, 2006.

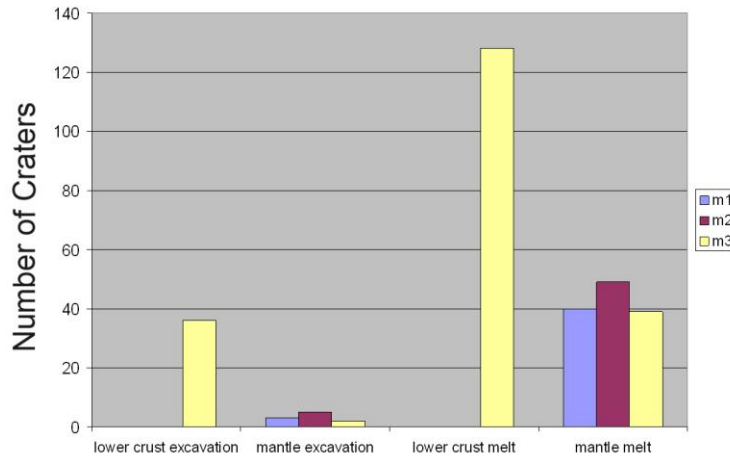


FIGURE 3.11 Sample data showing the number of craters that are supposed to excavate lower crust or mantle, or sample lower crust or mantle in the melt (meaning craters which have a proximity value <-5km) for each of Wieczorek's models. Models 1 and 3 are more consistent with each other. Only model 3 can provide data on the lower crust.

More accurate crustal thickness estimates based on data from the Kaguya mission have been published recently (Ishihara *et al.*, 2009) but have not yet been publicly released. Therefore global crust thickness maps from this paper are only used as a qualitative check for the models based on Clementine data.

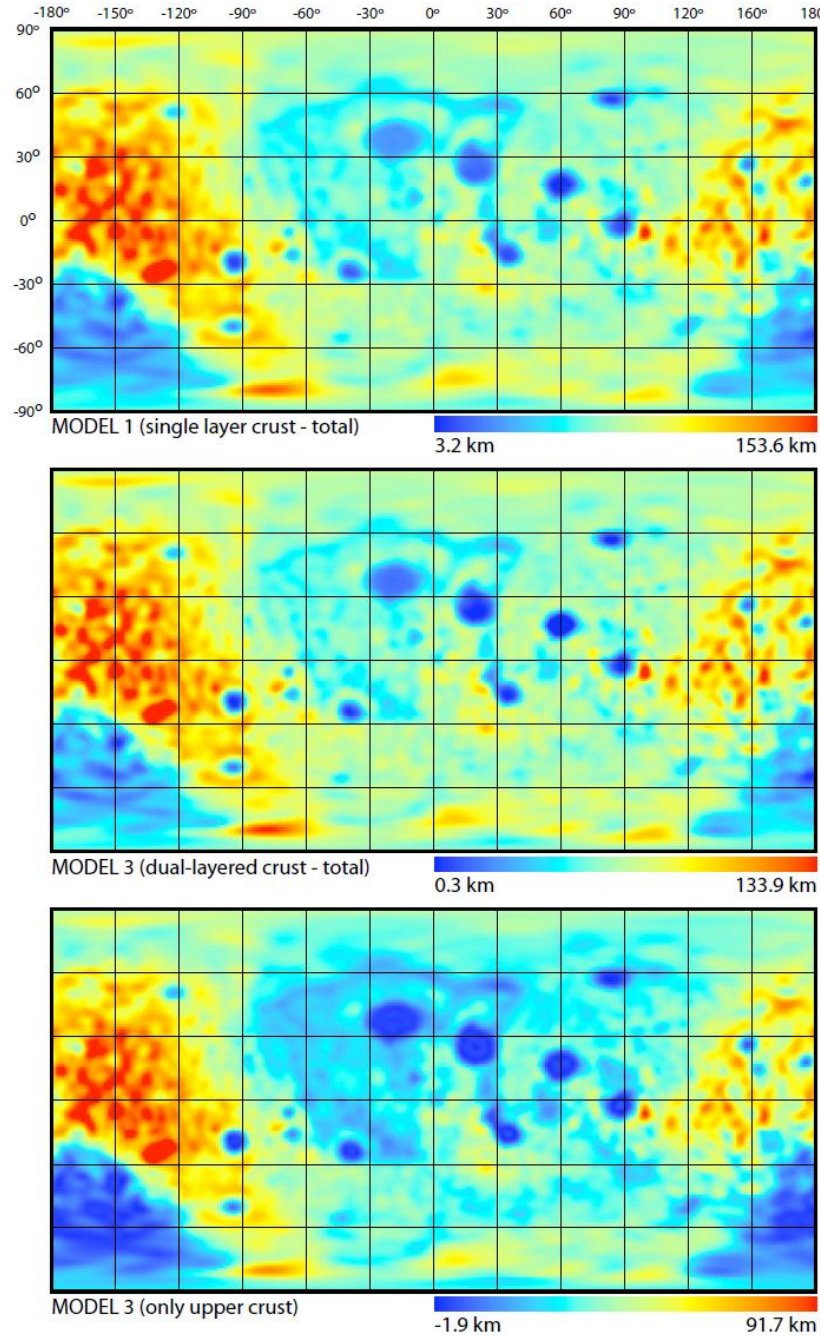


FIGURE 3.12 Global lunar crustal thickness maps based on models 1 and 3 from Wieczorek *et al.*, (2006). The top image shows the total lunar crustal thickness derived using model 1; the second image shows the total lunar crustal thickness derived using model 3 and the third image shows the upper crustal thickness derived using model 3.

Determining if a crater samples the upper crust, lower crust, or mantle material

To determine if the material excavated by a crater sampled the upper/lower crust or mantle, we integrate analyses of individual craters with models of crustal thickness where those impacts occurred. Our

calculations shown here are based on Cahill *et al.* (2009) (Fig. 3.13). Two parameters are compared to the crustal thickness at each of the crater locations: the excavation depth (D_e , which is the maximum depth from which the ejecta deposits are derived) and the maximum depth of melting (D_m , which is the maximum depth from which the central peak could sample material).

For all complex craters in the Lunar Impact Crater Database with diameter $>20\text{km}$, the following calculation can be performed:

$$P = T - D \quad (3.6)$$

Here, T is the pre-impact crustal thickness corresponding to each of the three crustal thickness models, D is the excavation depth or depth of melting, and P is the proximity to the crust-mantle boundary. This simple equation will then yield one of two responses:

- If P is positive, the ejecta blanket/central peak contains only crustal material.
- If P is negative, the ejecta blanket/central peak may sample mantle material.

To increase the reliability and accuracy of our results, we applied a down-sampling criterion to the returned proximity values. Any craters within a $\pm 5\text{ km}$ proximity to the crust-mantle boundary were not taken into account, as they are subject to errors of modeling techniques.

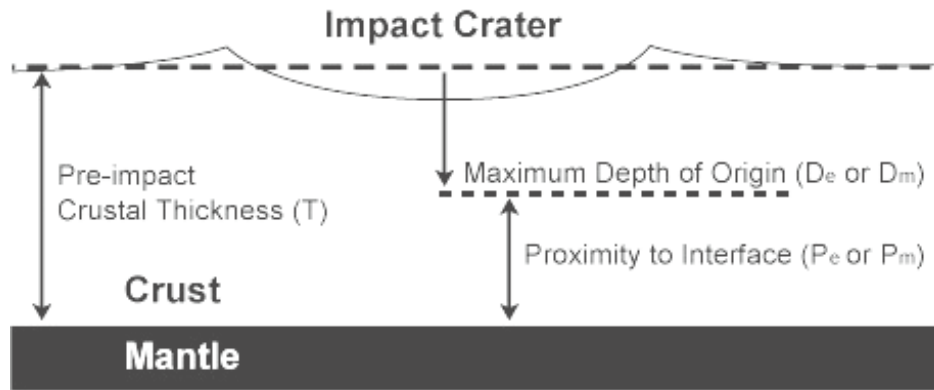


FIGURE 3.13 (Adapted from Cahill *et al.*, 2009). For each crater the proximity to the lunar crust-mantle boundary was calculated by subtracting the depth of origin (D_e or D_m , excavation depth and melting depth, respectively) from the crustal thickness (T). Here proximity to the crust-mantle boundary (P_e or P_m , excavation proximity and melt proximity) via the maximum depth of origin is illustrated.

Wieczorek's crustal thickness models have a resolution of 1 degree/pixel or approximately 30km/pixel. However, as shown in Fig. 3.13, the crustal thickness directly underneath the center of each crater cannot be used for our calculations, as it represents the thickness after the impacts in question. We thus need an estimate of the pre-impact crustal thickness to get an accurate measurement of the proximity to the crust-mantle boundary. To calculate the average pre-impact crustal thickness corresponding to each crater in the Lunar Impact Crater Database, we took an average of the crustal thickness corresponding to pixels located at a distance of $\pm 10\%$ of a crater diameter distance from the rim (Fig. 3.14).

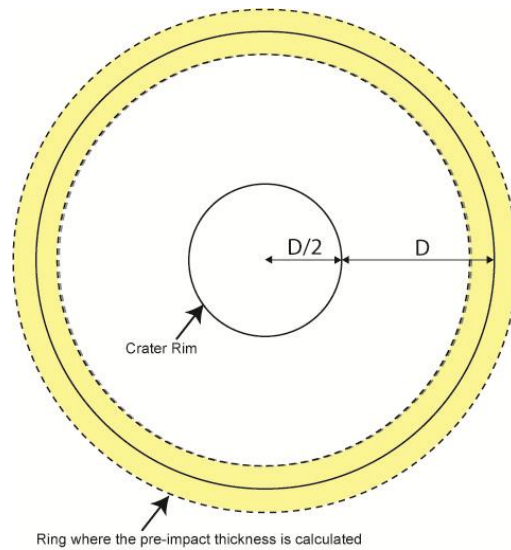


FIGURE 3.14 Calculation of the pre-impact crustal thickness for each crater. The inner solid circle shows the crater diameter while the outer solid circle shows a circle at a distance of 1 diameter away from the crater rim. The dashed lines show the $\pm 10\%$ ring of pixels that were used for calculating the average pre-impact crustal thickness.

Similar calculations were carried out for the boundary between the upper crust and lower crust, based on Wieczorek's dual-layered model.

Using the single-layered crustal thickness model 1, we identified 3 craters that might sample mantle material in their ejecta blanket and 40 that might sample mantle material in their central peak. Using the dual-layered crustal thickness model 3, we identified 2 craters that might sample mantle material in their ejecta blanket, 39 that might sample mantle material in their central peak, 36 that might sample lower crustal material in their ejecta blanket and 128 that might sample lower crustal material in their central peak (Table 3.4).

TABLE 3.4 Summary of results obtained using the crustal thickness models 1 and 3.

	Number of craters	
	Model 1 (single-layered)	Model 3 (dual-layered)
lower crust excavation	-	36
mantle excavation	3	2
lower crust melt	-	128
mantle melt	40	39

Results of model 1 and 3 are very similar, except for two craters. Here, results from model 1 (best fit) are used for mantle proximity calculations, while results from model 3 are used for lower crust proximity calculations, as model 1 does not distinguish between upper crust and lower crust.

Figure 3.15 shows a map of craters in which the central peaks (or peak rings) and melt sheets might sample material from the mantle according to our calculations (using crustal thickness model 1).

Figure 3.16 illustrates the methodology by showing where the material that was displaced by the Orientale basin impact can be found. The excavated material should be ejected around the basin, while deep material should be brought to the surface in the central peak or peak rings. Peak rings should be uplifted. Melt should be found within the crater, especially within the inner ring and inside it.

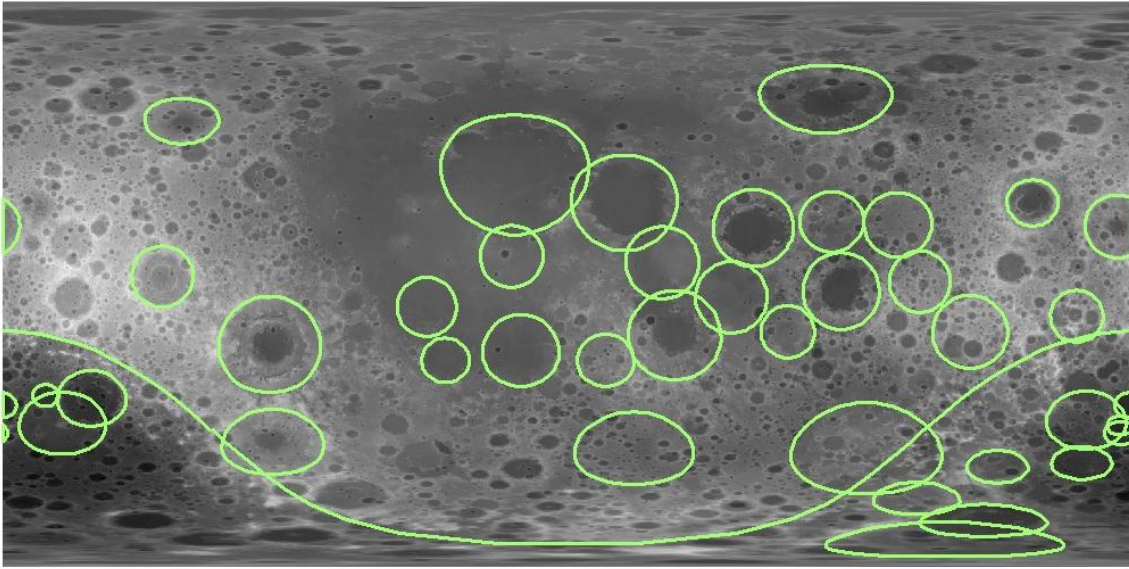


FIGURE 3.15 Craters in which the central peaks or rings (if preserved) should sample material from the mantle (according to the single-layered crustal thickness model 1). These craters were highlighted as they have proximity value (= crustal thickness - melt depth) lower than -5 km, meaning that they sample at least 5 km below the crust/mantle boundary.

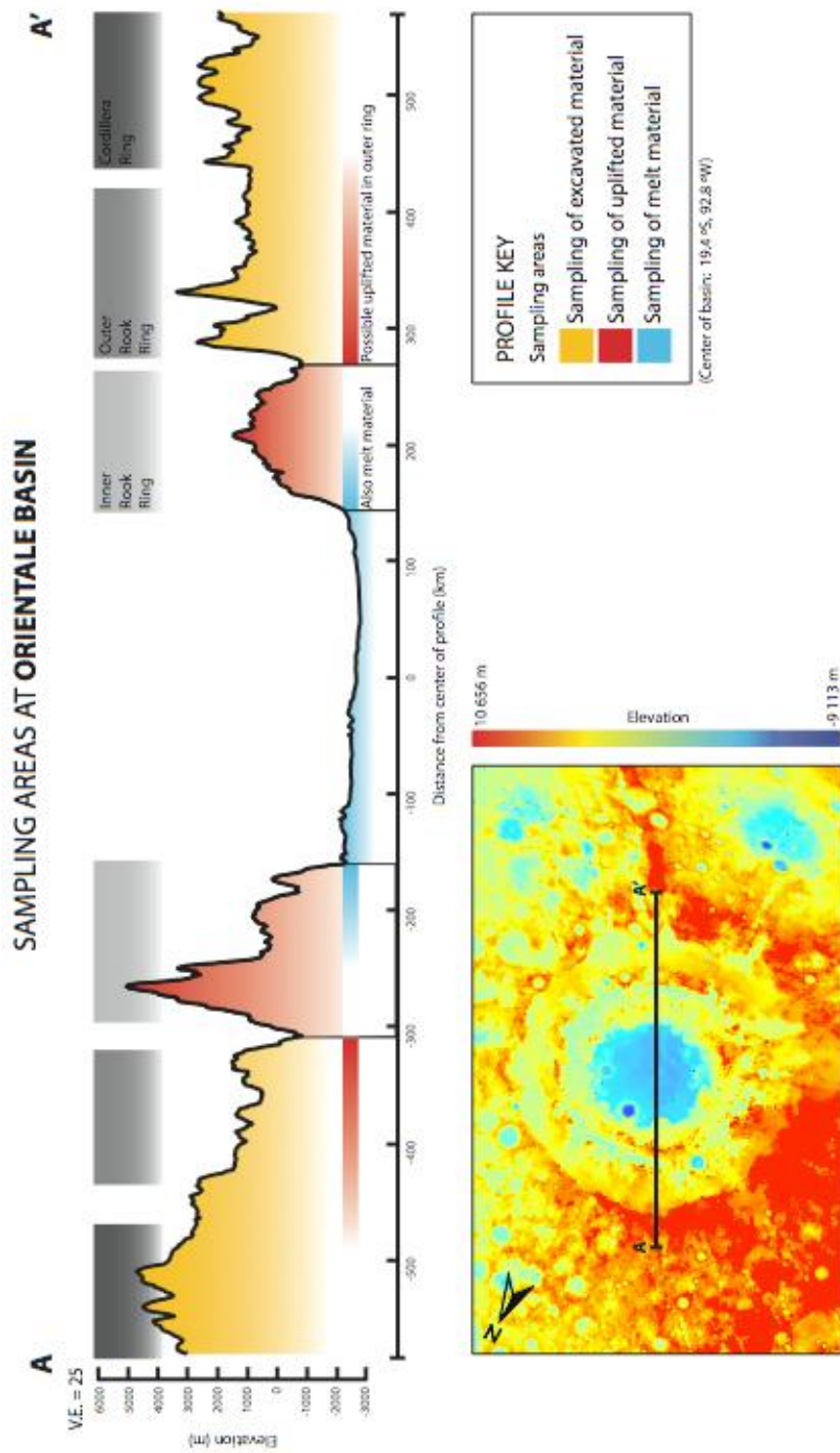


FIGURE 3.18 Elevation profile of the Orientale basin (19.4°S, 92.8°W) showing the sampling areas for different kind of impact materials. Vertical exaggeration is 25. The different colors in the profile shows where different kinds of impact material can be found *on the surface, immediately after the Orientale impact event* (i.e. ejecta material, melt material, uplifted material). Subsequent impacts might have mixed the surface material, laterally and vertically. Sampling areas at complex craters follow a similar pattern, except that the uplifted material can be found in the central peak and that the melt material can be found over the crater floor and on the rims of the crater. Elevation data were generated by the LOLA instrument on the Lunar Reconnaissance Orbiter. Resolution is 64 pixels/deg, or approximately 500m/px at the equator.

SCIENCE GOAL 3A: DETERMINE THE EXTENT AND COMPOSITION OF THE PRIMARY FELDSPATHIC CRUST, KREEP LAYER, AND OTHER PRODUCTS OF DIFFERENTIATION

Introduction

According to most widely-accepted lunar formation models, the Moon was completely molten to a depth of hundreds of kilometers right after its accretion (Wood *et al.*, 1970). The existence of a magmatic ocean at the surface of the Moon, inferred from the study of the Apollo samples, led to the process of planetary differentiation as the Moon was cooling, with denser crystallized material like pyroxene and olivine sinking, and lighter material like plagioclase-rich cumulates floating to form the upper crust. This process also triggered a segregation of chemical elements, as the last liquid to crystallize was enriched in incompatible elements, such as potassium (K), rare earth elements (REE) and phosphorus (P) (collectively known as (ur)KREEP, Fig. 3.17) (Warren and Wasson, 1979). Although this concept has served well since the days of the Apollo missions, remote sensing, geophysical measurements, and sample analysis reveal that the lunar crust is not simply vertically stratified, but also varies laterally, and that the traditional dichotomous mare/highlands classification developed from Apollo experience is inadequate for describing the formation, geology and evolution of the Moon. The Moon seems to be made of geologically distinct global provinces, which are inferred to be the result of asymmetry in the crystallizing lunar magma ocean (Jolliff *et al.*, 2000). Consequently, to improve the understanding of the formation and evolution of the Moon, it is important to determine the composition and the extent of each of the differentiation products: the primary feldspathic crust, the (ur)KREEP layer, and the mantle.

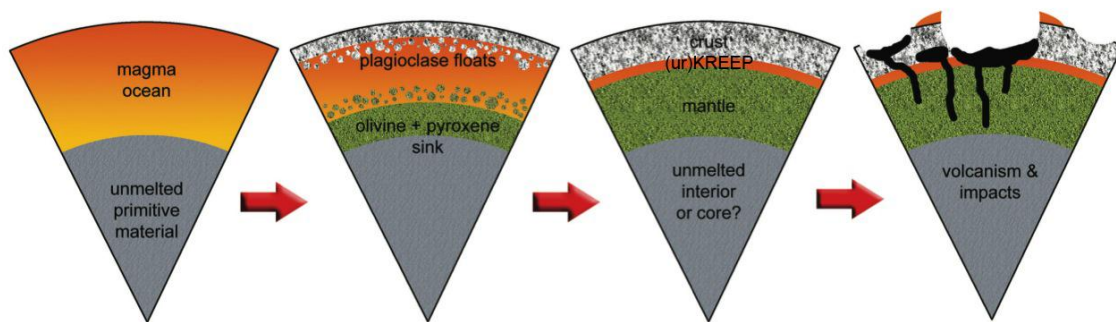


FIGURE 3.17 The lunar magma ocean hypothesis (adapted from NRC 2007, p.14).

This magma ocean hypothesis can also be applied to other planetary bodies, especially the Earth. But since the surface of the Earth and most other planets have encountered large modification since their formation 4.5Ga, the Moon remains the best most accessible place in the Solar System to study magma ocean processes.

Background

Geochemical terranes

Instead of the simple classification of mare and highlands, large regions of the Moon have distinct geologic and geochemical characteristics. Jolliff *et al.* (2000) defined at least three of these distinct provinces, or terranes (Fig. 3.18), using the FeO abundance map derived from Clementine UVVIS data by Lucey *et al.* (1998) and the Th data from Lawrence *et al.* (1998) calibrated to the Apollo gamma-ray-spectrometer (GRS) data as described by Gillis *et al.* (1999):

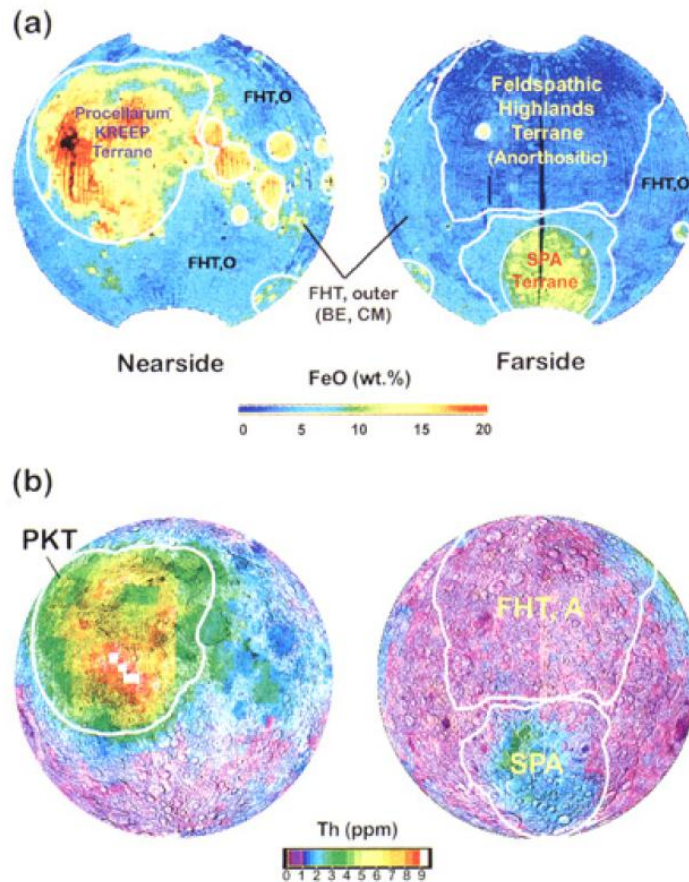


FIGURE 3.18 Surface expression of major lunar crustal terranes delineated on the Clementine global FeO map (a) and on a Lunar Prospector Th map, merged with topographic data (b) (from Jolliff *et al.*, 2000).

- The *Feldspathic Highlands Terrane* (FHT) consists in a region made of nearly pure anorthositic highlands (Jolliff *et al.*, 2000; Ohtake *et al.*, 2009).
- The *Procellarum KREEP Terrane* (PKT) has been defined by its high content in mafics and its enrichment in incompatible elements such as thorium (values >3.5 ppm were used to set the boundaries of PKT) (Lawrence *et al.*, 1999; Jolliff *et al.*, 2000; Haskin *et al.*, 2000).
- The *South Pole-Aitken Terrane* (SPAT) limits are given by the basin rim. The composition of the SPAT could be linked to the material excavated by the corresponding impact crater, which was derived from the lower crust and potentially mantle (Pieters *et al.*, 1997; Lucey *et al.*, 1998). The occurrence of low thorium value in this area also suggests that the KREEP layer may be absent (Jolliff *et al.*, 2000).

Highland variety

It is thought that the lunar highland crust was formed by the crystallization and floatation of plagioclase from the global magma ocean, although the actual generation mechanisms are still debated. The composition of the lunar highland crust is therefore important for understanding the differentiation of such a magma ocean and the subsequent evolution of the Moon.

The crustal igneous rocks are almost exclusively plagioclase-rich, making the lunar crust predominantly anorthositic. The crustal rocks have been subdivided into suites according to their major mineralogical composition (Fig. 3.19):

- The ferroan-anorthositic suite, which have high calcic plagioclase and anorthosite content >94%,

- The magnesian suite, where $\text{Mg}/(\text{Mg}+\text{Fe})$ values range from about 0.95 to 0.6,
- The alkali suite, which have alkali-rich bulk compositions.

Ferroan anorthosites are thought to be diagnostic of the pristine highlands, formed by crystallization in the magma ocean, while magnesian and alkali rocks are chronologically younger and might be secondary, KREEP-related products.

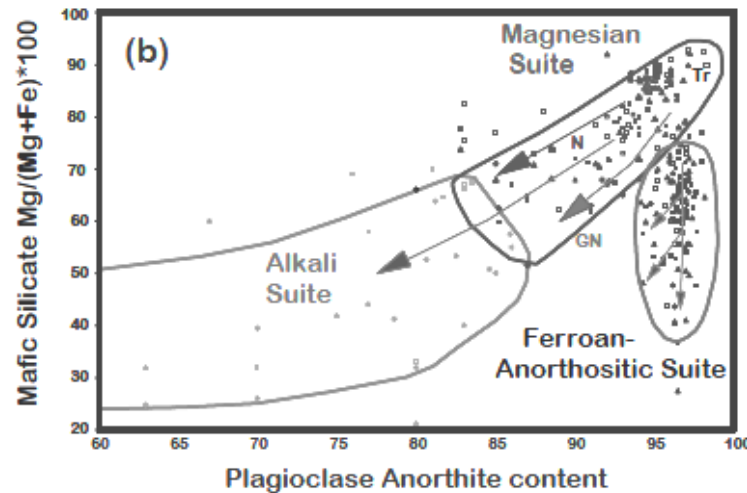
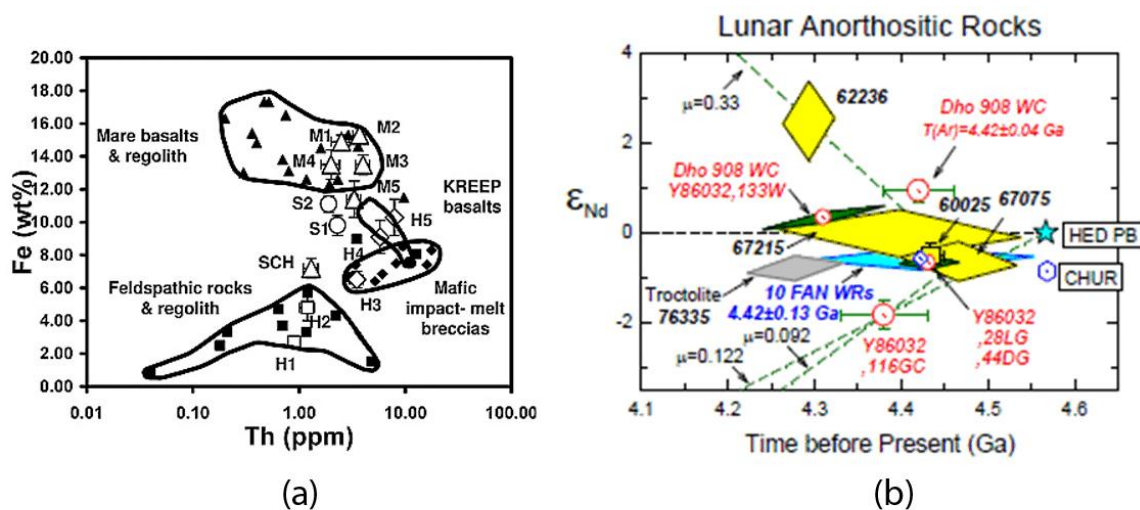


FIGURE 3.19 Compositions of the three main types of anorthosites. Typical trends resulting from fractional crystallization (arrows) suggest a possible relationship between the magnesian- and alkali-suite rocks. The overall trend from upper right to lower left is similar to trends observed for rocks of terrestrial layered mafic intrusive bodies. The Fe-anorthositic and Mg suites are difficult to relate through a common magmatic process. (image from Wieczorek *et al.*, 2006).

Based on chemical composition, especially the Th, Ti and Fe abundances, Chevrel *et al.* (2002) reported several other anorthosite types on the Moon, showing that the highland variety is more diverse than was first expected. There might be at least 5 different types of highlands to sample. Nyquist *et al.* (2010) came to the same conclusion looking at isotopic composition in lunar meteorites (Fig. 3.20). Ages of some of the ferroan anorthosites postdate the age estimates for crystallization of the lunar magma ocean, implying other mechanisms in the formation of the highlands. This evidence for multiple highland rock types raises questions on the global pervasiveness of the magmatic ocean, and on the possibility of the formation of anorthosite in secondary plutons (Nyquist *et al.*, 2010). The distinction between the pristine anorthosites that are primary products of the magma ocean versus those that originate from other post-differentiation processes is important for understanding the complex lunar formation process.



Rock and soil samples

- ▲ Mare basalts and regolith
- Feldspathic rocks and regolith
- KREEP basalts
- ◆ Impact melt breccias

PCA units

- H1, H2, Highland units
- ◇ H3, H4, H5, Th-rich units
- △ M1 to M5, Mare units
- S1, S2, SPA units
- △ SCH, Schickard unit

FIGURE 3.22 (a) Variety of lunar highlands and mare types according to their Ti, Fe and Th composition estimated from orbit (Chevrel *et al.*, 2002). Different highland types are classified from H1 to H5, H3 to H5 being Th-rich types. (b) Various ages and isotopic composition (ϵ_{Nd}) of highlands clasts from different lunar meteorites suggest that the lunar crust is composed of a variety of anorthosites, as least some of which must have formed as plutons in the earliest formed ferroan anorthosite crust (Nyquist *et al.*, 2010).

Recently, Ohtake *et al.* (2009) detected a possibly ubiquitous shallow layer of anorthosites containing more than 98% plagioclase using data from the Multispectral Imager instrument (MI) onboard the Kaguya spacecraft, and classified them as “purest anorthosite” (PAN). Spectral signatures characterizing PAN are found in the central peaks of almost all the fresh craters larger than 30 km in diameter (Fig. 3.21). They may represent remnants of the ancient anorthositic upper crust, that is now blanketed by a more-mafic rich layer. The presence of this pure anorthosite layer is critical for the understanding of the Moon as it could significantly modify the estimated content of the bulk Moon, and the magma ocean model. It is therefore crucial to sample PAN and perform chemical and isotopic analyses on it.

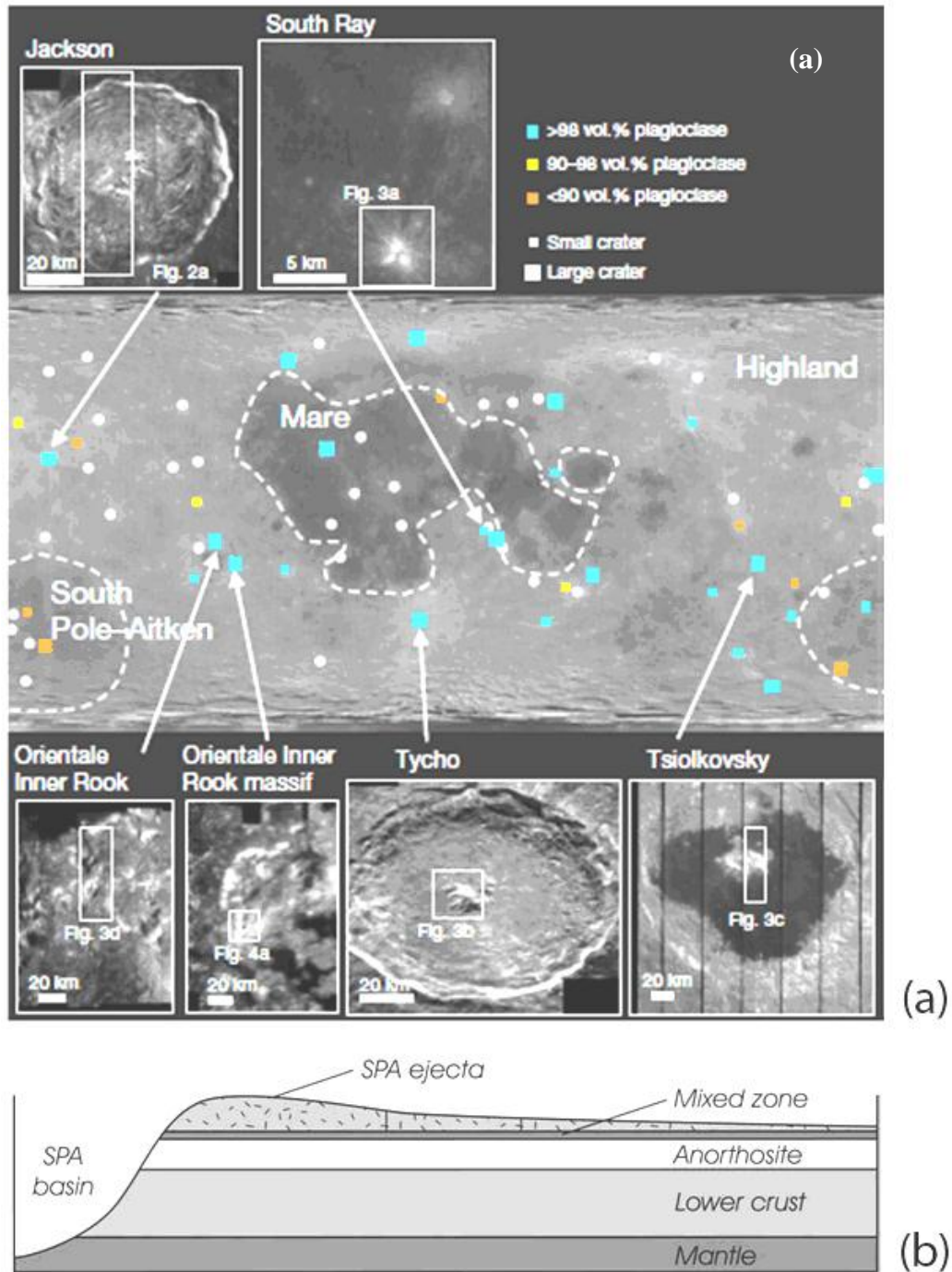


FIGURE 3.21 (a) MI (Kaguya) investigations plotted on the USGS Clementine 750 nm basemap. Plagioclase modal abundances of the 32 freshest and nearly regolith-free locations derived from the model analyses are indicated by orange (90 vol.%), yellow (90 to 98 vol.%) and blue (98 vol.%) squares. Investigated locations that do not have freshly exposed outcrops are plotted as white dots regardless of the crater diameter (Ohtake *et al.*, 2009). (b) Schematic diagram illustrating the generalized crustal cross-section at the margin of South Pole-Aitken basin, showing a pure anorthosite layer may lie beneath a layer of more mixed material (Hawke *et al.*, 2003).

KREEP

The concept of “KREEP” was first introduced after the Apollo 11 mission returned samples showing fragments of material rich in potassium (K), rare earth elements (REE), and phosphorus (P). To understand this concept, it is important to make a clear distinction between what is called “urKREEP” and “KREEP basalt”, as the terminology for KREEP is often misused or unexplained in the literature.

The urKREEP layer (the “ur”- prefix stemming from German meaning “original” or “primitive”) was first introduced after the return of the Apollo samples and the emergence of the magma ocean theory (Warren and Wasson, 1979). The urKREEP layer is believed to correspond to the last liquid that crystallized from the magma ocean, and is expected to be rich in incompatible elements. The formation of such a layer is a complex process that is still not well understood, but it has probably been formed as a global layer, ‘sandwiched’ between the primordial crust and mantle boundary at the very end of the crystallization process. The urKREEP layer is estimated to be approximately 2 km thick, assuming an average crustal thickness of about 40 km and initial global distribution. Even though it only represents less than 1% of the lunar magma ocean in volume, this thin layer is thought to have contained about half of the moon’s incompatible elements, while the other half remained incorporated within nonKREEPy rocks. Despite the very small volume, it is nevertheless a very important part of the model as it encompasses the majority of incompatible elements, themselves being useful tracers for different materials.

Remote-sensing results from recent missions such as Lunar Prospector and Clementine question the global extent of this theoretical layer. Contrary to the early theories of a global urKREEP layer (Fig. 3.22), current observations of patchy incompatible element abundances on the lunar surface would suggest an asymmetrical distribution of urKREEP since the early phases of planetary differentiation (Wieczorek *et al.*, 2006), making it a regional attribute of the PKT region (*e.g.*, Wieczorek and Phillips, 2000). For instance, the South Pole-Aitken Basin is supposed to have tapped deep enough to excavate the urKREEP layer, yet has comparably low thorium value (thorium being an indicator of KREEP-rich material). However, the primordial urKREEP layer (as well as the lunar mantle) has not been sampled by any of the missions or meteorites, making urKREEP material a priority sample in order to constrain its so far putative existence and debated distribution.

On the other hand, the analyses of Apollo samples did show the existence of rocks enriched in incompatible elements (potassium, rare earth elements and phosphorus), in varying amounts from sample to sample, but with a thoroughly constant relative ratio. These samples were named “KREEP basalt” as they have a unique mineralogy (Wieczorek *et al.*, 2006) with a different geochemical signature than the hypothetical urKREEP material (Warren 1988). Various amounts of KREEP basalt material were found in all of the Apollo mission samples, although they were the most abundant in samples from Apollo 14, 15, and 12 (Elphic *et al.*, 2000). KREEP basalts are thought to come from deep sources in the mantle that plowed through the molten urKREEP layer, thus assimilating some urKREEP material along the way (Warren, 1988) (Fig. 3.23). They are therefore a product of serial magmatism from the mantle and urKREEP layer.

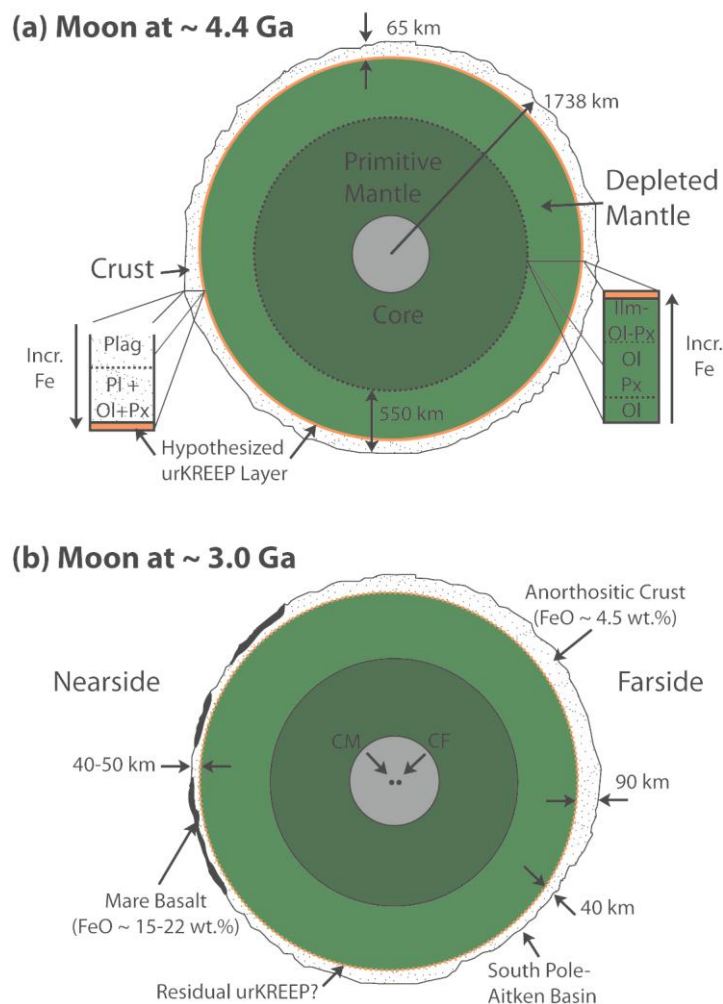
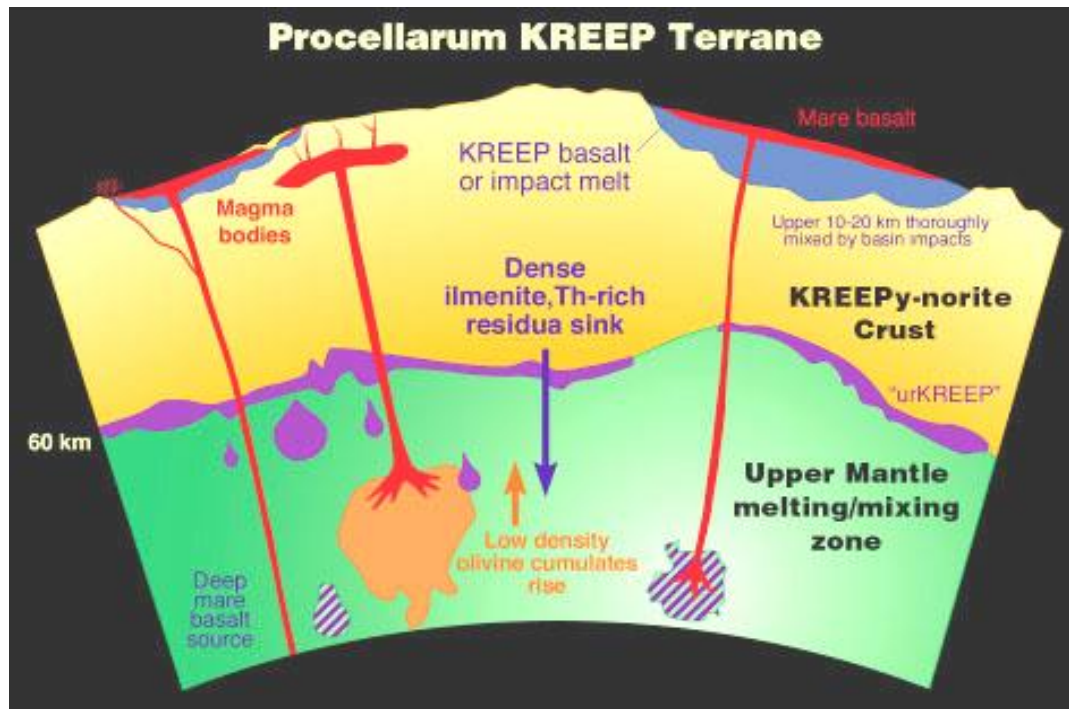


FIGURE 3.22 Cross sections of the Moon. (a) Depiction of lunar interior around 4.4 Ga, just after magma ocean crystallization. A thin urKREEP layer lies between the crust and mantle. (b) Depiction of lunar interior around 3 Ga, near the end of mare basaltic volcanism. Notice the asymmetry of the lunar crustal material, unknown extent of urKREEP layer (adapted from McCallum, 2001).

Given the high uncertainties that exist concerning the KREEPy material (origin, extent, etc.), representative samples of KREEP and urKREEP would provide invaluable insight regarding the accuracy of the lunar magma ocean theory and the bulk Moon, as it represents the last liquid to solidify. Ground truth data are also needed to provide more accurate global estimates of incompatible element abundances that have only been derived so far from orbital data. In addition, heat producing elements existing within KREEP material may have had a large effect on lunar volcanic processes. For such reasons, it is thus highly recommended to target areas with high KREEP signatures to gain important information about the extent and composition of the urKREEP layer, and target deep impact basins that could potentially sample pristine urKREEP.



(Graphic by Brooks G. Bays, Jr. based on diagram by Brad Jolliff.)

FIGURE 3.23 This diagram of the PKT region depicts the differences between the KREEP basalt and the urKREEP layer. Residua from the lunar differentiation process has left a ‘pristine’ layer of urKREEP wedged between the crust and mantle. The mixture of the urKREEP material with rising cumulates and possible lower crustal material lead to the emplacement of KREEP basalt. Image Source: Planetary Science Research Discoveries, University of Hawaii (adapted from Jolliff *et al.*, 2000).

Other differentiation products: lower crust, mantle, core

As mafics sink after their crystallization in the magma ocean, the deeper layers of the Moon are expected to be mafic-rich. This is the case of the lower crust, which is likely to be pyroxene-rich, and the mantle, which is likely to be olivine-rich. The Moon might also have a core of an unclear size and composition, though a metal-rich composition would be expected. However, very little information on the possible existence of a lunar core can be obtained from remote sensing data and geophysical measurements on the lunar surface.

Requirements

There are four main requirements for targeting potential landing sites that may accomplish Science Goal 3a:

- I. Target sites with potential to yield representative samples of planetary differentiation products (primordial anorthositic crust, lower crust, urKREEP, mantle).
- II. Target sites that could demonstrate the variety of lunar highlands.
- III. Target sites that will allow sampling of the three main geochemical terranes (FHT, PKT, SPAT).
- IV. Target sites that will allow the determination of the origin and extent of the urKREEP layer.

Methodology

To fulfill the requirement list, methods and procedures were devised for locating landing sites for Science Goal 3a:

1. Look for representative samples of planetary differentiation products:

- a. Analyze global maps of the lunar highlands and create contour maps to identify areas with high to low abundances of anorthosite. Use PAN detections to sample as pure as possible anorthosite.
 - b. Calculate excavation depth for all known craters and compare it with local crustal thickness to locate regions where ejecta may contain material from different depth layers (*i.e.* 0-5km, 5-10km, etc.) or material from the upper/lower crust and mantle in a broader sense (proximity calculations similar to the calculations of Cahill *et al.*, 2009, *cf.* section 3.3.3). Make maps showing all craters for which the ejecta blankets should contain material from a given depth range. Crater rim will have material from deeper regions.
 - c. Create maps depicting approximate depth from which central peaks material originates, using the maximum depth of melting as the minimum depth of origin of central peaks (Cintala and Grieve, 1998). Compare this to crustal thickness maps and find craters with central peaks material from upper/lower crust, mantle and different depth layers (proximity calculations similar to the calculations of Cahill *et al.* 2009, *cf.* section 3.3.3). Make maps showing all craters for which the central peaks reach a given depth range.
2. Determine the highland types variety:
 - a. Look at highland maps, and highland types maps (Chevrel *et al.*, 2002) to identify sites with various highland compositions.
 - b. Look at PAN detections to identify sites of extreme compositions.
 3. Sample the three main geochemical terranes:
 - a. Look at geochemical terranes maps to outline places that will be considered.
 - b. Look at elemental composition maps to identify locations that are representative of the entire terrane.
 4. Determine if the urKREEP layer is uniform or patchy:
 - a. ‘Bottom-up’ method: Assuming a global urKREEP layer sandwiched between the crust and mantle, it is safe to hypothesize that impacts that sample the mantle should also excavate material from the overlying urKREEP layer (as shown in Fig. 3.24). Thus, we identify craters reaching urKREEP-depth material and compare them to Lunar Prospector Th abundance maps to confirm the presence of urKREEP.
 - b. ‘Top-down’ method: Analyze geochemical maps of thorium, samarium, and potassium. Locate regions where these elements show the strongest signature, as well as areas of anomaly (both high and low). Target well-preserved craters such that samples may be representative of that area.

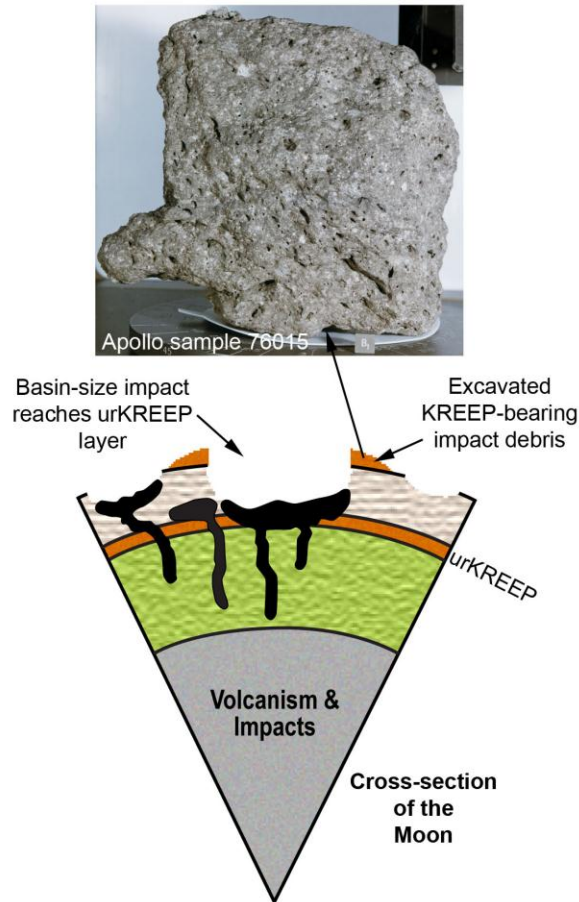


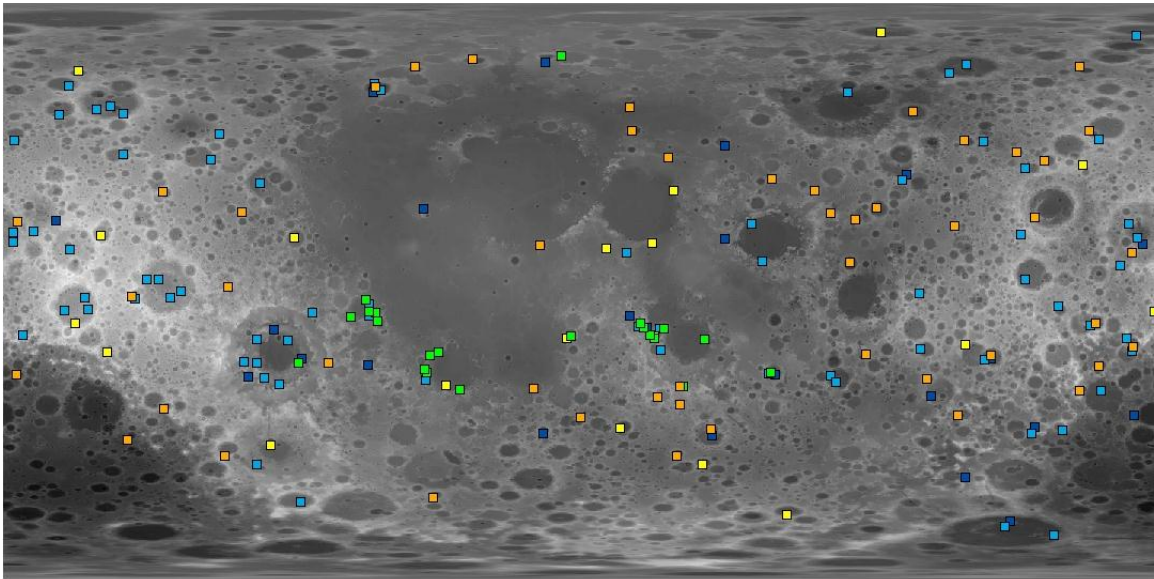
FIGURE 3.24 Excavation of the urKREEP layer by an impact basin.

Suggested landing sites

An integrated list of all candidate landing sites that are expected to fulfill each of the previous requirements is presented in Table A3.3, to assess the best places where the entire Science Goal 3a could be achieved.

Determining the best landing sites to sample each of the differentiation products.

Finding places that could yield representative samples of each of the differentiation products implies multiple landings at different sites. Differentiation products include the primary feldspathic crust, the lower crust, the urKREEP layer, the mantle and the core. As discussed earlier, the primary feldspathic crust is expected to be a ferroan-rich anorthosite, with very high and nearly pure plagioclase content. Therefore sites to investigate are the highland areas and the recent purest anorthosite (PAN) detections (Fig. 3.25). One can down-select a few specific places within the highlands (FHTa) by selecting fresh craters that should expose fresh outcrops of highlands (Fig. 3.26 and Table 3.5).



- Detection sources:
- Terrestrial observations (Hawke *et al.*, 2003)
 - SP onboard Kaguya (Ohtake *et al.*, 2010)
 - MI onboard Kaguya (Ohtake *et al.*, 2009)
 - Clementine observations of An (Tompkins and Pieters, 1999)
 - Clementine observations of An+1 other rock type

FIGURE 3.25 Combined map of all the purest anorthosite (PAN) detections from different missions and sources. The complete list of PAN detections is provided in Table A3.1. Background: LOLA topography.

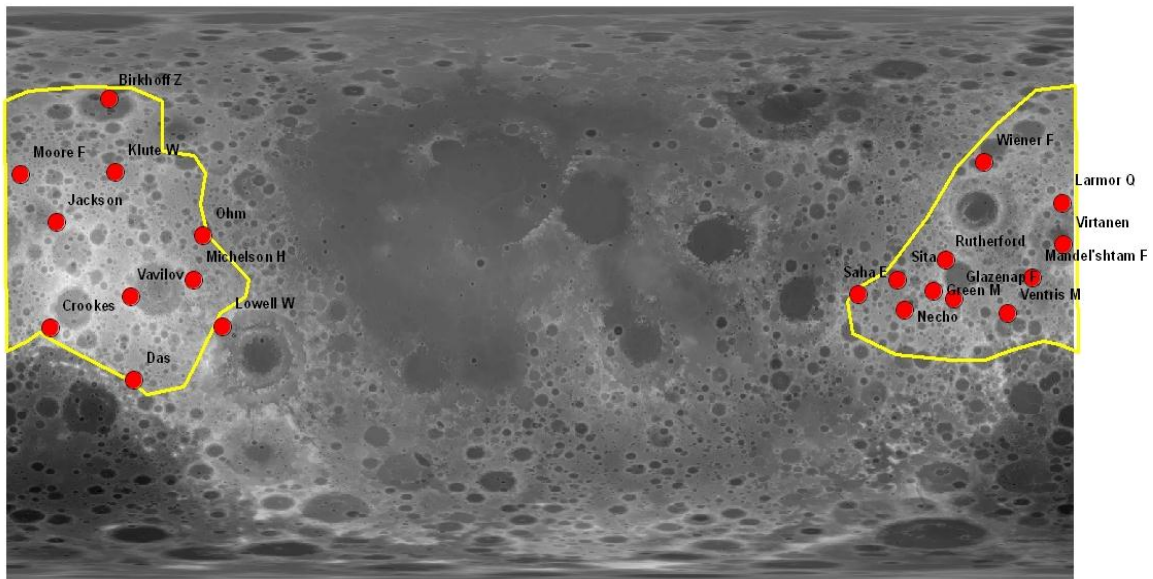


FIGURE 3.26 Map of fresh craters located within the 'typical highlands' (FHTa). Background: LOLA topography.

TABLE 3.5 List of fresh craters located within the FHTa highlands (*cf.* Fig. 3.26).

Name	Latitude (°N)	Longitude (°E)	Diameter (km)	Age
Das	-26.84	-137.01	38.00	Copernican
Crookes	-10.65	-165.20	49.00	Copernican
Lowell W	-10.00	-107.00	18.00	
Ventris M	-6.00	157.90	18.00	
Necho	-5.00	123.10	30.00	Copernican
Glazenap F	-1.50	139.70	11.00	
Vavilov	-0.80	-137.90	98.00	Copernican
Saha E	-0.20	107.60	28.00	
Green M	0.90	132.90	37.00	
Michelson H	4.60	-116.80	35.00	
Sita	4.60	120.80	2.00	
Mandel'shtam F	5.20	166.20	17.00	
Virtanen	15.50	176.70	44.00	Copernican
Ohm	18.40	-113.50	64.00	Copernican
Jackson	22.40	-163.10	71.00	Copernican
Larmor Q	28.60	176.20	22.00	
Moore F	37.40	-175.00	24.00	
Klute W	38.20	-143.00	13.00	Eratosthenian
Wiener F	41.20	150.00	47.00	Copernican
Rutherford	10.70	137.00	13.00	Copernican
Birkhoff Z	61.30	-145.30	30.00	Copernican

Possible sampling sites for lower crust and mantle are addressed in detail in Science Goal 3c, so that only the final map of Science Goal 3c is used here (Figs. 3.27 and 3.30). Lower crust and/or mantle materials can be sampled in crater ejecta or in central peaks or uplifted rings, if those are preserved (Fig. 3.28). An integrated list of all the potential sites to sample lower crust and/or mantle can be found in Table A3.2.

UrKREEP is generally expected where mantle is excavated, as this layer is located at the crust/mantle boundary. However, if this layer is not global (as suggested in previous parts of this section), one might not be able to sample urKREEP where it would be expected.

The core cannot be sampled anywhere on the lunar surface; it must be studied by geophysical means and is addressed as another Science Concept in the NRC report.

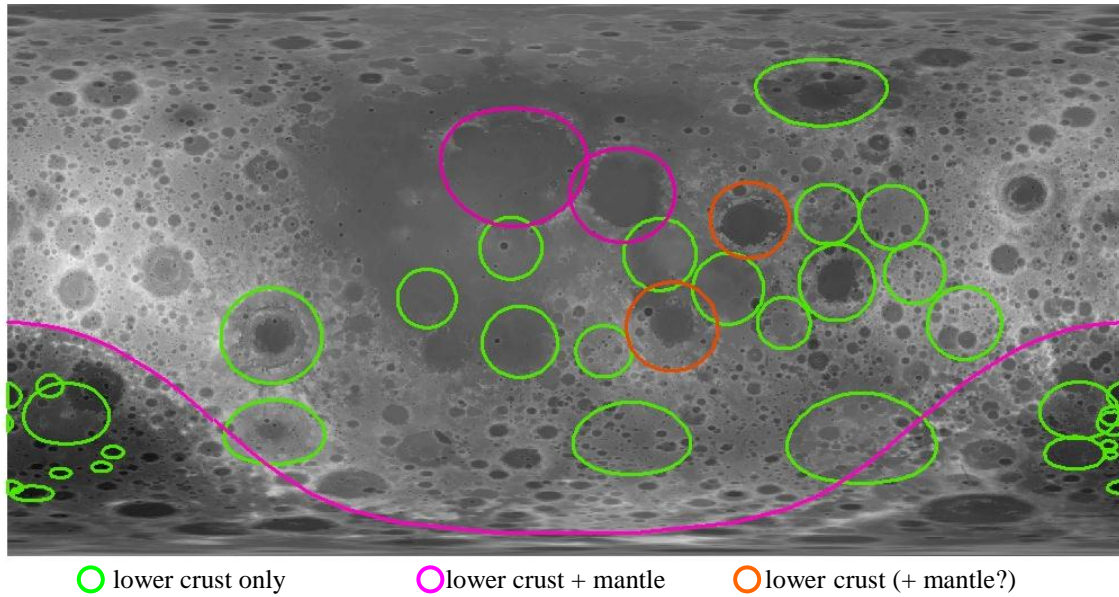


FIGURE 3.27 Map of all the craters that should have excavated lower crust and/or mantle in their ejecta. Green: lower crust only. Orange: lower crust and possibly mantle (within the 5 km error bar). Purple: lower crust and mantle. Background: LOLA topography.

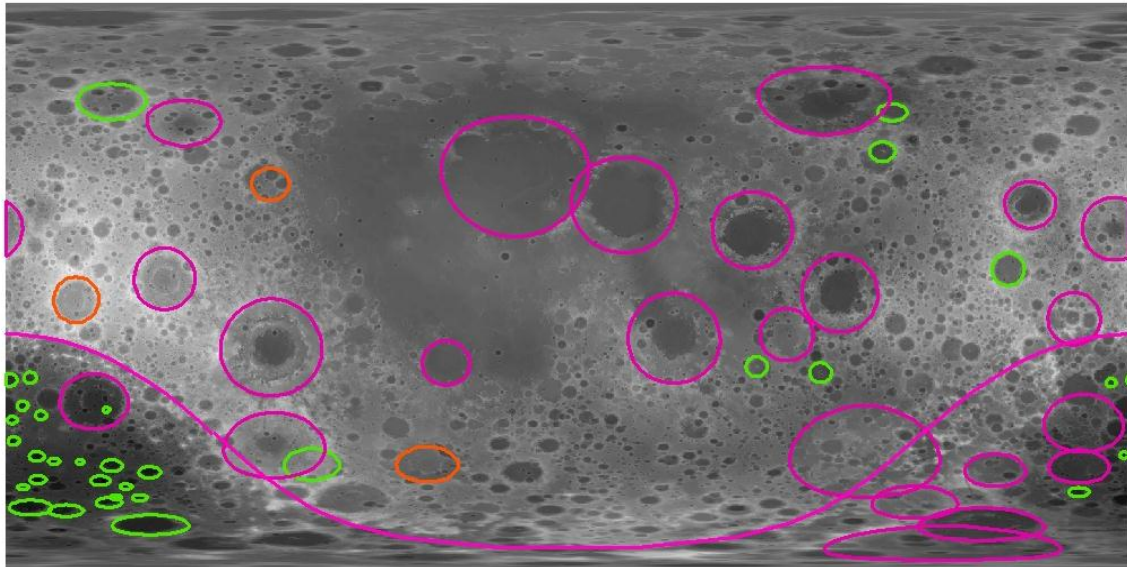


FIGURE 3.28 Map of all the craters that should have excavated lower crust and/or mantle in their central peaks or uplifted rings. Color code is the same as in Fig. 3.27, above.

Determining the best landing sites to assess the highland variety

Clementine and Lunar Prospector data suggest that the highlands can be divided into at least five types according to their composition (Chevrel *et al.*, 2002). There might be even more highland types based on different criteria like isotopic compositions but these can not be assessed with the currently available remote sensing data. Figure 3.29 shows the five types of highlands (H1 to H5) along with the Apollo (white stars) and Luna (purple stars) landing sites. Apollo and Luna highland samples come from H3 and H5 areas, whereas typical highlands areas seem to have a H1 or H2 composition. Therefore H1 and H2

sites, which might represent the most pristine anorthosite crust, should receive priority targeting, although samples from H4 sites would be useful as well .

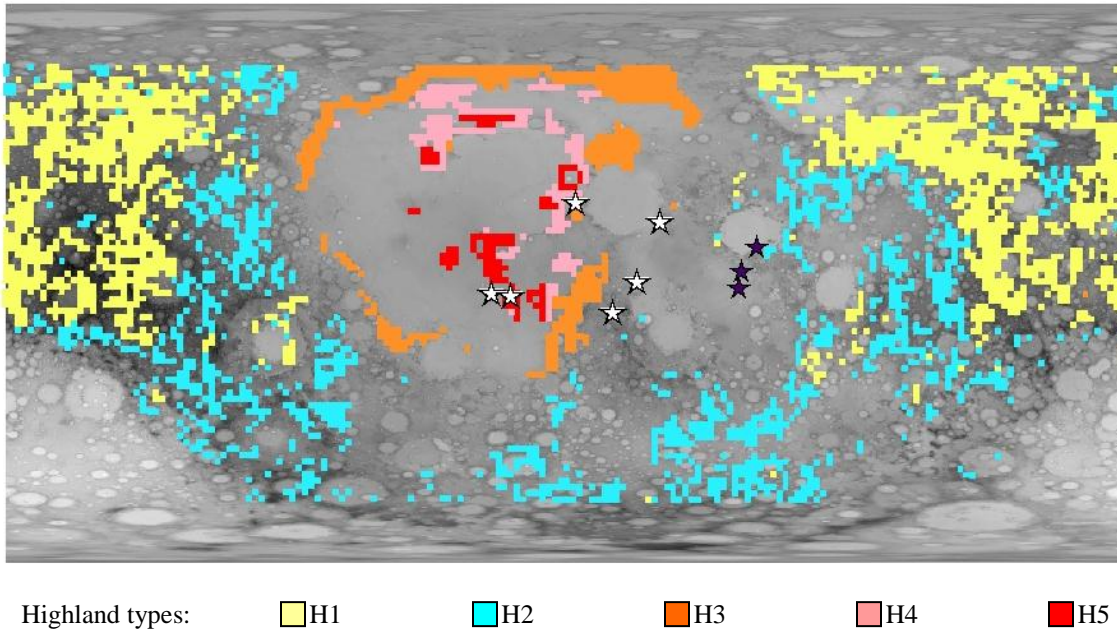
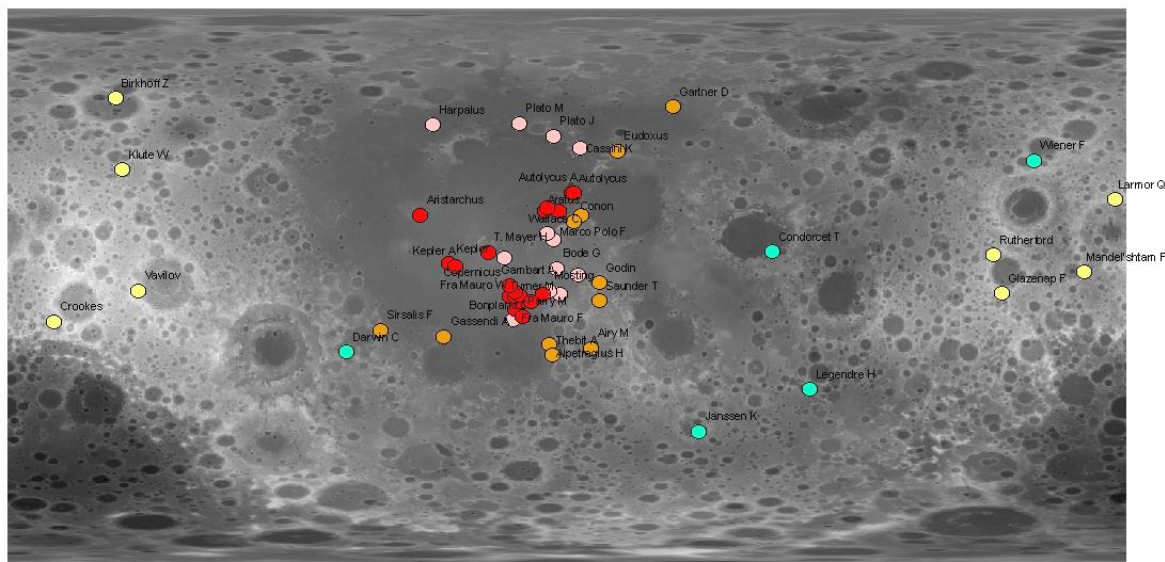


FIGURE 3.29 Chevrel *et al.* (2002) highland types map. Based on the Th, Fe and Ti compositions of the highland clasts and rocks in the Apollo collection, highlands were classified in 5 types (H1-H5), with H3 to H5 being Thorium-rich (KREEP-related). Background: LOLA topography.

Since the highlands are generally very old and have been superficially mixed, brecciated, and covered by regolith, careful selection of highland sample sites is required. Sites with fresh exposures of highland material are preferred; maps of young (*i.e.* Copernican) and rayed (bright rays are an indicator of young age) craters (courtesy of S. Werner, *DLR Berlin*) were projected on top of the highland variety map of Chevrel *et al.* (2002), and craters impacting different highland-type compositions were marked (Fig. 3.30). A list of these craters is provided in Table 3.6.



Craters that are impacting: ● H1 ● H2 ● H3 ● H4 ● H5

FIGURE 3.30 Map of fresh craters (Copernican or rayed) that are impacting one of the five highland types. Table 3.7 lists these craters along with important associated parameters. Colors are the same as those in Chevrel *et al.* (2002) and Fig. 3.29 just above. Background: LOLA topography.

TABLE 3.6 List of all the fresh craters (Copernican or rayed) that are impacting one of the five highland types H1 to H5 (*cf.* associated map in Fig. 3.30).

Name	Latitude (°N)	Longitude (°E)	Diameter (km)	Age	Highland type
Airy M	-19.20	7.60	1.00		H3
Alpetragius H	-18.00	-6.00	5.00		H3
Aratus	23.60	4.50	10.00		H3
Archimedes E	25.00	-7.20	3.00	Copernican	H5
Archimedes L	25.00	-2.60	4.00	Copernican	H5
Archimedes R	26.00	-6.60	4.00	Copernican	H5
Aristarchus	23.70	-47.40	40.00	Copernican	H5
Autolycus	30.70	1.50	39.00	Copernican	H5
Autolycus A	30.90	2.20	4.00	Copernican	H5
Birkhoff Z	61.30	-145.30	30.00	Copernican	H1
Bode G	6.40	-3.50	4.00		H4
Bonpland C	-10.20	-17.40	4.00		H4
Cassini K	45.20	4.10	4.00		H4
Condorcet T	11.80	65.80	15.00		H2
Conon	21.60	2.00	21.00	Copernican	H3
Copernicus	9.70	-20.10	93.00	Copernican	H4
Crookes	-10.65	-165.20	49.00	Copernican	H1
Darwin C	-20.50	-71.00	16.00		H2
Eudoxus	44.30	16.30	67.00	Copernican	H3
Flammarion A	-1.90	-2.50	4.00		H4
Fra Mauro F	-6.70	-16.90	3.00	Copernican	H5
Fra Mauro H	-4.10	-15.50	6.00	Copernican	H5

Name	Latitude (°N)	Longitude (°E)	Diameter (km)	Age	Highland type
Fra Mauro J	-2.60	-18.60	3.00	Copernican	H5
Fra Mauro K	-2.50	-16.70	6.00	Copernican	H5
Fra Mauro R	-2.20	-15.60	3.00	Copernican	H5
Fra Mauro W	-1.30	-16.80	4.00	Copernican	H5
Gambart A	1.00	-18.70	12.00	Copernican	H5
Gartner D	58.50	33.90	8.00		H3
Gassendi A	-15.50	-39.70	33.00	Copernican	H3
Glazenap F	-1.50	139.70	11.00		H1
Godin	1.80	10.20	34.00	Copernican	H3
Harpalus	52.60	-43.40	39.00	Copernican	H4
Janssen K	-46.10	42.30	16.00		H2
Kepler	8.10	-38.00	31.00	Copernican	H5
Kepler A	7.20	-36.10	11.00	Copernican	H5
Klute W	38.20	-143.00	13.00	Eratosthenian	H1
Larmor Q	28.60	176.20	22.00		H1
Legendre H	-32.50	78.10	7.00		H2
Mandel'shtam F	5.20	166.20	17.00		H1
Marco Polo F	15.70	-4.50	4.00		H4
Mosting	-0.70	-5.90	24.00	Copernican	H4
Mosting C	-1.80	-8.00	4.00		H5
Parry M	-8.90	-14.50	26.00	Copernican	H5
Plato J	49.00	-4.60	8.00		H4
Plato M	53.10	-15.40	8.00		H4
Rutherford	10.70	137.00	13.00	Copernican	H1
Saunder T	-4.00	10.40	6.00		H3
Sirsalis F	-13.50	-60.10	13.00		H3
T. Mayer H	11.70	-25.50	3.00		H5
Thebit A	-21.50	-4.90	20.00	Copernican	H3
Triesnecker	4.20	3.60	26.00	Copernican	H4
Turner M	-4.20	-11.80	4.00	Copernican	H5
Vavilov	-0.80	-137.90	98.00	Copernican	H1
Wallace C	17.60	-6.40	5.00		H4
Wiener F	41.20	150.00	47.00	Copernican	H2

Determining the best landing sites to find representative samples of the three main geochemical terranes

A map of the three main terranes was generated based on criteria defined by Joliff *et al.* (2000) (Fig. 3.31):

- The PKT area is circled by the Thorium 3.5 ppm contour line;
- The SPAT area has Fe abundances larger than 5% wt (up to 8 % wt in the inner SPAT);
- The FHT is divided in 2 areas: the FHTa, which correspond to the farside 'highlands', where the crust is thicker than 70 km, and the FHTb which correspond to everything outside all of the previous defined terranes.

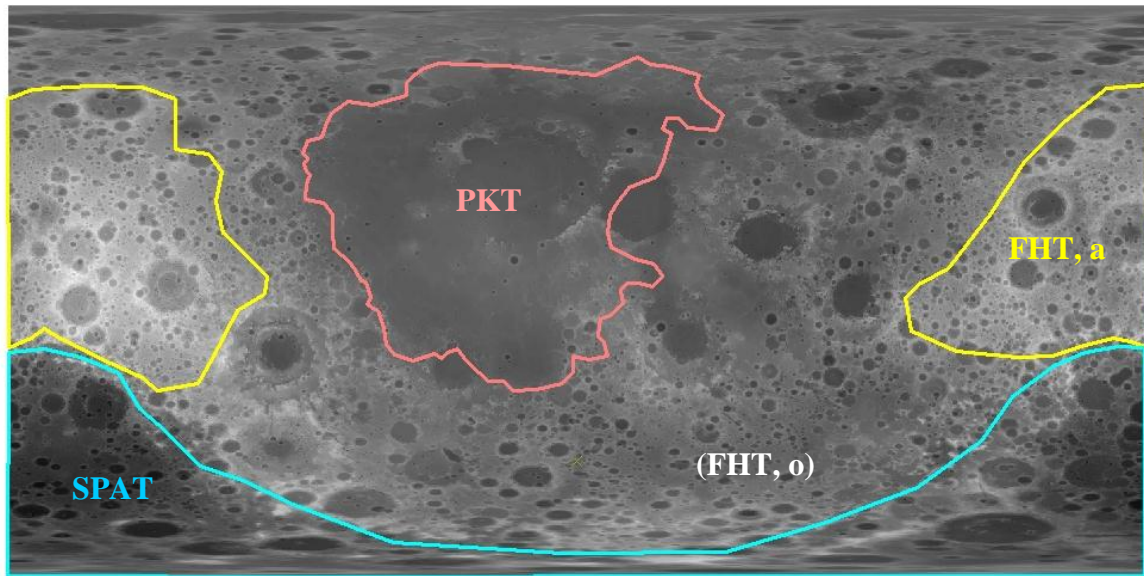


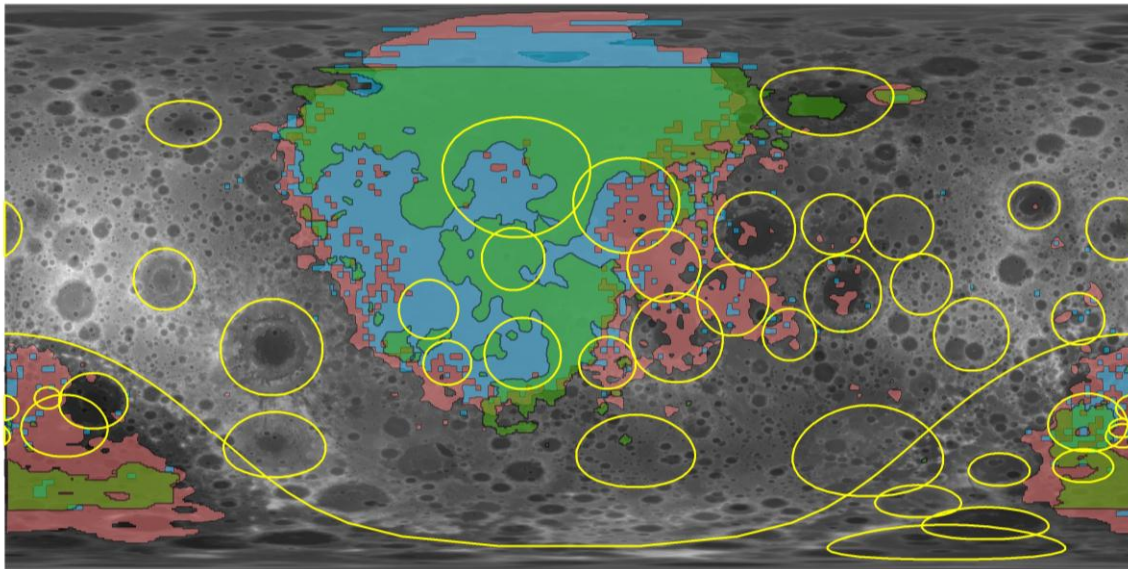
FIGURE 3.31 Map of the 3 main geochemical terranes defined by Jolliff *et al.* (2002). Any place located within these 3 distinct regions is a possible landing site to fulfill this requirement. Samples for the 3 terranes are required, implying multiple landings.

Ideally, we would like representative samples from each of the individual terranes, so this requirement can be fulfilled by landing anywhere within the three distinct provinces.

Determining the best landing sites to find representative samples of KREEP and assess its global extent

Utilizing the ‘bottom-up’ method of exploring the extent of the KREEP layer, we identify areas indicating impact excavation or melting of mantle material, and therefore possible urKREEP sampling. In Fig. 3.32, the yellow lines depict craters or basins that would likely excavate material from a global urKREEP layer in their melt or central peak. Interestingly, not all of these features show KREEP signatures, suggesting possible heterogeneity of the urKREEP layer. Note that mantle (and thus urKREEP) material could also be found in the ejecta of Imbrium and Serenitatis basins, but since they are located in the PKT, it might be hard to distinguish urKREEP from KREEP basalt.

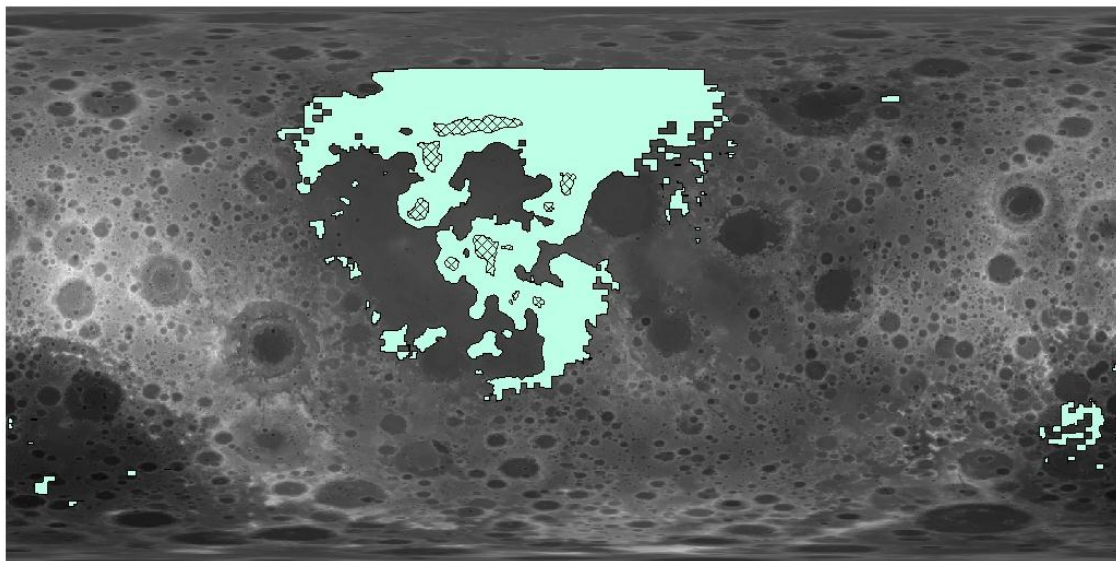
Utilizing the ‘top-down’ method of analyzing geochemical data, we combine contour maps of incompatible elemental abundance associated with KREEP to distinguish where to find the best samples. Figure 3.33 presents these KREEP-rich regions. Note that the low resolution of these data do not suggest specific sites on a small scale, but large-scale KREEPy regions of interest. For this reason, it is suggested that any site located within the boundaries of the contours should be considered for sampling high KREEP material. Of particular interest may be anomalous regions located outside of the PKT (*e.g.*, the northern rim of Compton crater; Antoniadi crater in SPAT).



Legend

- Craters sampling mantle (therefore possibly urKREEP)
- Th > 2.2 ppm
- Sm > 49 ppm
- K > 1000 ppm

FIGURE 3.34 Distribution of craters sampling a hypothetical global urKREEP layer, compared to contours depicting enriched abundances of thorium, potassium, and samarium. Background: LOLA topography.



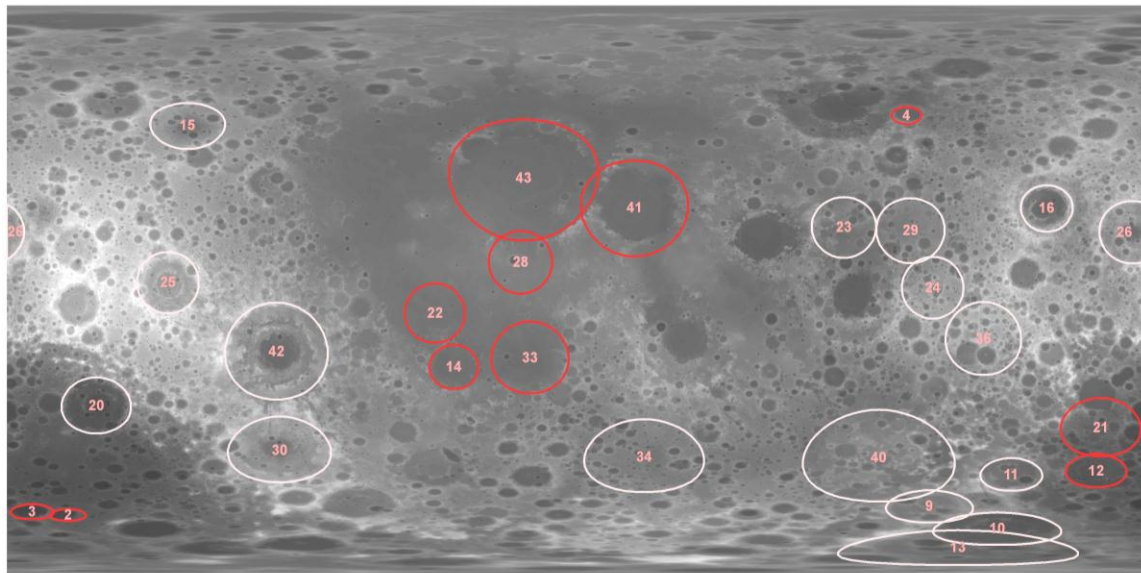
Legend

- High enrichment of Th, Sm, K
- Elevated abundance of Th, Sm, K

FIGURE 3.35 Combined elemental abundance maps of thorium, samarium, and potassium. Areas in cross-hatch correspond to regions of high enrichment for all three elements. This map conveys areas of especially KREEP-rich material. Background: LOLA topography.

High KREEP areas have been determined through a combination of these ‘top-down’ and ‘bottom-up’ methods. These regions, marked in bright red in Fig. 3.34, could provide representative samples of KREEP material, possibly even pristine samples of urKREEP. Included in Fig. 3.34 are some geochemically anomalous regions, specifically the Compton crater region in the northern hemisphere and Antoniadi and

Numerov craters in the South Pole-Aitken basin. Areas marked in light pink do not show incompatible-rich material in the superficial layer, yet are thought to sample mantle material.



Legend

KREEP

	high
	low

FIGURE 3.34 Global map showing regions of interest for determining the lateral and vertical extent of KREEP. Not included are sites that show inconclusive geochemical signatures. Background: LOLA topography. Table

TABLE 3.7 Craters of interest which provide essential information regarding KREEP, associated with Fig. 3.34.

ID	Name	Latitude (°N)	Longitude (°E)	Diameter (km)	KREEP	Age
2	Numerov	-70.7	-160.7	113	high	Nectarian
3	Antoniadi	-69.7	-172	143	high	Upper Imbrian
4	Compton	55.3	103.8	162	high	Lower Imbrian
9	Sikorsky-Rittenhouse	-68	111	310	low	Nectarian
10	Schrodinger	-75	132.4	312	low	Lower Imbrian
11	Planck	-57.9	136.8	314	low	Pre-Nectarian
12	Poincare	-56.7	163.6	319	high	Pre-Nectarian
13	Amundsen-Ganswindt	-81	120	335	low	Pre-Nectarian
14	Humorum	-24	-39	425	high	Nectarian
15	Coulomb-Sarton	52	-123	440	low	Pre-Nectarian
16	Moscoviense	26	148	445	low	Nectarian
20	Apollo	-36.1	-151.8	537	low	Pre-Nectarian
21	Ingenii	-43	165	560	high	Pre-Nectarian
22	Flamsteed-Billy	-7	-45	570	high	Pre-Nectarian
23	Marginis	20	84	580	low	Pre-Nectarian
24	Al-Khwarizmi-King	1	112	590	low	Pre-Nectarian
25	Hertzprung	2.6	-129.2	591	low	Nectarian

ID	Name	Latitude (°N)	Longitude (°E)	Diameter (km)	KREEP	Age
26	Freundlich-Sharonov	18.5	175	600	low	Pre-Nectarian
28	Insularum	9	-18	600	high	Pre-Nectarian
29	Lomonosov-Fleming	19	105	620	low	Pre-Nectarian
30	Mendel-Rydberg	-50	-94	630	low	Nectarian
33	Nubium	-21	-15	690	high	Pre-Nectarian
34	Mutus-Vlacq	-52	21	700	low	Pre-Nectarian
36	Tsiolkovsky-Stark	-15	128	700	low	Pre-Nectarian
40	Australe	-52	95	880	low	Pre-Nectarian
41	Serenitatis	26	18	920	high	Nectarian
42	Oriente	-19	-95	930	low	Lower Imbrian
43	Imbrium	35	-17	1160	high	Lower Imbrian

Integrated list of all the suggested landing sites for Goal 3A in general

Candidate sites can be combined to determine the best places to achieve the entire Science Goal 3a. Figure 3.35 shows a map of the 227 proposed landing sites for Science Goal 3a. An integrated list of all the landing sites determined for each of the requirements is presented in Table A3.3. Priority sites are those where 3 out of the 4 previous requirements can be achieved. There is no one single site where all the Science Goal 3a requirements could be completed, so multiple landing sites are required.

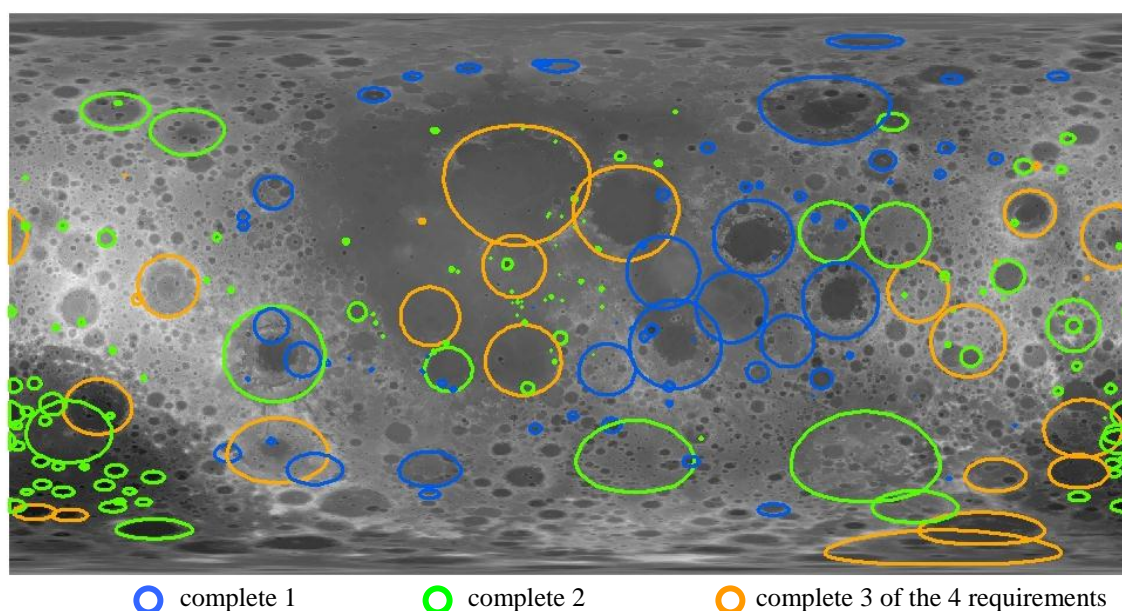


FIGURE 3.35 Map of all the craters or basins where Science Goal 3a could be addressed. The color scale indicates how many of the requirements defined for Science Goal 3a could be completed at this location. Due to the scale, the figure does not show well the much smaller rayed craters.

SCIENCE GOAL 3B: INVENTORY THE VARIETY, AGE, DISTRIBUTION, AND ORIGIN OF LUNAR ROCK TYPES

Introduction

The current understanding of the formation and evolution of the Moon is framed by the lunar magma ocean (LMO) hypothesis, a concept developed on the basis of Apollo samples studies (*cf.* Science Goal 3a). However, new insight provided by geophysical, remote sensing, and especially sample analyses since the Apollo era shows that the lunar crust exposed at the surface varies in composition, age, and mode of emplacement, a fact that the LMO cannot account for. The Apollo samples, which originate from a limited surface area of the Moon, reveal a variety of rock types. Some of these rocks were expected (such as basalts), and some varieties were unexpected (the occurrence of granites, for instance). Moreover, some hypothesized types of rocks are not even in the sample collection yet, such as pristine anorthositic crust, urKREEP, or mantle material. In addition, there may exist some smaller regions containing unique materials that can be of great interest to science and in-situ resource utilization, but have not been identified or sampled yet (*i.e.* the recent discovery of spinel-rich outcrops by M³). Compiling a database of all the lunar rock types and their ages is crucial to understand the history and evolution of the Moon.

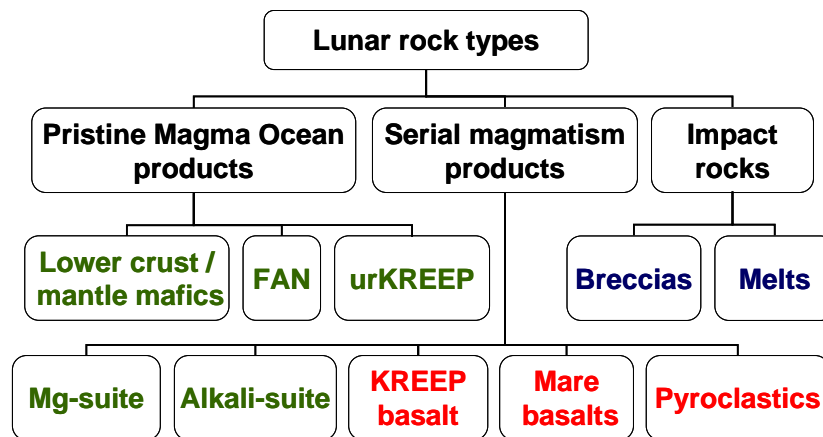


FIGURE 3.36 Global overview of the lunar rock types. Green font corresponds to plutonic rocks, red font to volcanic rocks, and blue font to impact rocks.

As discussed below, the lunar crust can schematically be divided into crustal and plutonic rocks (ferroan anorthosites [FAN], magnesian suite, alkali suite, KREEP, and mafic rocks of the lower crust and mantle), volcanic rocks, and more complex structures like breccias and regolith. The lunar surface is traditionally spatially divided into three different geological crustal provinces that have been defined using maps of Th, Fe and Ti (PKT, FHT and SPAT, *cf.* Science Goal 3a). But the more precise the available data, the more complex this view becomes. Even though Science Goal 3B could be addressed virtually everywhere on the lunar surface that has not yet been sampled, the integration of all the available data (*e.g.*, elemental maps, crater excavation depths, volcanic features), can help assess places where multiple rock types, or high scientific interest ones (*e.g.*, granites), could be sampled.

Background

Crustal and plutonic rocks

Lower crust and mantle mafic-rich rocks, ferroan anorthosite, and urKREEP: The formation and background of these types of igneous rocks are described in detail in Science Goals 3a and 3c of this report, and therefore will not be discussed further here, although these rock types will be taken into account for landing site selection in this section.

Magnesian suite rocks: The earliest evolution of the Moon likely included the formation of a magma ocean and the subsequent development of anorthositic flotation cumulates. This primitive crust was then intruded by mafic magmas which crystallized to form the lunar highlands magnesian suite (Mg-suite)

(Snyder *et al.*, 1995a). These plutonic rocks exhibit a range of compositions that include dunites, troctolites, norites, and gabbronorites. A distinguishing characteristic of this suite is that they contain some of the most magnesium-rich phases that had crystallized from lunar magmas, yet they also are significantly enriched in KREEP (Shearer and Papike, 2005).

Dating of Mg-suite rocks from lunar samples shows a partial overlap of the Mg-suite rocks ages with those of the FAN rocks, implying that they formed during or early after the formation of crust from the magma ocean, and not necessarily as later remelting and intrusion events into an already solid ferroan-anorthositic crust. The global distribution of Mg-suite intrusives within the crust is not known yet, although they appear to have depths of origin deeper than 20 km (Wieczorek *et al.*, 2006) (*i.e.*, they are expected to be found in the lower crust).

These Mg-suite rocks can also be mapped using remote sensing data. A study of rock types exposed in the central peaks of large craters (Tompkins and Pieters, 1999) allowed the detection of gabbro, norite, troctolite, gabbronorite, anorthositic troctolite, anorthositic gabbro, and anorthositic gabbronorite, which were inferred to be Mg-suite lithologies from known rock type samples (Shearer *et al.*, 2006). However, the presence of pyroxene or olivine-rich material (especially norite and dunite) could also be indicative of the lower crust material that was brought to the surface by the impact. As Mg-suite rocks and lower crust rocks can have similar mineralogical composition, it is difficult to distinguish between them with spectroscopic data only. With the exception of places with troctolite detections that are diagnostic of these Mg-suite rocks, or places where the high resolution observations show clear intrusive contacts, the distribution of Mg-suite plutons cannot be determined with certainty. Isotopic measurements could be used to distinguish between Mg-suite and lower crust rocks, but this cannot be done in-situ, implying that samples would have to be brought back to Earth.

Recent studies coupling the Mg-suite to KREEP-rich parent magmas make it likely that their primary occurrence is controlled by the early distribution of KREEP, which appears to be concentrated in the regions of Mare Imbrium and Oceanus Procellarum. It is still uncertain whether Mg-suite rocks are special products of the PKT or if they represent plutonic activity throughout the lunar crust. In this regard, sampling craters that should have excavated lower crust materials (Fig. 3.37) would be a key test of the global distribution of Mg-suite rocks, and could help to better understand their petrogenetic relationship to latter stages of lunar magmatism (mare basalts) that still remains obscure.

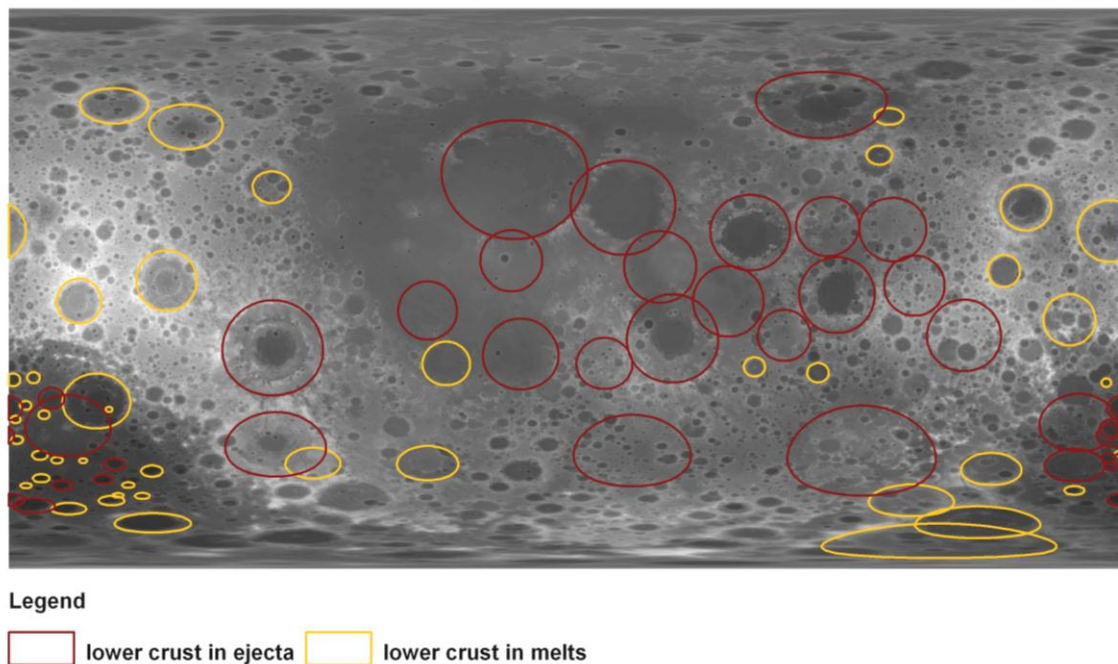


FIGURE 3.37 Map showing craters whose ejecta and melts should contain lower crust materials. Background: LOLA topography.

Alkali Suite: The alkali suite comprises a variety of assemblages including sodium-rich norites, gabbros, gabbro-norites, alkali anorthosites, quartz monzodiorites, and granites. It is surprising to find granite on the Moon as the presence of highly differentiated silica-rich magma there was not expected. Granites are rare in the Apollo samples and occur mainly as small rock fragments or clasts in impact breccias. Nevertheless, their presence reveals that the Moon has a much more complex geology than expected.

Sample analyses points toward a relationship between KREEP basalt and members of the magnesian and alkali suites (Snyder *et al.*, 1995b), as the trend among the mineral compositions of these rock types suggests that fractional crystallization of a KREEP basalt-like magma could produce both the Mg- and alkali suite rocks. Mineral compositions and textures of members of the alkali suite appear consistent with a rapid cooling associated with shallow emplacement and crystallization (Jolliff *et al.*, 1999), within one or two kilometers of the surface. The extent and distribution of the alkali suite remains unknown, though Lunar Prospector results suggest a general confinement of concentrations of these materials to the PKT. Whether the alkali suite rocks form extensive outcrops (*e.g.*, domes and other volcanic constructs observed in parts of Oceanus Procellarum), are exposed by impacts such as Aristarchus (*e.g.*, Chevrel *et al.*, 1999; Hagerty *et al.*, 2006), or are separate intrusive bodies remains to be determined.

Thus, sampling crater materials that have been excavated from the lower and upper crust could help better constrain the alkali suite locations, both horizontally and vertically. Excavated material from the shallow crust may be done virtually at any crater site (excavated depth of at least 2 km to penetrate the regolith), and craters that might have excavated deeper in the lower crust are presented in Fig. 3.37.

Volcanic rocks

KREEP basalts: A detailed description of KREEP formation and background is presented in Science Goal 3a.

Mare basalts: Mare basalts are large, dark basaltic plains that are observed often within large impact structures on the Moon. They are thought to be formed by ancient volcanism. Lunar mare basalts cover about 17% of the lunar surface, the majority of which being exposed on the lunar nearside. They also occur, although spatially less extensively, on the lunar farside. Basaltic mare materials show variations in terms of age, chemical and isotopic composition (*e.g.*, titanium content), and mineralogy.

Figure 3.38 shows the latest results for mare dating, which highlights the fact that lunar volcanism was active over a long period of time, starting at ~4 Ga and ending at ~1.1 Ga (Hiesinger *et al.*, 2008). Sampling the youngest and oldest mare basalts within the PKT is needed to understand how volcanic processes varied as a function of time within this terrane. The youngest basalts are located in Oceanus Procellarum, in the vicinity of the Aristarchus Plateau, while very old mare basalts are preferentially located within Mare Tranquillitatis, Mare Australe, Mare Marginis, Mare Humboldtianum, Mare Orientale and Mare Humorum.

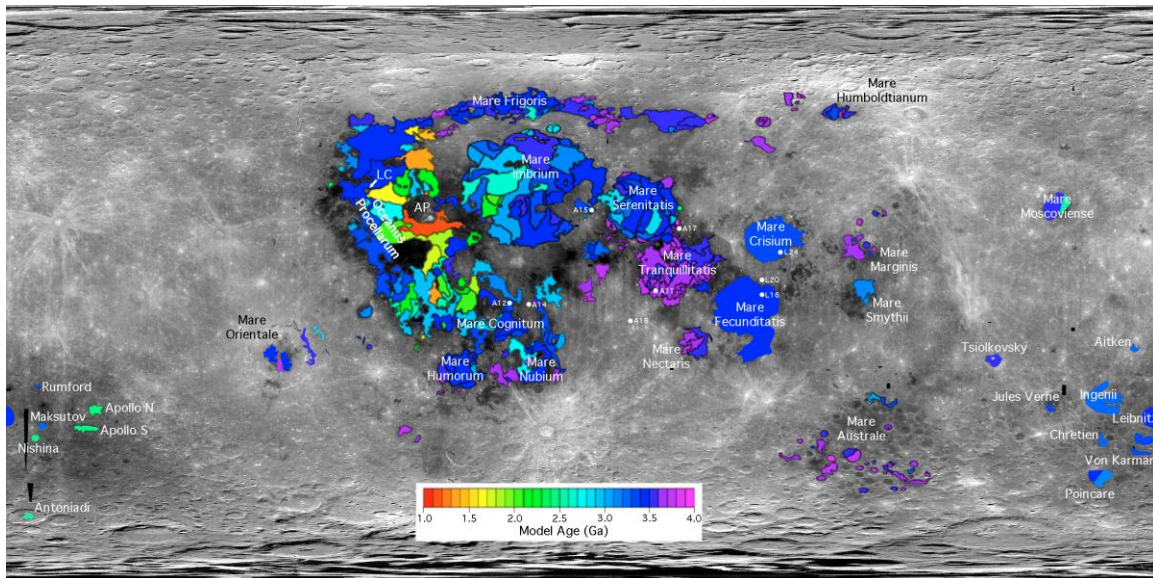
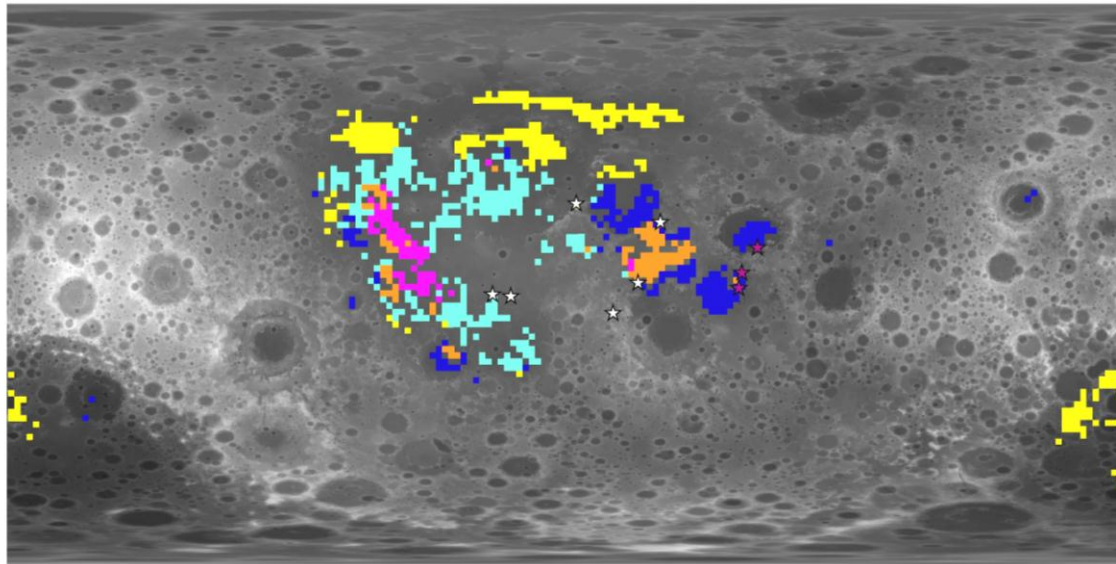


FIGURE 3.38 Estimated surface ages of mare basalts based on crater counts (map compiled using the data of Tyrie, 1988; Greeley *et al.*, 1993; Neukum and Ivanov, 1994; Hiesinger *et al.*, 2000, 2003, 2006, 2008; Haruyama *et al.*, 2009).

The integration of maps of thorium, iron, and titanium that helped define the three main lunar terranes (FHT, PKT and SPAT) led to a more precise subdivision of these terranes and relates them to specific types of rocks (Chevrel *et al.*, 2002). Figure 3.39 shows the spatial extent of five types of mare materials (M1 to M5), whose compositions in Fe, Ti and Th are presented in Table 3.8, along with the Apollo and Luna landing sites. M1 and M2 are high-Ti mare basalts, with different Th content, while M3 and M4 units are less rich in Ti, again with different Th content. M5 is the only unit with very low Ti levels, and the lowest Fe content as well. Mare rocks gathered during the Luna and Apollo missions sample mainly M1, M3, and M4 types, although this evaluation remains quite imprecise. M2 and M5 types are clearly lacking in the sample collection, and sampling and analyzing them would greatly improve our knowledge on the variety of mare rock types.

TABLE 3.8 Ranges of concentration in Fe, Ti, and Th for the mare units presented in Fig. 3.39 (From Chevrel *et al.*, 2002)

Mare unit	Fe, wt % (mean)	Ti, wt% (mean)	Th, ppm (mean)
M1 (orange)	14.5–15.3 (14.9)	6.0–7.0 (6.5)	2.0–3.0 (2.5)
M2 (violet)	14.9–15.7 (15.3)	5.8–6.8 (6.3)	3.2–4.2 (3.7)
M3 (light blue)	13.5–14.7 (14.1)	3.0–4.0 (3.5)	3.4–4.6 (4.0)
M4 (dark blue)	12.6–14.4 (13.5)	3.0–4.0 (3.5)	1.6–2.4 (2.0)
M5 (yellow)	10.3–12.5 (11.4)	0.3–0.9 (0.6)	2.8–3.8 (3.3)



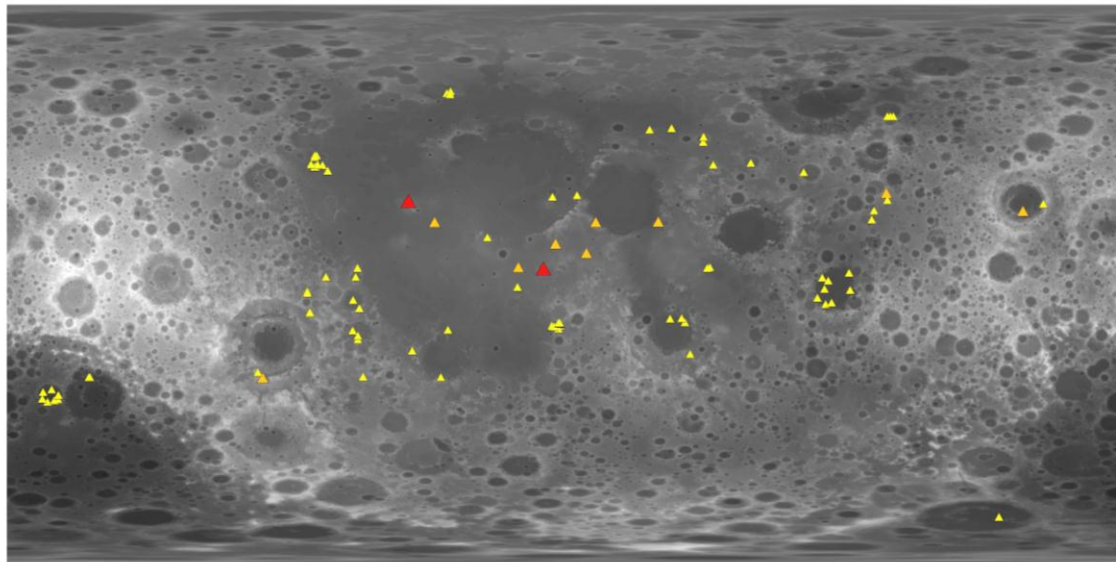
Legend

■ M5
 ■ M3
 ■ M4
 ■ M2
 ■ M1
 ☆ Apollo landing site
 ☆ Luna landing site

FIGURE 3.39 Mare units determined using a multi-element principal component analysis applied to the Fe and Ti (CSR) and Th (GRS) datasets (adapted from Chevrel *et al.*, 2002). Background: LOLA topography.

Pyroclastic deposits: Pyroclastic deposits and cryptomare formation are detailed in the Science Concept 5, and so only the different lithologies that are related to these volcanic processes will be addressed here, with very few details on their morphology.

Volcanic glasses are formed during “fire-fountain” eruptions that leave pyroclastic deposits made up of glass droplets (quenched iron-bearing glass and crystallized beads with volatile-element coatings) that have chilled from the spray of molten lava (Lucey *et al.*, 2006). Pyroclastics provide precious clues on mantle reservoir origin and the type and extent of lunar volcanism. Most of lunar pyroclastic deposits are of late Imbrian age, generally 3.2 to 3.7 Ga, corresponding to the age of the peak period of ancient lunar volcanism (Gaddis *et al.*, 2003). Figure 3.40 and Table A3.5 shows that pyroclastic deposits are widely distributed on the whole surface of the Moon, and that they can greatly differ, in terms of both spatial extent (from 1 km² to 49,000 km²) and composition (Fe- and Ti-rich with black beads; Ti-rich with black and orange beads; Fe rich and lower Ti content). An illustration of these deposits is presented in Fig. 3.41.



Legend

Pyroclastic deposits ▲ 2 - 3000 km² ▲ 3001 - 10000 km² ▲ 10001 - 37400 km²

FIGURE 3.40 Map of pyroclastic deposits from the USGS Lunar Pyroclastic Volcanism Project (Lisa R. Gaddis *et al.*, 2008) and additional sources (Giguere *et al.* 2003, 2007; Sunshine *et al.* 2010). Background: LOLA topography.

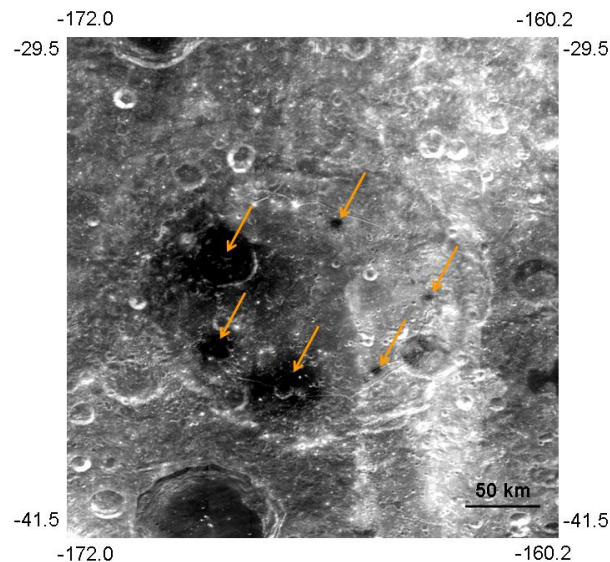


FIGURE 3.41 Example of pyroclastic deposits of various extents in Oppenheimer crater (USGS 750 nm filter Clementine basemap); orange arrows point to the 6 deposits that have been detected in this area (*cf.* Table A3.5).

Cryptomare basalts: The oldest mare basalts on the lunar surface are widely considered to be the buried mare basalt termed “cryptomare” (*e.g.*, Schultz and Spudis, 1979; Antonenko *et al.*, 1995), which refer to mare-like volcanic deposits that have been obscured from view by subsequent emplacement of material of higher albedo, commonly ejecta from craters and basins (thus primarily detected by the presence of dark-haloed craters – Fig. 3.42). Evidence for the old age of cryptomare is mostly in the form of stratigraphic relationships, as many cryptomaria are suspected to lie beneath material as old as pre-Nectarian in age (Hawke *et al.*, 2005b). Cryptomare basalts have not been sampled yet, though the lunar meteorite Kalahari

009 has been interpreted to be a sample of cryptomare. Kalahari 009 has been radiometrically dated at ~4.35 Ga and shows extremely low abundances of incompatible elements such as thorium and the rare earth elements (Terada *et al.*, 2007). Cryptomaria are interesting places to sample as they might represent the oldest mare basalts on the Moon, and could bring information on the early mantle and volcanism, and their evolution.

Figure 3.43 shows the distribution of dark-haloed impact craters larger than 1 km in diameter determined by Schultz and Spudis (1979), and the locations where cryptomaria areas have been detected (Bell and Hawke, 1984; Pieters *et al.*, 2001a, 2001b; Antonenko 1999; Antonenko and Yingst, 2002; Hawke *et al.* 2003, 2005a, 2005b; Giguere *et al.*, 2003, 2007; Campbell *et al.* 2005, *cf.* Appendix B3 for details). It should be noted that both the dark-haloed craters and the cryptomare presented here do not constitute a comprehensive list, as many potential cryptomare sites may still be unidentified (Antonenko *et al.*, 1999). Apart from the cryptomare mapped in the regions of Lomonosov-Fleming, Balmer-Kapteyn, Schiller-Schickard, SPA, and the South-West margin of Procellarum, which have been studied in detail, all the other contours are very imprecise and should only be taken as approximate locations of cryptomare. Figure 3.43 also maps the units that have been interpreted as being mixtures between highlands and mare materials by Chevrel *et al.* (2002), with 6.6–7.8 wt% in Fe, 0.15–0.35 wt% in Ti and 1.1–1.5 ppm in Th. Their locations correspond mostly to otherwise detected cryptomare deposits, and thus add evidence to their presence in these parts of the Moon.

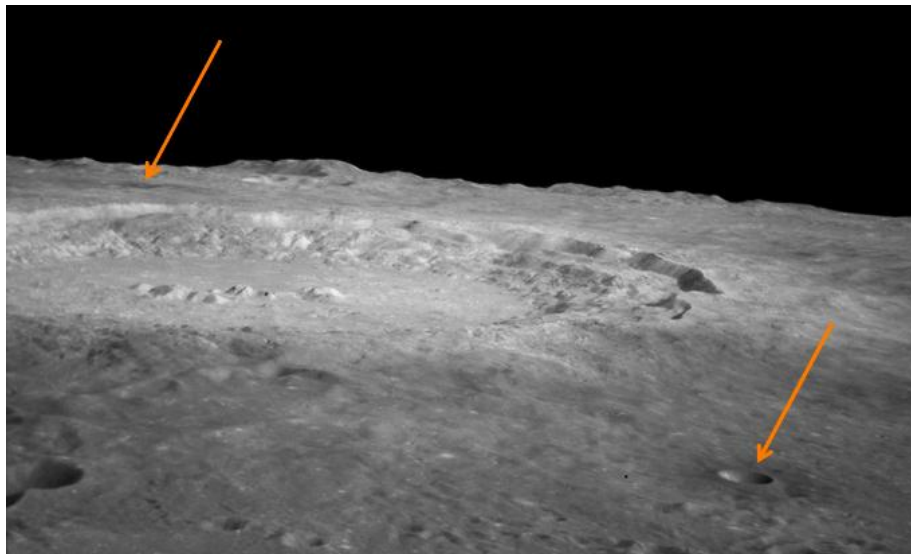
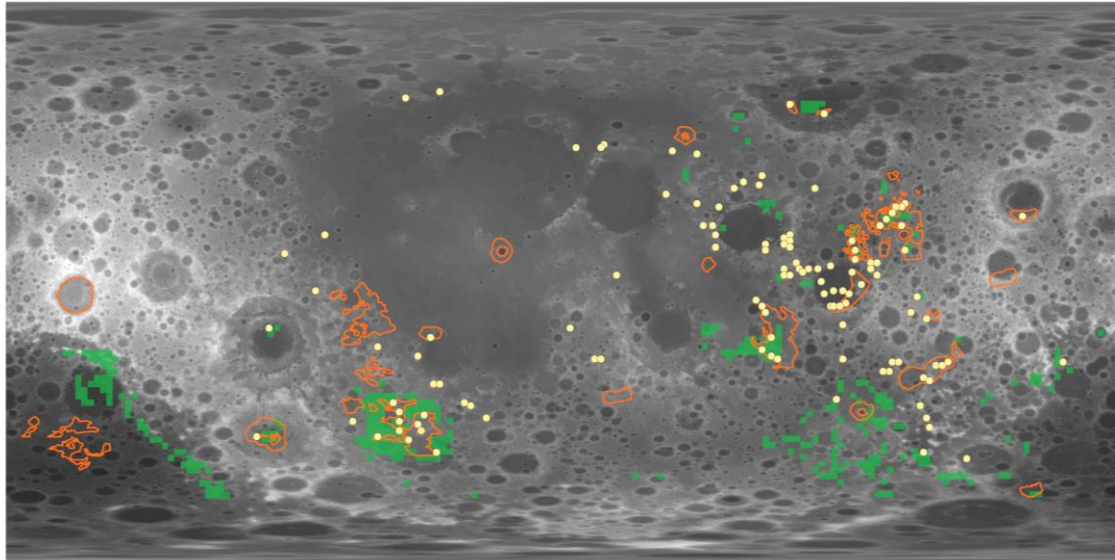


FIGURE 3.42 Oblique view of Copernicus crater (93 km in diameter) from the south (Apollo 12 photo AS12-52-7738). Yellow arrows indicate two dark-haloed craters: Copernicus H (4.6 km in diameter) on the right and a nameless crater north of Copernicus on the left (Bell and Hawke, 1984).



Legend

• dark-haloed impact craters cryptomare highland / mare mixed material

FIGURE 3.43 General distribution of dark-haloed impact craters larger than 1 km in diameter determined by Schultz and Spudis (1979), and the locations where cryptomaria areas have been detected (Bell and Hawke, 1984; Pieters, 2001; Antonenko 1999; Antonenko and Yingst, 2002; Hawke *et al.* 2003, 2005a, 2005b; Giguere *et al.*, 2003, 2007; Campbell *et al.* 2005). Green areas represent mixed mare and highland materials (Chevrel *et al.*, 2002). Background: LOLA topography.

Impact rocks – breccias

Breccias are the most abundant rock types found within a crater area and comprise the majority of Apollo samples. These are rocks composed of pieces from older rocks that were disaggregated or melted by meteoroid impacts. They can exist as rock fragments, crystallized impact melts or glassy impact melts, and most contain fragments from many different older rocks (Fig. 3.44). Figure 3.45 illustrates where the different types of breccias would occur in an impact structure.

Regolith breccias are composed of regolith that was lithified by shock compaction or heating. They generally contain glass spherules and agglutinates that can only be produced or acquired at or above the lunar surface. As they may be formed in any regolith, they display a wide range of compositions. Their main interests lie in the facts that (1) they are fossil regolith that at some point became closed to further input of material, so that some may represent very ancient regolith and provide information about condition in the past, and (2) since they are polymict rocks consisting of soil, their compositions are more likely to represent the average composition of the surface upon which they formed (Lucey *et al.*, 2006).

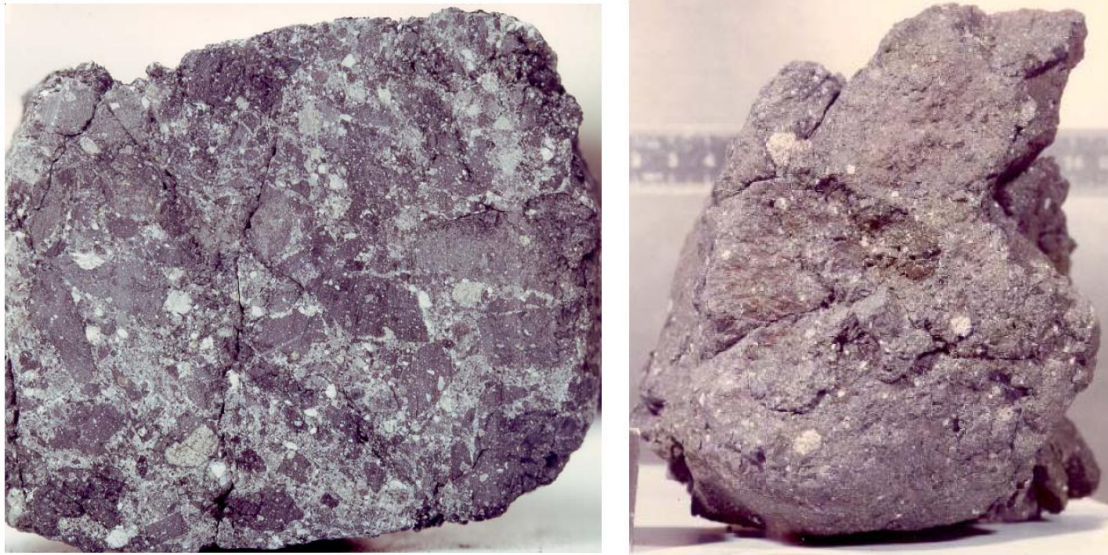


FIGURE 3.44 Examples of a polymict breccia on the left (sawn surface of sample 14306,21, about 6 cm across, NASA # S77-22103) and a regolith breccia on the right (sample 15299,0, the scale in background is in cm, NASA # S74-32566).

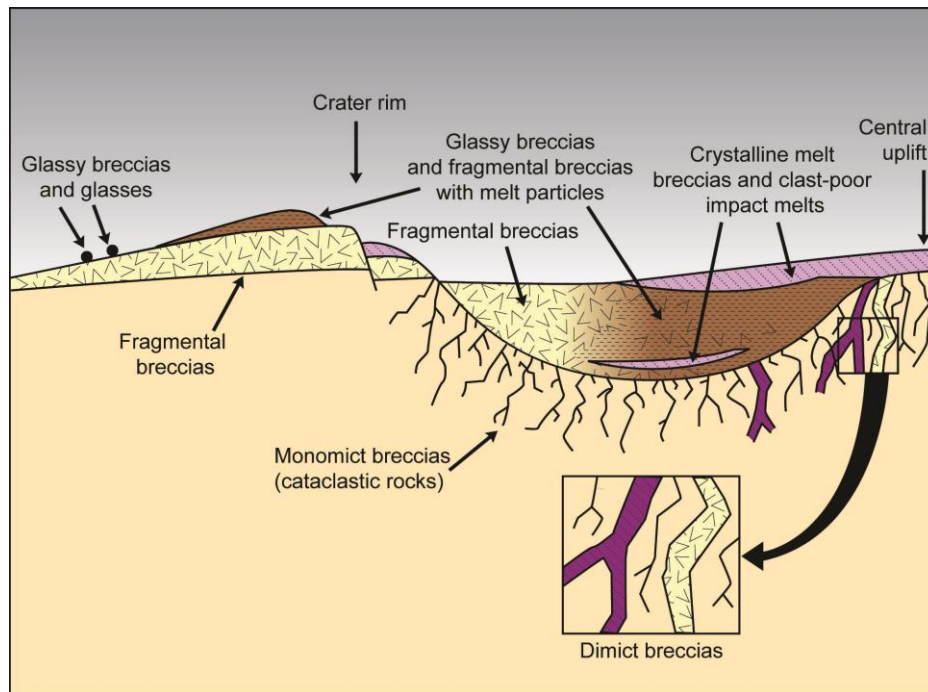


FIGURE 3.45 Cross-section of an ideal lunar crater showing the relationship of different breccia types to the geological environment of the crater. Regolith breccias and granulitic breccias are not indicated for clarity (adapted from Stöffler, 1981).

Granulitic breccias and granulites are commonly found as clasts in breccias, including lunar meteorite fragmental and regolith breccias, which reflects their common and widespread occurrence on the lunar surface (Korotev and Jolliff, 2001). Their textures suggest heating and recrystallization, and composition as well as shock features in some indicate a relationship to impact processes. Granulitic lithologies have radiometric ages ranging from 3.75 to slightly older than 4.2 Ga (Hiesinger *et al.*, 2006 and references

therein), average compositions which cover a relatively restricted range (such as high Al_2O_3 and low FeO), and extremely low incompatible element concentrations. The most common interpretation of these compositions is that they represent upper-crustal materials uncontaminated by the excavation of KREEP-rich materials from the Procellarum KREEP Terrane, and thus the formation of most of these rocks appears to predate the formation of the large, late basins such as Imbrium and Serenitatis. (Wieczorek *et al.*, 2006).

On the basis of their Mg/Fe ratios, granulitic breccias have been divided into ferroan and magnesian varieties (which does not necessarily imply any relationship to the Mg-suite igneous rocks, especially those that are trace-element-rich). While the composition of ferroan granulitic breccias is consistent with their derivation from the ferroan anorthositic-suite of lunar plutonic rocks, the magnesian granulitic breccias compositions are not easily explained as mixtures of known igneous or plutonic rocks. This suggests the possibility that the magnesian granulitic rocks may have an igneous rock precursor that is not yet recognized among the current samples of the Moon (Korotev and Jolliff, 2001). Their origin within the crust is also still debated. Cushing *et al.* (1999) suggest a relatively rapid cooling at shallow depths lower than 200 m and a formation in craters of 30–90 km in diameter, thus physically associated with impact-melt breccias or fine-grained fragmental precursor lithologies. At odds with this theory, Korotev and Jolliff (2001) find it more likely that granulitic rocks were assembled by very large impacts (for instance, basins) that penetrated to mid-crustal levels, and that later impacts re-excavated these rocks and brought them to the surface.

Other rock types – spinel-rich lithologies

Spinel group minerals (MgAl_2O_4) are common in lunar samples, but only occur as accessory phases (abundances <10%). Investigation of spectral anomalies in global data acquired with the Moon Mineralogy Mapper (M^3) reveal a spinel-rich lithology on the central nearside, found among the Sinus Aestuum pyroclastic deposits (5.1°N, 15.2°W and 6.0°N, 8.4°W), thus consistent with a volcanic origin, but notably absent from the adjacent Rima Bode pyroclastic deposits (12.0°N, 4.1°W) (Sunshine *et al.*, 2010). While these pyroclastic deposits are spatially extensive (10000's km^2), the most spinel-rich signatures occur at much smaller scales (<1 km). A possible explanation for the presence of these spinel-rich deposits is that they may have been underlying the thin layer of pyroclastic glass deposits above, and exposed by subsequent cratering of the region. Given that the whole region is embayed by mare volcanism, with the spinel-rich and pyroclastic deposits exposed only on topographic highs, this suggests that the spinel-rich deposits are ancient (Sunshine *et al.*, 2010).

M^3 data also allowed the detection of a rock type dominated by Mg-rich spinel with no other detectable mafic minerals on the western edge of Mare Moscoviense, which does not easily fit with the current crustal evolution models and has been interpreted as being a new, unsampled rock type (Pieters *et al.*, 2010).

Requirements

There are three main requirements for targeting potential landing sites that may accomplish Science Goal 3b:

- I. Target multiple sites that will provide samples cataloging the chronological history of the Moon.
- II. Target multiple sites that will provide samples cataloging the lithological diversity of the lunar rocks.
- III. Target enough sites to collect samples from all of the main regions of the Moon.

Methodology

To fulfill the requirement list, methods and procedures were devised for locating landing sites for Science Goal 3b:

1. Complete rock type database.
 - a. Categorize rock types in Apollo, Luna, and lunar meteoritic samples.
 - b. Assess rock types or minerals (*e.g.*, pure anorthosite, granite, spinel) for which samples are needed.
 - c. Focus primarily on the rock types that have not been presented in Science Goal 3a.
2. Compile surface age maps of mare basalts to locate and categorize by oldest and youngest.

3. Compile surface maps of mare types and highland types (*cf.* Chevrel *et al.*, 2002) to locate regions of greater variety.
4. Examine the extent of pure anorthosite, mafics, and other lithologies (*e.g.*, spinel) and where on the lunar surface they can be found.
 - a. Determine whether this would be an interesting mineral to sample.
 - b. Determine its importance in regards to lunar formation theories.
5. Make maps of volcanic product locations (mare, cryptomare, and pyroclastic deposit).
6. Overlay all of the previous maps and find areas of diversity that could address most of Science Goal 3b's requirements.

Suggested landing sites

Cryptomare and mare materials of extreme ages (youngest and oldest), of various compositions, and from diverse locations can give valuable insight in the complex lunar volcanic history and its earliest and latest phases. Some sites can be of great interest to science and in-situ resource utilization, such as the high-Ti mare basalts regions (M1 and M2) that appear to be located mainly within Mare Tranquillitatis and in the East of Oceanus Procellarum. As it is still uncertain whether farside magmas were derived from a similar source composition and depth as the nearside basalts (Wieczorek *et al.*, 2006), sampling both farside and nearside mare basalts appears necessary.

Volcanic glasses are of critical importance both in characterizing the lunar interior and as a starting place for understanding the origin and evolution of lunar basaltic magmatism, but have also been recognized as having commercial potential, such as the black bead deposits at Taurus–Littrow that have been suggested as sources of oxygen, iron, and titanium. Thus the need to sample both large and small pyroclastic deposits, in order to better understand the whole compositional range that pyroclastic materials can span.

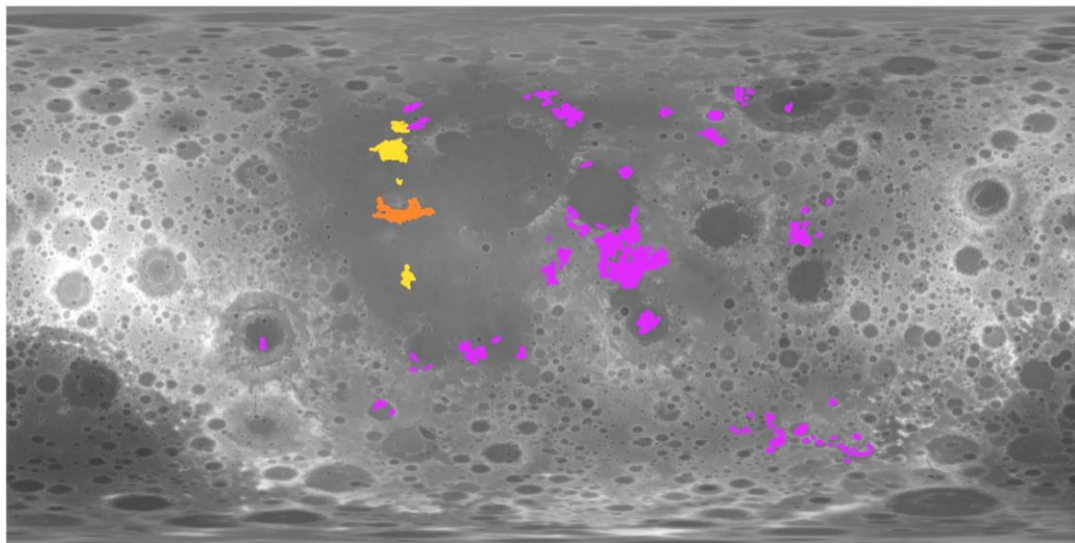
Sampling and subsequent analyzing of spinel-rich lithologies could bring new invaluable insight on the early lunar volcanism and probably add constraints on the lunar evolution models, as the entire variety of the lunar rock has still to be uncovered.

There is an important need to understand the geological context and the origin of Mg-suite and alkali-suite rocks. Unfortunately, however, they cannot be positively identified with remote sensing data and therefore cannot be mapped, so we do not have any landing sites suggestions for these rock types.

Pristine highlands, lower crust, urKREEP, and mantle material are also needed to implement the lunar rock type catalogue, but as they are investigated in Science Goal 3a and 3c, they will not be considered again here.

The sampling of all impact rocks can be done at virtually any crater site on the Moon. However, given the variety of composition that can be displayed by the different types of breccias according to the crater age, size, and excavation depth, sampling at a variety of crater sites is advised. Precise cataloging of the types of breccias that may be found on the floor or rims of craters would improve the understanding of cratering processes. For instance, in the case of granulitic breccias, their presence (or absence) and precise location at different sites could help settle debates on the origins of these still poorly known lithologies.

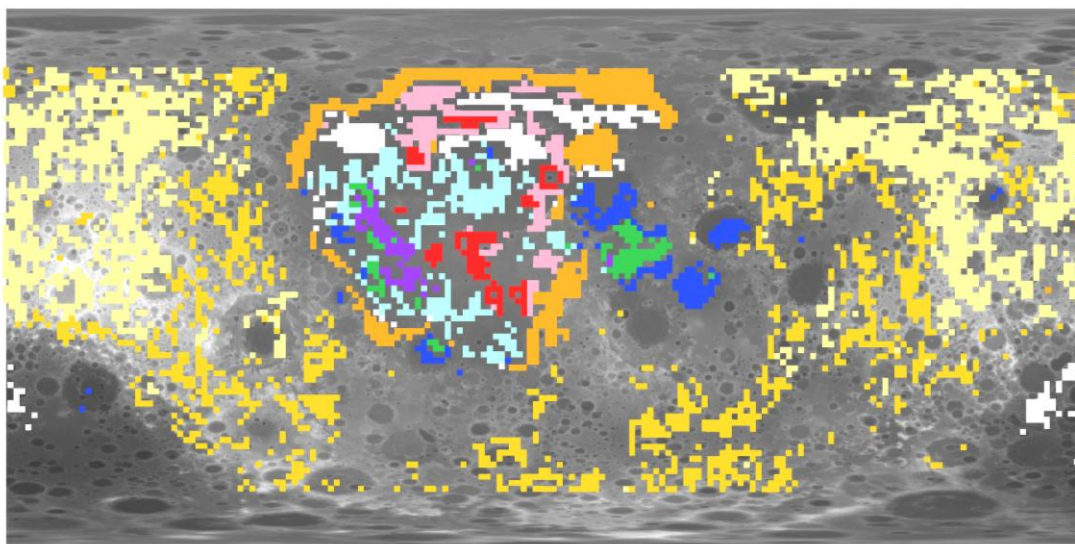
Determining landing sites specific to Science Goal 3b implies the integration of the locations of the different types of rocks that have been presented above (with the exception of breccias). Even though nearly all the different lithologies of the lunar crust can be found mixed together in the regolith (usually in a brecciated form), information regarding their respective geologic contexts is lost in this case. That is why direct sampling of the different rock types in their original geological context is so important. Consequently, Science Goal 3b requires multiple landing sites at multiple places on the Moon. Integrated maps for Science Goal 3b sample sites are presented in Figs. 3.46, 3.47 and 3.48. Figure 3.46 presents the locations of the youngest and oldest mare basalts, Fig. 3.47 represents a global view of the different regions of mare and highlands that have been defined by Chevrel *et al.* (2002), and Fig. 3.48 shows the location of the different lithologies that need to be sampled within their geological context.



Legend

- oldest mare (3.6 - 4 Ga)
- young mare (1.2 - 1.4 Ga)
- youngest mare (1.1 Ga)

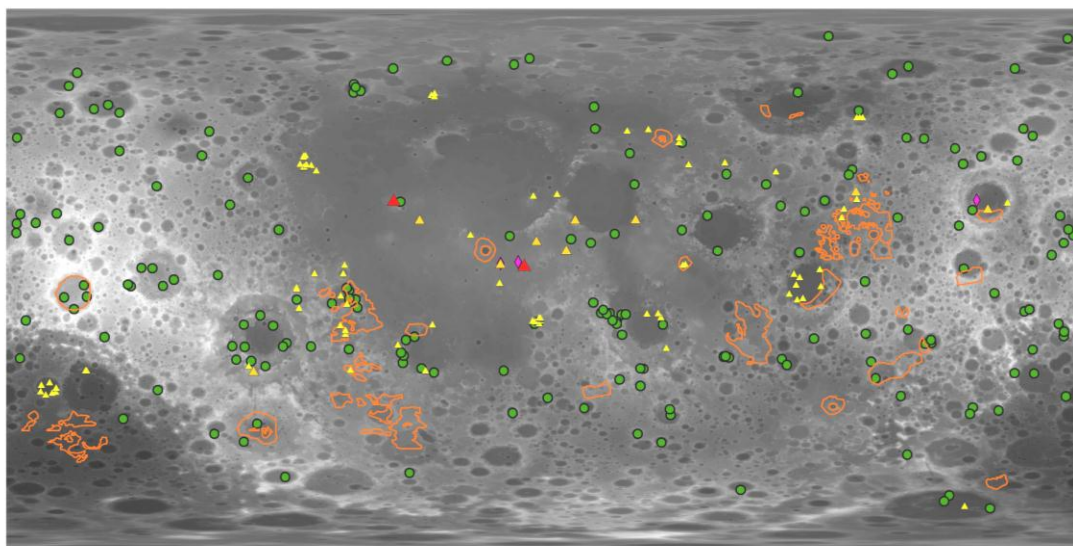
FIGURE 3.48 Map showing the locations of the youngest and oldest mare basalts (see also Figure 3.5.3). Background: LOLA topography.



Legend

- | Highland types | Mare types |
|---|--|
| ■ H5 | ■ M5 |
| ■ H1 | ■ M3 |
| ■ H2 | ■ M4 |
| ■ H3 | ■ M2 |
| ■ H4 | ■ M1 |

FIGURE 3.49 Map showing the different types of highland and mare materials classified according to their content in Fe, Ti and Th (Chevrel *et al.*, 2002). Note that some colors were changed from Pictures 3.4.13 and 3.5.4 for clarity. Background: LOLA topography.



Legend

- pure anorthosite
- ◆ spinel
- cryptomare
- ▲ pyroclastics (2 - 3000 km²)
- ▲ pyroclastics (3001 - 10000 km²)
- ▲ pyroclastics (10001 - 37400 km²)

FIGURE 3.48 Map showing where particular types of rocks that need to be sampled within their geological context have been detected: pure anorthosite, spinel, pyroclastics, and cryptomare. Background: LOLA topography.

SCIENCE GOAL 3C: DETERMINE THE COMPOSITION OF THE LOWER CRUST AND BULK MOON

Introduction

The magma ocean hypothesis was conceptualized from the results of geochemical analyses of Apollo samples. This concept has shaped our understanding of the composition and structure of the Moon, and its bulk composition. Key to this understanding are the proportion of different rock types (plagioclase, mafics and KREEP, which are expected to form different layers of the crust and mantle), their variability, precise composition, and origin. For instance, the difference in composition between the pristine crust and that of the intrusive rocks (plutons) is still not clear, and understanding it could shed some light on the two main processes responsible for the formation of the crust, namely differentiation and volcanism. Intrusive rocks could exist in most of the lower crust, the composition of which is still unknown but has already been partly sampled in the Apollo collection as norites, troctolites and dunites. Although the lower crust is covered by the upper portion of the crust and the megaregolith, it can still be sampled by impact craters that excavate material from depths close to the crust/mantle boundary. Collecting samples from these locations is critical to understanding the organization of the lower crust and the extent of plutons within the crust. Determining the precise composition of the mantle of the Moon is important because the mantle occupies most of the Moon's volume and therefore contributes the most to the lunar bulk composition estimates. Moreover, the lunar mantle has never been directly sampled, placing high value on samples from locations exposing mantle material on the surface of the Moon. The question of whether the Moon has a core or not, and what is its size and composition (Science Goal 2c) is also important in determining bulk lunar composition and understanding the differentiation process.

Background

Bulk composition of the Moon

Like most large bodies in the Solar system, the Moon is expected to have differentiated and formed a metal-rich core, an olivine-rich mantle, and a crust. The bulk composition of the Moon refers to its global composition when all these layers are mixed homogeneously, representing the composition of the initial Moon prior to its differentiation (with the exception of volatiles, which may have been lost during the formation stage).

The bulk composition of the Moon is still unclear; it has been proposed to be close to either the Earth's upper mantle composition or to chondritic silicates (Warren, 1993). These uncertainties are mainly due to the fact that there are still uncertainties regarding the way the Moon was formed. If the Moon was formed from debris after the impact of an object twice the size of the Moon with the early Earth then the lunar bulk composition should be close to the Earth's primitive mantle composition. Depending on how much of the Earth was differentiated at this time, the bulk composition might also be closer to the Earth's current upper mantle. In contrast, if the Moon formed by accretion, as did the other terrestrial planets, then a chondritic bulk composition similar to the bulk Earth is expected. Current datasets and lunar samples cannot explicitly rule out either of these two hypotheses. Information on the composition of the lunar mantle, and possible core, both of which together constitute the largest part of the bulk Moon, is therefore required.

Lower crust

The origin and precise composition of the lower crust of the Moon is still unknown. Different hypotheses for the formation of the lower crust have been proposed:

- The lower crust is a basaltic intrusion similar to maria (Head and Wilson, 1982), but with a different composition, as it seems more noritic (enriched in orthopyroxenes) than gabbroic (enriched in clinopyroxenes).
- The lower crust is entirely made of Mg-suite plutonic rocks (Reid, 1977; Ryder and Wood, 1977). However, this hypothesis does not fit Lunar Prospector gamma-ray observations (Wieczorek and Zuber, 2001). The occurrence of Mg-suite rocks seems rather local, and would be linked to Mare Imbrium and Oceanus Procellarum (Jolliff *et al.*, 2000).
- The lower crust was formed as a differentiation product of the magma ocean (Wieczorek and Zuber, 2001). In the Lunar Magma Ocean hypothesis, plagioclase cumulates float on the surface, whereas mafic-rich minerals sink to the bottom. This process could have reasonably formed a mafic-rich basal layer, underlying the upper crust. This last hypothesis seems the most plausible and fits existing orbital observations. According to crater central peak compositions, the lower crust is enriched in mafics and has probably a noritic to gabbro-noritic composition (Ryder and Wood, 1977; Pieters *et al.*, 1997; Tompkins and Pieters, 1999).

The current general definition of the lower crust includes a noritic-rich bulk, with intrusive material from the Mg-suite rocks (norites, troctolites, dunites) which are suggested to be post-magma ocean serial magmatism (Warren, 1993), and a possibly intermittent urKREEP layer (Warren and Wasson, 1979; Spudis and Davis, 1986) (Fig. 3.50).

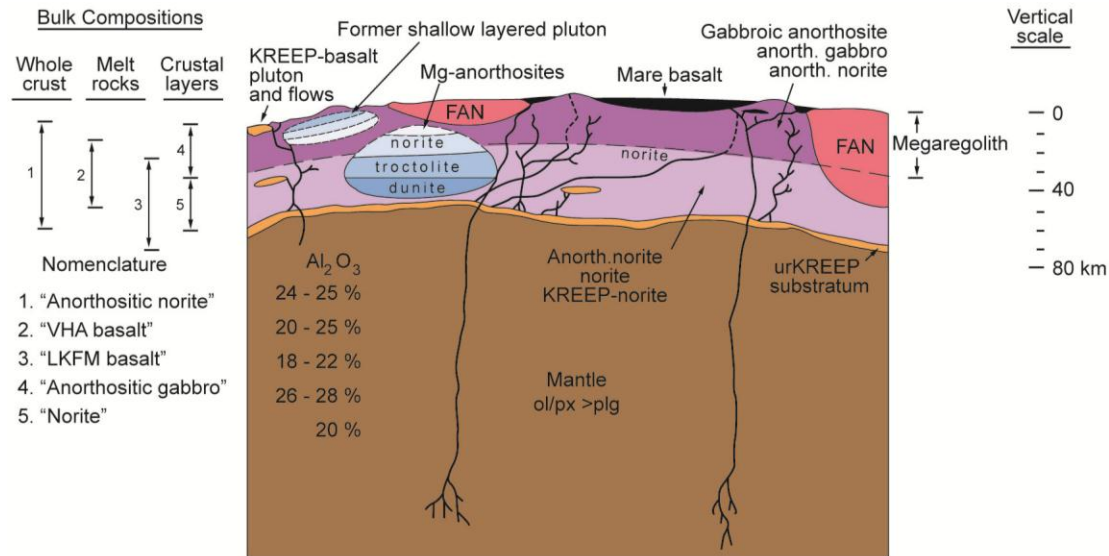


FIGURE 3.50 Suggested lunar crustal model from Spudis and Davis (1986). Contact between the upper crustal layer ("anorthosite gabbro") and the lower crustal layer ("norite") is gradational on a scale of kilometers. "FAN" refers to ferroan anorthosites. Bulk compositions are given on the left.

As discussed in Science Goal 3b, Mg-suite rocks are intrusive rocks or plutons which are considered part of the norite-rich lower crust that they are intruding. Their compositions vary from norite to gabbro, troctolite or dunite. They are very difficult to identify from orbit as they can have the same composition as lower crust and mantle, and would probably be exposed in outcrops much smaller than the resolution of most orbital spectrometers and imagers. They may also be present or absent where lower crust is exposed. They will be considered here as a component of the lower crust.

Another component of the lower crust is the urKREEP layer. This layer is expected to have infiltrated the lower crust as KREEPy basalts such as are found on the surface of the Moon, especially in the PKT area. But it is not clear if the KREEP-rich samples in the PKT are diagnostic of the urKREEP layer, and if the urKREEP layer is uniformly distributed around the Moon. It is consequently important to find areas where one could sample this pristine urKREEP material. It should be exposed in craters that have excavated mantle, if there is any, as the urKREEP layer is posited to lie just above the crust/mantle boundary.

The Moon's crust can no longer be viewed as a simple globally stratified structure (anorthosite-rich upper crust / mafic lower crust / urKREEP horizon). Variations are not only vertical, but also lateral (Pieters *et al.*, 1993; Joliff *et al.*, 2000). Several geochemically distinct provinces (or terranes) have been identified, and show that the upper crust may be absent in some locations (PKT), or the whole crust may be very thin, and the mantle close to the surface. In other cases, the KREEP layer may be absent as well, as in SPA, where thorium is detected in an unexpected low amount (Parmentier *et al.*, 2002).

Attempts to estimate the lower crustal depth and thickness have been made (Neumann *et al.*, 1996; Wieczorek and Phillips, 1998; Ishihara *et al.*, 2009). Such studies have shown important lateral and vertical variations that must be taken into account when looking for sites where the lower crust or mantle could be exposed (*cf.* proximity calculations earlier in this report).

Mantle

The deep lunar mantle has never been sampled to date, yet the properties and composition of the interior of the Moon can be inferred by indirect evidence. Geophysical surface measurements by Apollo crews revealed that the density of the mantle is high enough so that common surface rocks cannot make up a significant portion of it; the mantle rocks must then contain large amounts of heavy minerals such as olivine and pyroxene. In addition, mantle rocks were partially melted to form the mare basalts that cover

the surface in some places. The chemical composition of these lava flows show that they were made by melting rocks rich in magnesium and iron.

Most planets, including the Earth, are olivine-rich; this idea is extended to the Moon, inferring olivine to be the major component of the lunar mantle. Therefore, it is very important to identify this mineral on the lunar surface, as it could indicate places where the lunar mantle is exposed. The presence of olivine has been reported in many Apollo samples; this mineral is especially abundant in troctolite and dunite samples which are thought to be part of the Mg-suite rocks, meaning the lower crust. None of the Apollo samples or lunar meteorites containing olivine have been related to a mantle sample. One reason for this lack of mantle sampling is that the lunar mantle is not supposed to outcrop directly on the surface, as it is overlain by less dense crustal material. However, it is possible that it might have been excavated through impact processes. Olivine has also potentially been detected from orbit with Clementine, yet the low spectral resolution (and discrete spectrum of five wavelengths within the UVVIS domain) does not provide high reliability on these detections. An olivine map (Lucey *et al.*, 2004) was derived from the Clementine observations, and can be used to infer olivine-rich sites, keeping the above-mentioned uncertainties in mind. Recent missions such as Chandrayaan-1 and Kaguya, which are equipped with the high-resolution VNIR spectrometers, the Moon Mineralogy Mapper (M³) and Spectral Profiler SP), respectively, have confirmed Clementine detections of olivine. Even if many locations referred to as ‘possible olivine’ (*e.g.*, Olivine Hill, Langrenus, Keeler, Crookes and Tsiolkovsky craters) turn out to be mixtures of pyroxene and plagioclase after analyzing Clementine’s five UVVIS bands, olivine has clearly been identified in other locations (Yamamoto *et al.*, 2010). Kilometer-wide olivine exposures have been detected in 34 olivine-rich sites, mainly around impact basins: Mare Moscoviense, Crisium, Imbrium, Humorum, the SPA basin (especially Schrödinger and Zeeman craters), Nectaris, Serenitatis, Humboldtianum and Australe. These basins are located in areas where the crust is generally thinner, suggesting that mantle could be outcropping there. Radiative transfer modeling of the olivine-rich spectra obtained with SP confirms that there may be pure olivine in many locations, where it is thus likely to be mantle olivine, and not pluton’s troctolites. Most of these olivine-rich sites are concentrated on the near side. Olivine is generally found in crater walls and ejecta, but sometimes also in crater terraces or central peaks, as for Theophilus, Copernicus and Erastosthenes.

Requirements

Requirements defined for accomplishing Science Goal 3c are:

- I. Target sites with potential to yield representative samples of the lower crust.
- II. Target sites where mantle material was brought to the surface and can be sampled to provide insight on the bulk composition of the Moon.

Science Goal 3c targets sites that should have the potential to yield representative samples of the lower crust and mantle. To assess the bulk Moon, a sample of mantle would be the most useful. If it is not possible, sampling a broad range of rock types to perform chemical analysis and isotopic measurements would nevertheless be helpful. It is also impossible to determine the bulk Moon without determining precisely the lower crust composition.

Sample return is crucial to fulfilling this goal and determining the composition of the lower crust and bulk Moon. Information on isotopic composition and crystallization ages is still missing and can only be obtained through analyses in terrestrial laboratories. In-situ measurements could also supplement information on the lower crust, mantle, and possibly the core (see Science Concept 2). For instance, seismometers and gravity and radar measurements at the landing sites would give a better idea of the vertical extent and stratification of the crust and its lateral variations could be refined by extensive multispectral mapping from orbit.

Methodology

To fulfill the requirement list, methods and procedures were devised for locating landing sites for Science Goal 3c:

1. Use map of crater excavation depth proximity, and compare with crustal thickness estimates to determine areas where ejecta may contain some lower crust or mantle material, and from what depth range it originated. Younger craters or basins will be considered as better targets

as they are more likely to have less regolith and more well-preserved features. Since no maps of the ejecta contours are available yet, and since crater formation mechanisms predict that the deepest excavated material will be deposited close to the transient crater cavity, crater rims are considered the best place to get samples of deep material within ejecta.

2. Use map of melt depth proximity to determine where the lower crust or mantle may be sampled in the melt sheet or in the central peak, if preserved. Topographic data from LOLA should be used to determine craters where the central peak has not been eroded away.
3. In low topography regions, such as SPA, look for fresh craters within craters, which may also be good sites to identify lower crust material.
4. Use recent spectral olivine detections as complementary material to spot potential mantle outcrops (Yamamoto *et al.*, 2010) within the previous craters.
5. Similar methods as in Science Goal 3a can also be considered to find representative samples of rock types. Geochemical studies of primordial differentiation products should help determine the bulk composition of the Moon.

Suggested landing sites

Sites of interest for lower crust samples and for mantle samples are investigated separately and combined together at the end to determine the best sites to achieve the entire Science Goal 3c. The best tool to sample vertically into the Moon's interior is impact processes; therefore all the suggested landing sites should be within craters or basins, or on rims or ejecta. Places where mantle is exposed should also expose lower crust, but as such areas generally correspond to old basins, we can also consider fresher craters with only lower crust exposures as potential targets. Sampling mantle and lower crust from different depths would enable assessment of the vertical variability of these units. Suggested landings in diverse sites, sampling a range of materials from different depths, is essential, as Science Goal 3c could not be completely achieved in a single location. The following sections give a precise description of the criteria used to select potential landing sites for mantle, lower crust, and then those addressing both.

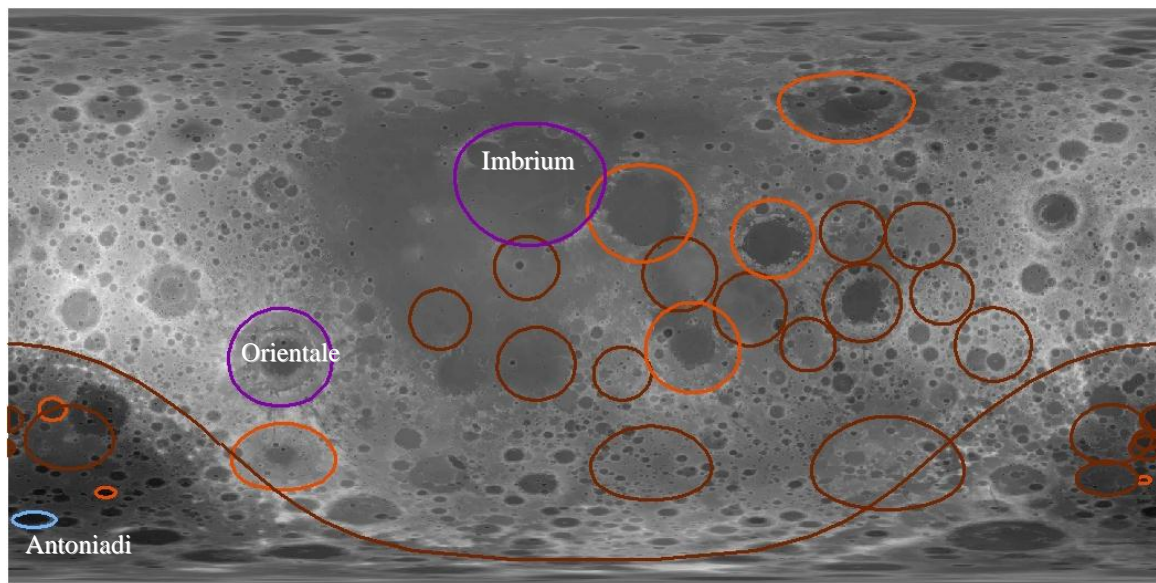
The lunar mantle or lower crust can be sampled in three different types of locations in the vicinity of an impact crater (or basin): within the crater ejecta, in the crater melt sheet, or in the crater central peak or peak ring(s). Ejecta blankets cover wide areas and generally extend until ~3 radii away from the crater center (Melosh, 1989), but the deepest material should be excavated close to the crater rim. Since ejecta maps are missing among the current datasets, we focus on the rims of craters and basins that should excavate lower crust or mantle, as deep material and preserved ejecta are expected in these locations. If craters or basins are old, ejecta is likely to be buried under a thick regolith layer, and therefore it is advised to focus on young locations when sampling of excavated material is considered.

The same issue occurs in old craters and especially in basins when trying to sample the impact melt sheet, probably buried under kilometers of regolith and not directly accessible on the surface. For large basins there is also a possibility that the melt is not homogenous due to differentiation after the impact (Science Goal 6a), and it is uncertain whether mantle components would be present at the top of the melt sheet. Therefore, melt sheets should not be considered as prioritized targets for this Science Goal. On the contrary, central peaks or peak rings of craters and basins, which are often well-preserved, should expose material at least as deep as the one reached by the melt sheet. Outcrops might be available on the vertical steep structures of central peaks and pieces of rocks rolling down the slope of the central peak could be sampled at the peak's base.

In summary, all the possible landing sites we suggest to sample lower crust and/or mantle are presented in craters rims, central peaks and peak rings.

Assessing the best landing sites to sample the lunar lower crust

According to our proximity calculations, the lower crust should be excavated by approximately 36 craters or basins. Figure 3.51 displays these according to their ages. Many of these are old large impact basins or craters that are located within SPA. Lower crust material should be found in their ejecta, especially the ones close to the crater rim. For old craters or basins, these ejecta are likely to be buried by other ejecta or regolith, therefore only the youngest and fresher basins and craters should be considered: Imbrium, Orientale and Antoniadi. The rims of these three craters are potential sampling sites.



Age: Pre-Nectarian Nectarian Lower Imbrian Upper Imbrian

FIGURE 3.51 Map displaying the craters or basins that should excavate lower crust in their ejecta (meaning those whose proximity value = crustal thickness - excavation depth is lower than -5 km). Color scale indicates their ages. The youngest ones have their name written in white. Background: LOLA topography.

Lower crust can also be sampled within craters or basins through their central peak or peak rings. Figure 3.52 shows all the craters or basins that have a melt proximity (= crustal thickness - melt depth) lower than -5 km, meaning all the craters or basins that should reach at least -5 km between the upper crust/lower crust boundary. Most of them are old large impact basins, or craters located within SPA, as this is where the lunar crustal thickness reaches its lowest values. Among these 128 craters or basins, only the 58 ones with well-preserved central features are considered for potential landing sites.

Some of these craters are actually large enough to sample the entire lower crust range, as they reach the mantle. Others are too shallow and only reach the uppermost part of the lower crust. Figure 3.54 shows the minimum depth reached by the 58 selected craters or basins.

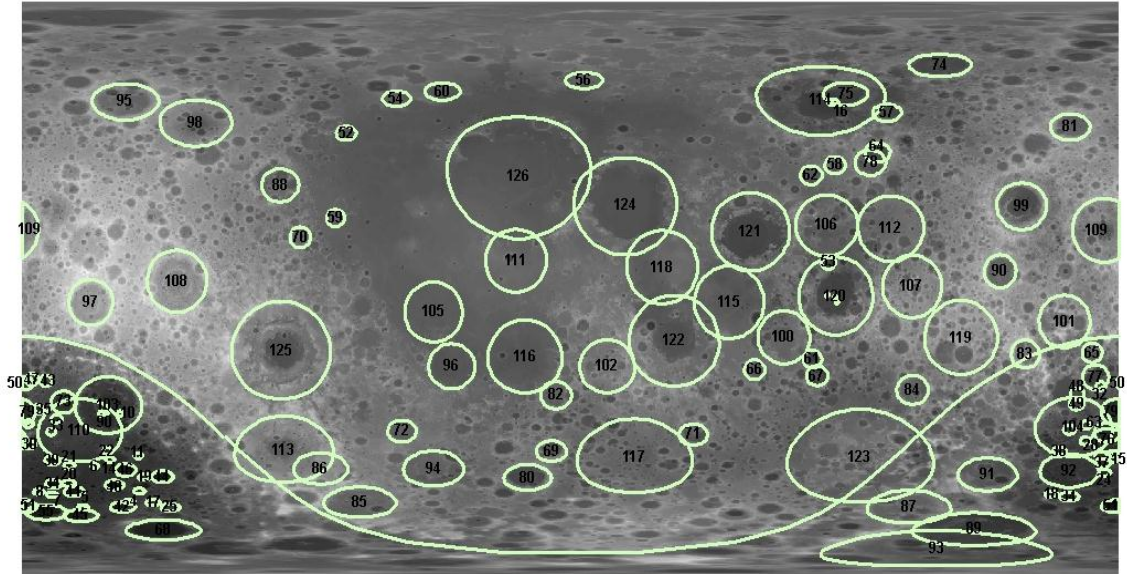


FIGURE 3.52 Map displaying the craters or basins that could theoretically contain lower crust material in their central peak or peak rings, if those are preserved (meaning those whose melt proximity value is lower than -5 km). Background: LOLA topography. A list of these craters and basins can be found in Table A3.7.

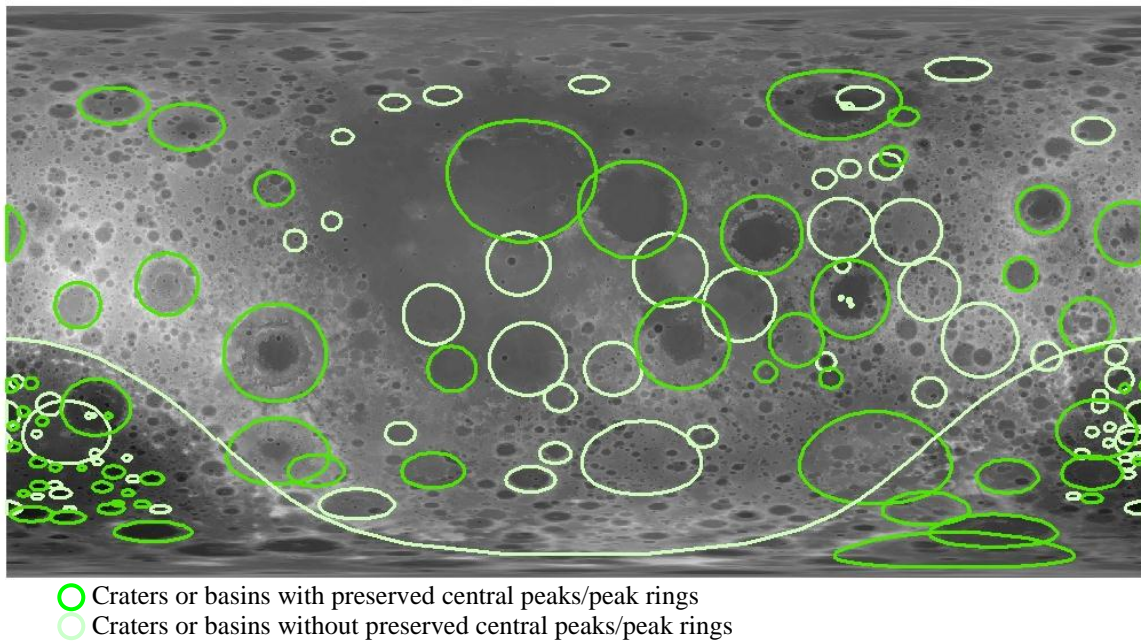


FIGURE 3.53 Map displaying the craters or basins that should contain lower crust material in their preserved central peak or peak rings (In red). Craters or basins represented in white seem to have been filled with material or eroded. Background: LOLA topography.

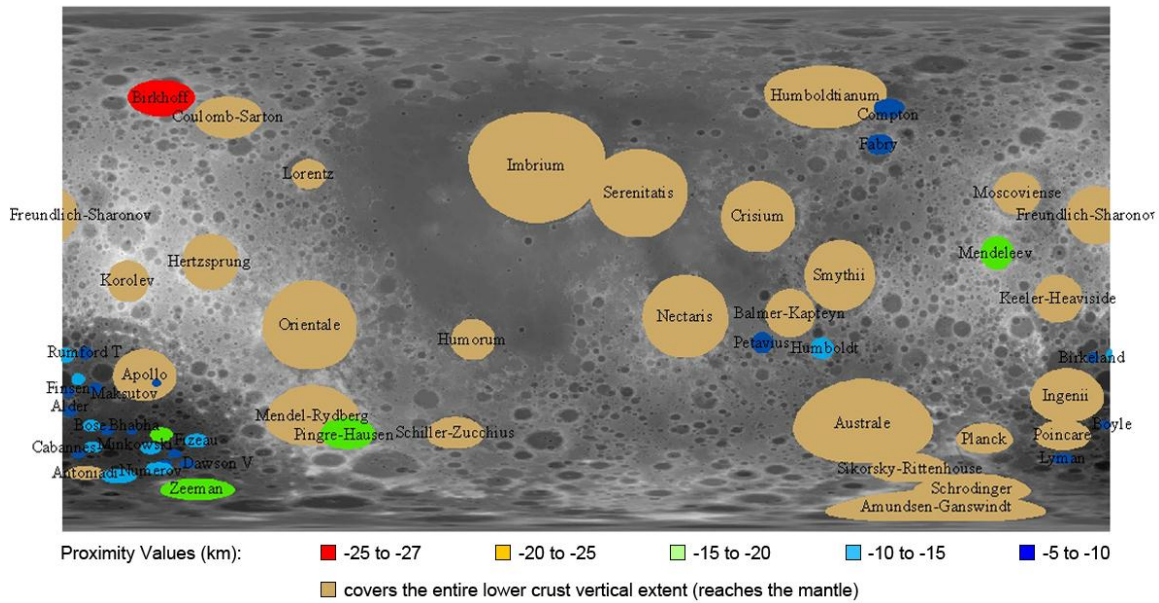


FIGURE 3.54 Map displaying the craters or basins that should contain lower crust material in their preserved central peak or peak rings as a function of their proximity value, meaning the depth they reach below the upper crust/lower crust boundary. Craters or basins that reach the mantle, are displayed in black. Background: LOLA topography.

Gathering lower crust samples from different depths would yield important information on the formation of the crust through the magma ocean process, its variability, and the occurrence and extent of plutons in the lower crust. We suggest sites in a few craters or basins of different proximity values, located at different places on the surface of the Moon, to compare the samples' homogeneity. For instance, one may want to obtain samples of Imbrium (nearside mare, proximity = -175 km, it reaches the mantle), Birkhoff (farside highlands, proximity = -26km), Mendelev (farside highlands, proximity = -15 km), and Rumford T (SPA, proximity = -6km).

A list of all the craters and basins that tap into the lower crust, ranked by their proximity value, is provided in Table 3.9. A detailed list of all the localization and parameters of these craters and basins can be found in Table A3.7.

TABLE 3.9 List of possible sites (total = 58) where lower crust material could be sampled, ranked according to the depth at which they sample the lower crust, below the upper crust/lower crust boundary. All suggested target are central peak of craters or peak rings of basins except for the ones in blue that correspond to crater rims or ejecta.

depth sampled below the upper crust/lower crust boundary (= proximity value)	number of craters	names
sampling the whole lower crust range + Mantle	23 + 1	<i>cf. mantle Table</i>
sampling the whole lower crust range + maybe mantle (-5 < proximity value from mantle < 0)	4	Antoniadi, Korolev, Lorentz, Schiller-Zucchi
from - 30 to - 25 km	1	Birkhoff
from - 25 to -20 km	1	<i>Oriente</i>
from - 20 to -15 km	4	Mendelev, Minkovski, Zeeman, Pingre-Hausen

from - 15 to -10 km	9	Humboldt, Fizeau, Crommelin, Lemaitre, Cabannes, Bose, Numerov, Davisson, Leeuwenhoek
from - 10 to -5 km	17+1	Rumford T, Borman, Matsukov, Finsen, Alder, Bhabha, Stoney, Dawson V, Crommelin C, Cabannes Q, Eijkman, Petavius, Birkeland, Boyle, Lyman, Fabry, Compton, Antoniadi

Lower crust exposure on the surface of the moon could also be inferred from spectroscopic data (Tompkins and Pieters, 1999). Nevertheless the spectral resolution of the Clementine imager, with only 5 bands in the UV-Visible domain, and 11 total, does not allow for a precise mineralogical identification. Some highland anorthosites may also bear a mafic-rich signature even if mafics are not the most abundant mineral in the rock. Indeed plagioclase are hard to detect when lower than 95 % in composition, and such a rock may then appear mafic-rich in the spectral data, even if it is not. This motivated our decision to assess Science Goal 3c landing sites with calculations only.

Assessing the best landing sites to sample the lunar mantle

According to our proximity calculations, only 3 basins should be deep enough to excavate mantle in their ejecta: SPA, Imbrium and Serenitatis (Fig. 3.55). Since they are large old basins, their ejecta should be widespread on the planet, but might be buried under a thick regolith layer. Therefore these possible landing sites should not be considered as high-priority ones. Crisium and Nectaris are within the 5 km error bar and may or may not have excavated mantle, so that they are not considered as potential landing sites for mantle sampling.

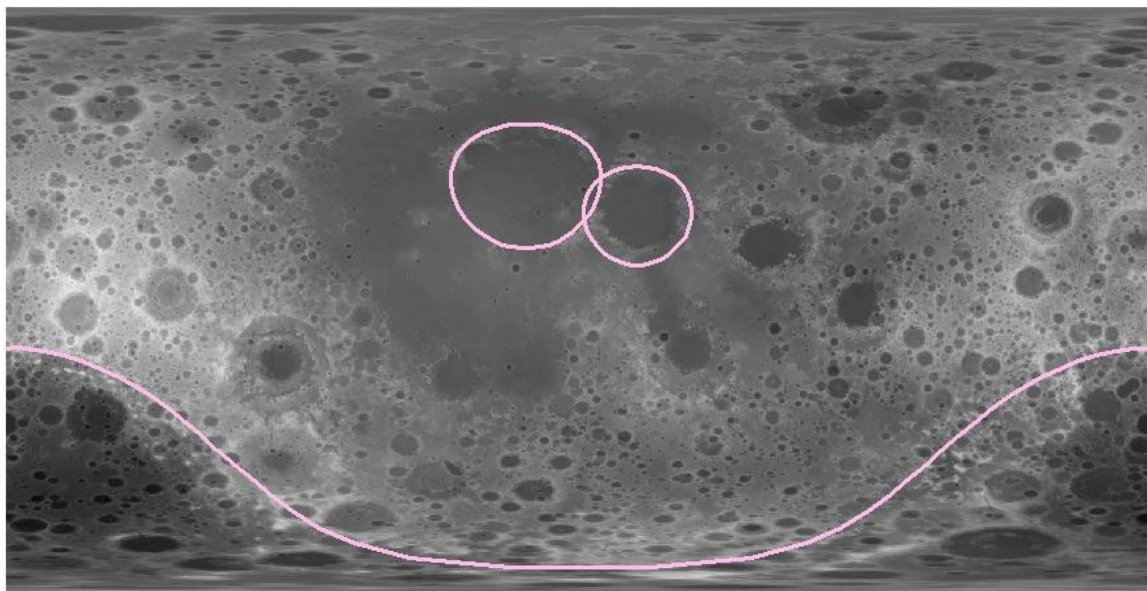


FIGURE 3.55 Map of the basins that are presumably excavating mantle in their ejecta (maps of these ejecta are not available). Potential landing sites should be on the rims of these basins. Excavation depth calculations are uncertain for SPA due to its size, but Imbrium should be excavating as deep as 60 km, meaning approximately 12 km below the crust/mantle boundary, while Serenitatis should be excavating as deep as 50 km, meaning 5.5km below the crust/mantle boundary.

Thirty nine craters or basins should have mantle material present in their melt sheet, or central peaks or peak rings (Fig. 3.56). They all correspond to old basins and have been studied in details. Topographic profiles with LOLA altimetry data and imagery from Lunar Orbiter were used to assess the presence of peak rings. 23 of them have one or several preserved rings (Fig. 3.57). Basins without peak rings are excluded from the potential landing sites (Table A3.8). Plotting the recent Yamamoto *et al.* (2010) olivine detections, we observe that at least half of the olivine detection locations correspond to the rings of large basins such as Imbrium, Crisium, Nectaris and Serenitatis (Fig. 3.58), suggesting a precise indicator for where to land to ensure that olivine outcrops. It is however very difficult to assess the presence of other minerals such as plagioclase in spectral data, and it is uncertain that these olivine detections correspond to mantle rocks (dunite) or lower crust rocks (troctolite).

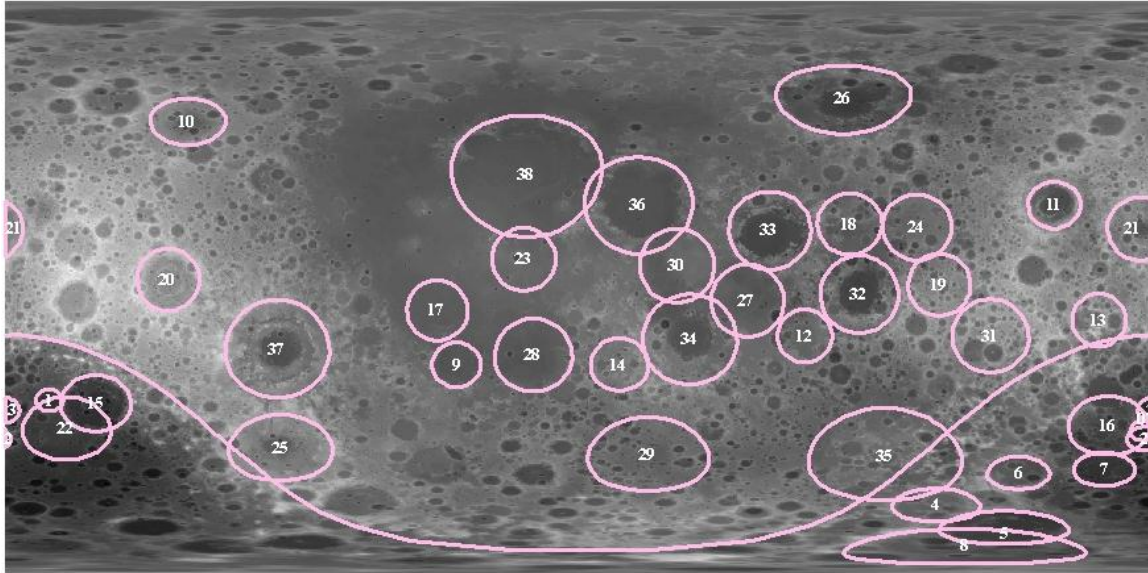
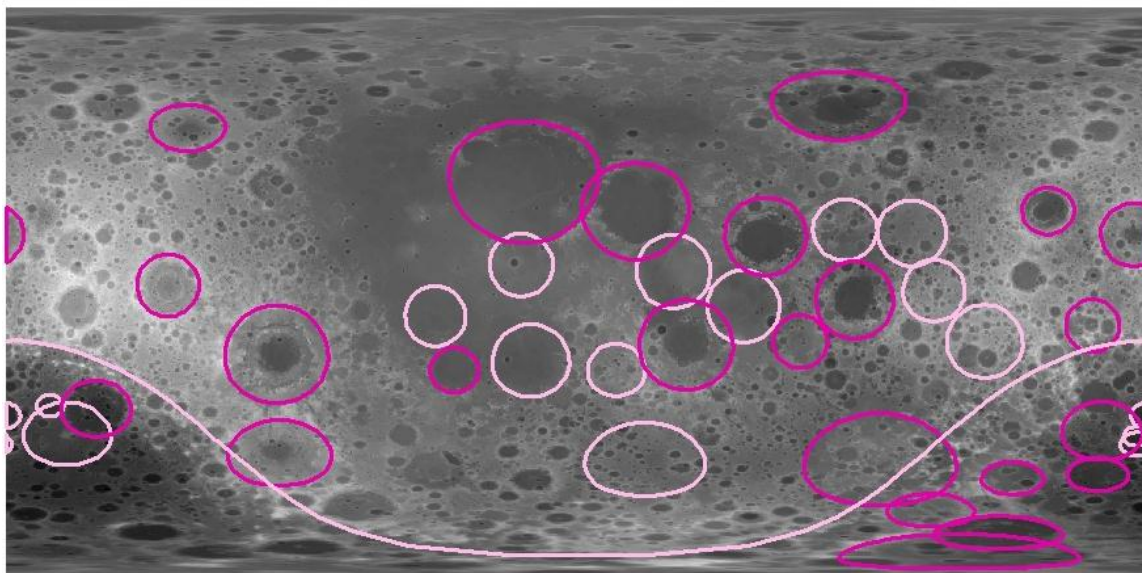
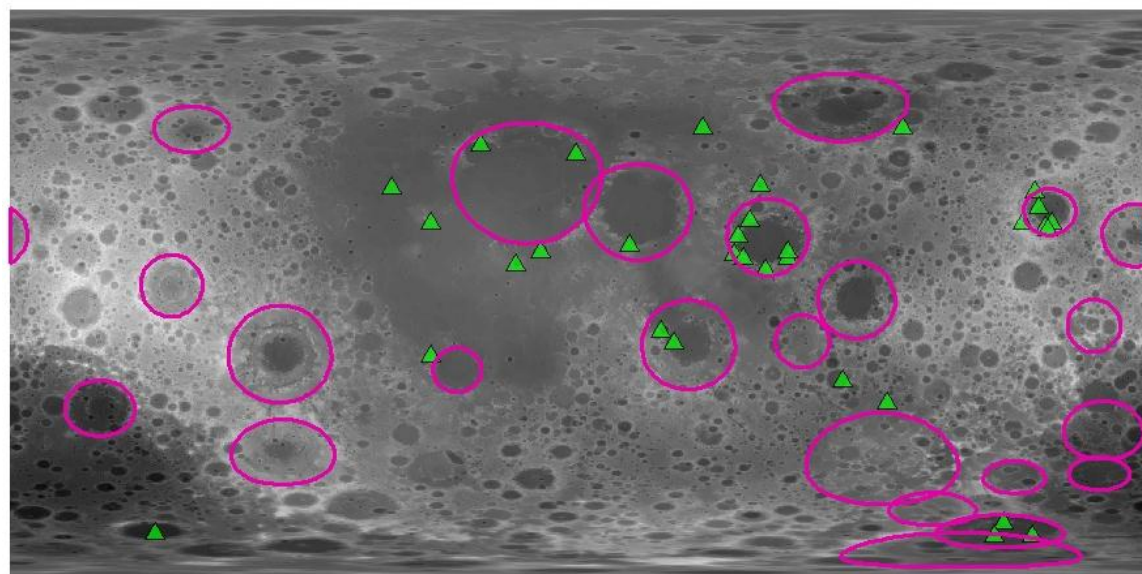


FIGURE 3.56 Map of the basins that are thought to have mantle material in their uplifted rings Potential landing sites should be around the uplifted rings of these basins. Labels are removed for clarity, but a complete list of these basins can be found in Table A3.8.



- Craters or basins with preserved central peaks/peak rings
- Craters or basins without preserved central peaks/peak rings

FIGURE 3.57 Map of the basins that are thought to have mantle material in their preserved uplifted rings. Craters in hollow are the ones without any visible uplifted rings or central features. They are therefore excluded from the final potential landing sites list. Edit images so they are hollow rings.



- Craters or basins with preserved central peaks/peak rings
- ▲ Olivine detections from Yamamoto *et al.* (2010)

FIGURE 3.58 Olivine detections from Yamamoto *et al.* (2010) (purple triangles) overlain on Fig. 3.57. In Imbrium, Moscoviense, Nectaris, Serenitatis, Crisium and Schrödinger, olivine detections perfectly match the uplifted rings location, but the few detections realized outside of the places where mantle is expected to outcrop may rather be indicative of the presence of troctolite in plutons.

Mantle samples from different depths would provide important information on the formation of the Moon and the magma ocean processes. The depth ranges from which material exposed in central peaks or peak rings were computed and are presented Fig. 3.59. It is suggested to land in two or three craters or basins of different depth ranges to compare the samples' homogeneity. For instance, one may want to bring back samples of mantle from Imbrium (Proximity = -175 km), Ingenii (Proximity = -58 km), and Moscoviense (Proximity = -12 km). A complete list of the proximity values for the 39 basins that are reaching the mantle is given in Table 3.10.

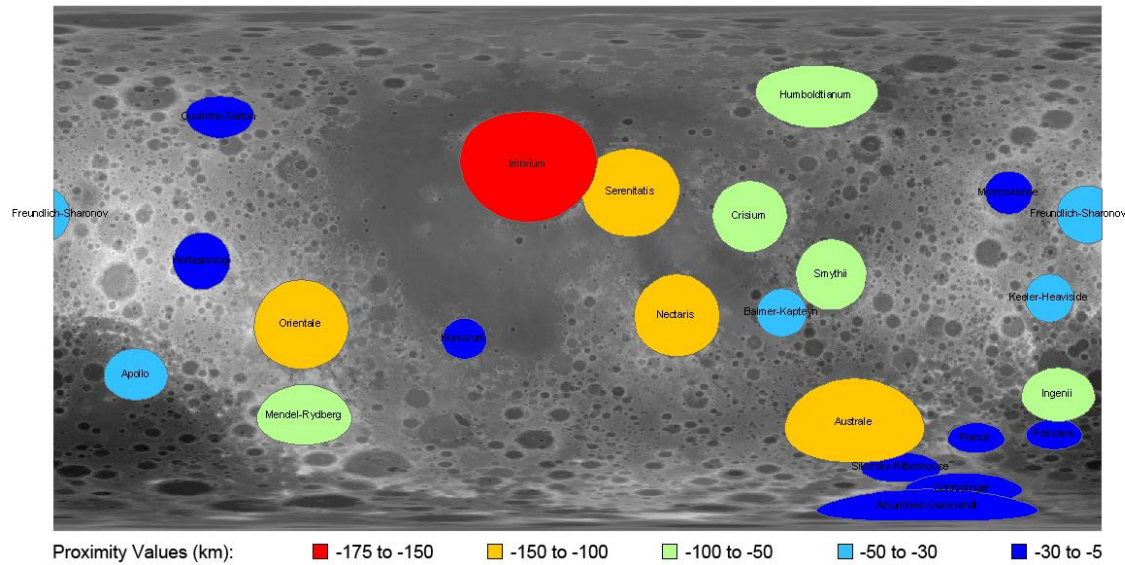
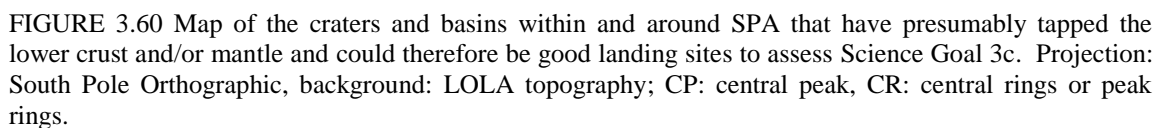


FIGURE 3.59 Map of the basins that are presumably containing mantle material in their preserved peak rings, color-coded as a function of their proximity value, i.e the depth they are supposed to reach and sample below the crust/mantle boundary.

TABLE 3.10 List of possible targets ranked according to the depth they reaching below the crust-mantle boundary. All suggested target are uplifted rings, except for the ones in blue that correspond to crater rims or ejecta. *Calculations are unsure for SPA. **Correlated with olivine detections.

Depth sampled below the C/M boundary	Number of craters	Names
around -400 km	1	SPA*
from - 200 to - 150 km	1	Imbrium**
from - 150 to -100 km	4	Orientele, Serenitatis**, Nectaris**, Australe
from - 100 to -50 km	5+1	Smythii, Ingenii, Mendel-Rydberg, Crisium**, Humboldtianum, SPA*
from - 50 to -30 km	4	Freundlich-Sharanov, Keeler-Heaviside, Balmer-Kapteyn, Apollo
from - 30 to -5 km	9+2	Coulomb-Sarton, Hertzprung, Humorum, Moscoviense**, Poincare, planck, Schrodinger**, Admunsen-Gandswindt, Sikorsky-Rittenhouse, Imbrium, Serenitatis

Excavation depth, melt depth, and proximity calculations are difficult to process for SPA, which is the oldest and largest impact basin. Although its size exceeds the limit size for which the equations used are valid, we applied them as no other tools or models exist for such large scale calculations. Therefore we urge caution in using computed values, and consider the results to have an associated error. It is very likely that SPA tapped deep into the mantle. SPA ejecta is buried, and its possible central features, if it had any, are probably not preserved. However, craters within SPA could be very interesting targets as they could penetrate the SPA melt sheet, even if they are shallow, and thus may present mantle components, as the crust below SPA is very thin.



An integrated Table of both landing sites where lower crust and mantle could be sampled is provided in Table A3.9. Selecting sites that sample mantle would allow the sampling of urKREEP (if present) and lower crust at the same time, but the quality of the sample might be better in fresher craters. We therefore recommend sampling in multiple sites. The final selection should respect equilibrium between the diversity of material that might be sampled there and the age of the location.

SCIENCE GOAL 3D: QUANTIFY THE LOCAL AND REGIONAL COMPLEXITY OF THE CURRENT LUNAR CRUST

Introduction

Early lunar formation models describe the lunar crust as the floating anorthositic crystallization cumulates from the lunar magma ocean. This topmost layer was later intruded by mantle material during an epoch of lunar volcanism, with the surface constantly being modified by impact events. While this general formation model may be sufficient for studying lunar features on a global scale, it does not adequately explain the complexity of the crust on a smaller scale. Here we wish to quantify the complex lithologies of the lunar crust by examining the lateral and vertical extent of intrusive and anomalous features, specifically on regional scales that cannot be explained by overarching models of planetary differentiation.

Where Science Goal 3b is concerned with categorizing the different types of rocks on the Moon, Science Goal 3d specifically addresses the structure and physical extent of each lithology. Of particular interest are plutonic intrusions, which are local scale features and will be discussed in detail in the following section. While Science Goal 3c examines the lower crust (where plutons are believed to reside) on a global scale in terms of composition in order to identify the representative characteristics of that layer, Science Goal 3d instead focuses on how small-scale variations in composition lead to a more heterogeneous crustal environment.

Background

Science Goal 3d aims to target sites that will expand our knowledge of the complicated crustal lithology on a local scale. A regional crustal thickness dichotomy exists between the nearside and farside of the Moon's crust. Investigations of specific craters within these two dichotomous regions may yield key information on lunar formation and differentiation. In addition, investigation of gravity anomalies from remote sensing data will present information on crustal processes and the possibility of intrusions which occurred after differentiation was complete. We will also investigate "red spots", which are spectral anomalies that may indicate the presence of underlying intrusive features. Finally, plutonic intrusions will be considered, as they represent local-scale anomalies in the lower crust (Mg-suite rocks; Science Goal 3b) and in the upper crust (anorthositic-rich plutons, Nyquist *et al.*, 2010; Science Goal 3a) whose extent is not well constrained.

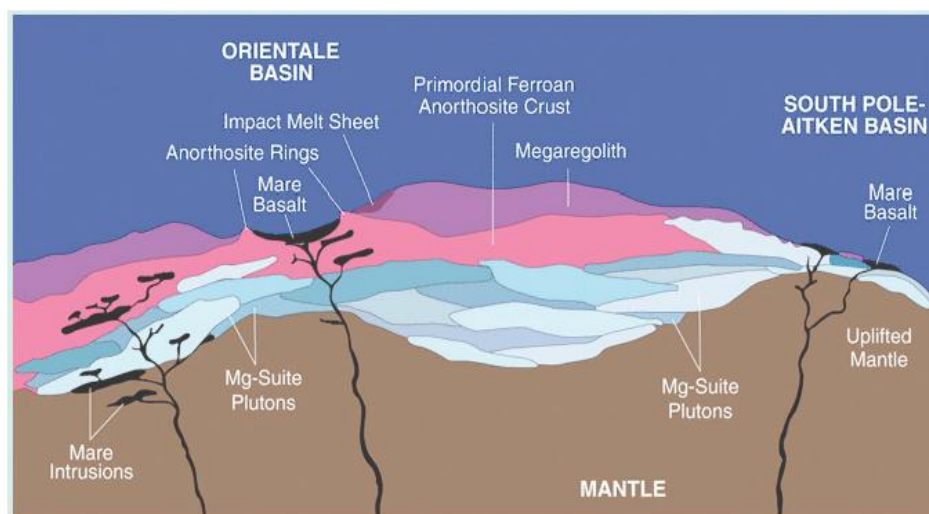


FIGURE 3.61 Cross section of the lunar crust, demonstrating complexity of plutonic layering. Image from NRC (2007), courtesy of Planetary Science Research Discoveries, University of Hawaii. Based on concept by Paul D. Spudis.

Nearside-Farside Dichotomy

The crustal thickness of the Moon has been a topic of study since the early Apollo missions. However, due to the low resolution of remote sensing data, as well as limited coverage of gravity and topography studies, not much progress was made until recently (Wieczorek *et al.*, 1998). Clementine topography and Lunar Prospector gravimetry show a clear dichotomy of the lunar crustal thickness, with the average nearside crust being thinner than that of the farside. The most accurate data to date is from the Kaguya lunar gravity and topography model, which allows the investigation of differences between farside basin structures (Fig. 3.62). While the crustal thickness data is similar to results from Wieczorek models (Wieczorek *et al.*, 1998), there exist some major differences. The most notable discovery is that the thickest crust appears to be located in the southern rim of the Dirichlet-Jackson basin ($6.91^\circ, -160.21^\circ$), with a maximum of ~ 110 km, while the thinnest crust is located in the Moscoviense basin ($26^\circ, 147^\circ$), with a minimum of nearly zero. The crustal maximum corresponds to the highest topography, while the thinnest crust occurs at the bottom of a farside basin, which could possibly be due to an abnormally large mantle plug (Ishihara *et al.*, 2009).

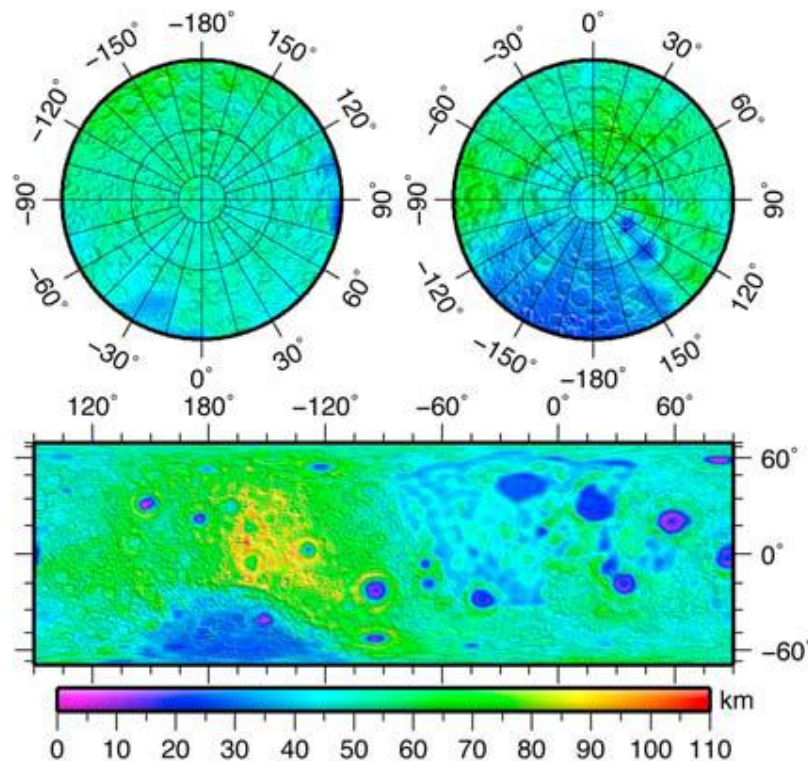


FIGURE 3.62 Total lunar crustal thickness (crustal materials and mare basalt fills) map for a uniform density crust with compensation occurring at the lunar Moho. Projections and areas are (bottom) Lambert cylindrical equal area projection for global, Lambert azimuthal equal area projection for (top left) north and (top right) south polar regions above latitude of 60 degrees. Contour interval is 10 km (Ishihara *et al.*, 2009).

Gravity anomalies / mascons

Study of the lunar gravity field — in particular the long-known positive gravity anomalies called mascons, associated with features like depressed basins that might otherwise have been expected to have negative anomalies — plays an important role in understanding the structure and the evolution of the Moon. Figure 3.63 presents the variations of gravity on the lunar surface in terms of free-air and Bouguer gravity anomalies as modeled by Matsumoto *et al.* (2010). Distinctive differences appear between the nearside principal mascons and the farside basins. These differences are particularly important for thermal

evolution of the Moon because the basin structure possibly reflects the state of the lithosphere in the early development of mare volcanism (Namiki *et al.*, 2009).

The nearside principal mascons on Imbrium, Serenitatis, Crisium, Nectaris, Humorum, and Smythii have sharp shoulders, with a weakly negative gravity anomaly in the surroundings. In contrast, the farside basins are characterized by concentric rings of positive and negative anomalies. Farside basins have been divided into two types (Table 3.12 and Fig. 3.63). Type I basins have similar peak heights for both the free-air and Bouguer anomalies, whereas Type II basins have smaller peak magnitudes in the free-air anomalies (40–80% compared to those in the Bouguer anomalies) and broader peak shapes (Namiki *et al.*, 2009; Matsumoto *et al.*, 2010). Basins that do not show distinct central peaks either in the free-air or Bouguer anomalies have been described as “nonmascon basins” to distinguish them from others by the lack of obvious gravity anomalies (Matsumoto *et al.*, 2010).

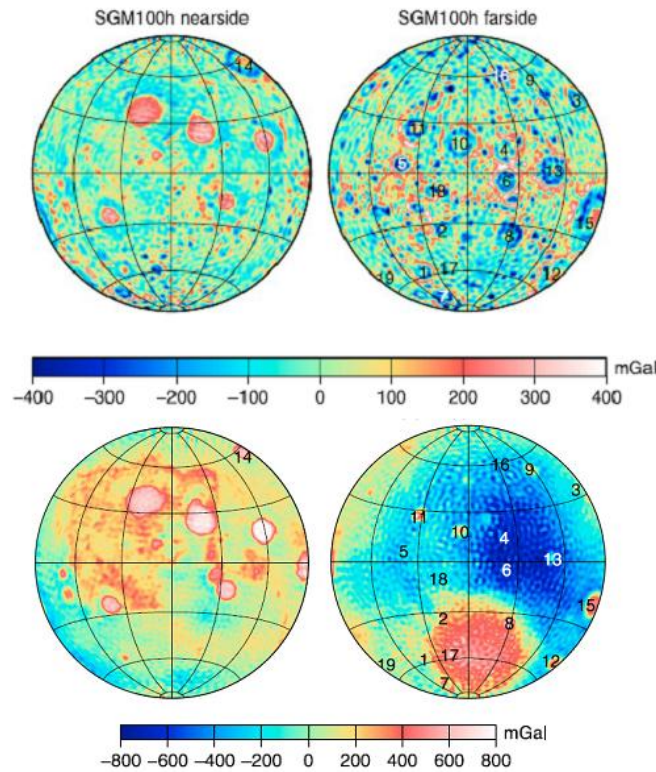


FIGURE 3.63 Free-air (top) and Bouguer (bottom) gravity anomalies at the lunar surface for the SGM100h model, computed with respect to a reference radius of 1738.0 km. The nearside maps are on the left and the farside on the right. The numbers on the figure indicate the locations of the basins tabulated in Table 3.12 (Matsumoto *et al.*, 2010).

Nevertheless, the explanation of these anomalies is still unclear. Combined gravitational attraction of lava fills in the mare basins, and uplifted mantle beneath the basins, are thought to be the mechanisms that support the positive gravity anomaly of the nearside mascons, but the relative contribution of these sources remains difficult to evaluate (Namiki *et al.*, 2009). A clear relation between basin types and crustal thickness has also been detected. Type I basins have a thicker surrounding crust and thicker crust at the basin center. On the other hand, Type II basins (with the exception of Moscoviense) have a relatively thinner surrounding crust and thinner crust at the basin center. The difference between type I and type II is probably due to the difference of the ratio between the preimpact crustal thickness (Moho depth) and impact scale (Ishihara *et al.*, 2009).

Local complexity of the lunar crust

Plutonic Intrusions: A pluton is an intrusive igneous rock body that crystallized from magma slowly cooling below the surface. In practice, 'pluton' usually refers to a distinctive mass of igneous rock, typically kilometers in dimension, without any particular shape.

Compositional and petrographic relations among lunar samples suggest that unmapped plutonic activity contributed significantly to early crustal evolution. Plutons might have been formed early after the magmatic ocean crystallized by intense and repeated periods of serial magmatism. Remote sensing study of Bullialdus crater (21°S, 22°W) showed the probable existence of a pluton at this site, whose size was estimated at least to have to be on the order of the size of the crater (~60 km) (Pieters *et al.*, 1991). Based on the character of mafic minerals present and compositional diversity with depth, most additional candidate areas for pluton excavation appear concentrated in the western hemisphere: for instance Copernicus, Aristarchus, Tycho (Pieters *et al.*, 1991). Seven highland craters (namely Jackson, King, Langmuir, Orlov, Ohm, Stevinus and Tycho), in which the central peaks are more mafic as compared to central peaks of other highland craters, were identified using Clementine UVVIS data (Tompkins, 1998). These seven mafic craters are not thought to have tapped the deep mafic-rich lower crust; their particular composition can reasonably be interpreted by the occurrence of excavated plutons at these locations.

Anorthosite-rich plutons may also exist on the Moon, as Nyquist *et al.* (2010) identified highland material that had a different age and isotopic composition than the primordial highlands, formed from the magma ocean. This suggests that not only the lower crust is intruded with Mg-suite rocks (mafic-rich plutons described above), but also the upper crust might be intruded by a more anorthositic-rich material.

Unfortunately, plutons are hard to identify as their composition might be similar to the upper (for anorthosite-rich plutons) or lower (for mafic-rich plutons) crust. The only ways to distinguish them from the material of the crust, formed by the magma ocean, is by their geological context (e.g., outcrops in central peaks of small craters that are only reaching the subsurface material or intrusive contacts in craters, walls, or cliffs). Rocks formed in plutons will have a different age and isotopic composition from those of the rocks formed from the magma ocean, as they have different formation processes, but these parameters cannot be assessed with remote sensing data or in-situ measurements. It is therefore crucial to return samples of plutonic intrusions for further analyses.

Intrusive domes/laccoliths: On Earth, subsurface magmatic intrusions often form laccoliths, where magma flows under a surface of solidified lava and lifts it up (Fig. 3.64), forming flattened or dome-shaped features. On the Moon there exist similar features, called intrusive domes. Intrusive domes do not display effusive vents and differ morphologically from the common effusive domes. They are characterized by very low flank slopes of less than 0.9°, often have larger diameters than effusive lunar domes of 30 km and more, and display regular but non-circular outlines (Wöhler *et al.*, 2009). These domes tend to be associated with tectonic faults or linear rilles, which are indicative of tensional stress and may suggest their possible intrusive mode of formation. Wichman and Schultz (1996) attributed the modification processes observed in floor-fractured lunar craters to the formation and growth of laccoliths.

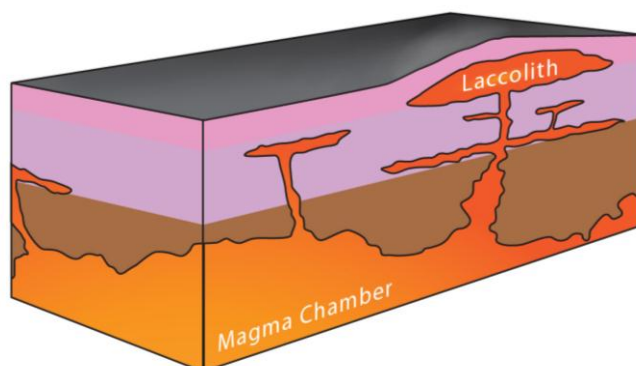


FIGURE 3.64 3D representation of the geological setting of a laccolith. The magma stays in subsurface, spreads laterally and cools slowly forming igneous rocks. Note the surficial uplift creating a dome-shape on the surface, due to the emplacement of a laccolith beneath.

Red spots: Features characterized by steep flank slopes, high albedo similar to lunar highlands, and strong absorption in the ultraviolet have been identified on the nearside of the Moon (Whitaker, 1972). Because of this latter feature they appear spectrally red and therefore were termed “red spots” (Wagner *et al.*, 2010). Detailed studies of these spectral anomalies show that red spots are located in a variety of geologic settings and commonly appear as domes, smooth plains units, and rugged highlands patches (Fig. 3.66). Their morphology suggests that these domes were created by much more viscous, silica-rich lava (Wagner *et al.*, 2010), and some models show that Hansteen Alpha dome, the Gruithuisen Domes, and the Lassell massif have Th abundances that are consistent with evolved lunar lithologies such as lunar granites (Hagerty *et al.*, 2006).

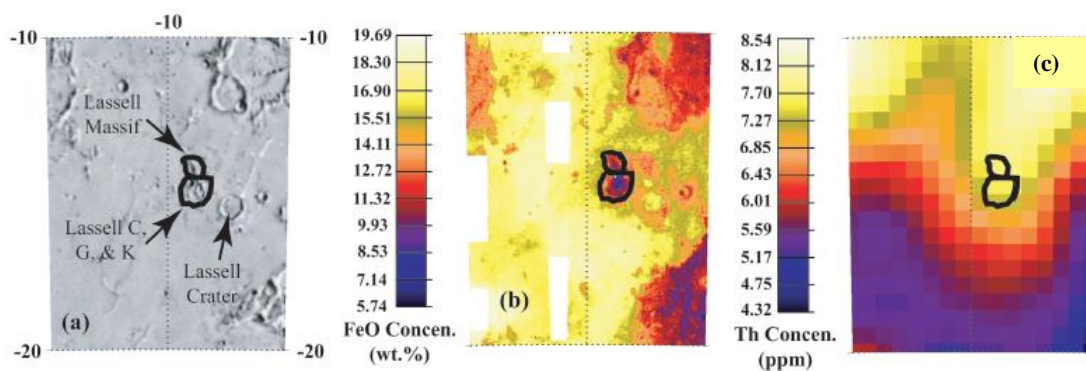


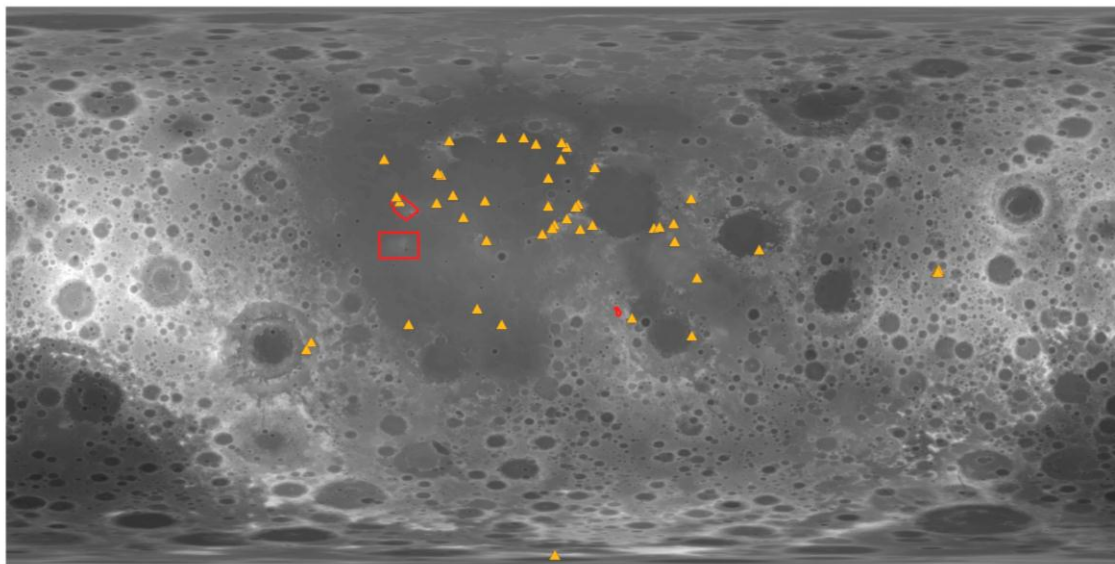
FIGURE 3.65 Geological context of the Lassell red spot. (a) Shaded relief map for the Lassell region. (b) Clementine FeO map for the Lassell region. Note the low FeO concentrations of the massif and crater cluster. (c) LP-GRS Th map for the Lassell region. The Lassell massif and the crater cluster are outlined in black (from Hagerty *et al.*, 2006).

As no samples collected and returned from the Apollo and Luna landing sites match the red spots' spectral characteristics (Hiesinger and Head, 2006), retrieving rocks from at least the Hansteen Alpha dome, the Gruithuisen Domes, and the Lassell massif would provide new information about the full range of volcanic and crustal processes that could have occurred on the Moon.

Massifs and plateaus

Lunar massifs are thought to be blocks of crust that were tilted and uplifted by the shock of a major impact (Harland, 2008). Plateaus are also uplifted crustal material whose origin still remains uncertain, although they appear connected with volcanic processes. Both these features are of interest as they have unclear origins and could expose thick and complex cross-sections through the upper crust.

Figure 3.67 displays the location of recognized lunar massifs and plateaus: the Aristarchus Plateau, a rectangular elevated crustal block about 170×220 km that is surrounded by younger mare basalts from Oceanus Procellarum; the Marius Hills plateau, which encompass an area of approximately 35,000 km² and rises several hundred meters from the surrounding plains of Oceanus Procellarum; and Kant plateau, smaller in size, near the Apollo 16 landing site. Note that the massifs' locations presented in Fig. 3.67 are only those that have been recognized as such and named accordingly, although there are probably far more of them on the lunar surface; thus those sites should only be considered as examples of massifs and not as a comprehensive list.



Legend

▲ massif □ plateau

FIGURE 3.69 Locations of recognized lunar massifs and plateaus. Background: LOLA topography.



FIGURE 3.66 Locations of the red spots identified by Hagerty *et al.* (2006). All of the lunar red spots are located within the Procellarum KREEP Terrane (*cf.* Science Goal 3a), which is demarcated by the dashed white line. Note that Apennine Bench Formation, although associated with large exposures of Th-rich lithologies, is not classified as a red spot.

Sinuuous rilles

Sinuuous rilles are long channel-like structures on the lunar surface that have been supposed to be related to basaltic lava flows because they are usually observed in the lunar maria which are filled with basaltic rocks (Honda and Fujimura, 2005). Although rilles share many common characteristics, their basic parameters vary greatly, ranging from several kilometers in length and tens of meters in width and depth to

100's of kilometers in length, over a kilometer in width, and hundreds of meters in depth (Chen *et al.*, 2008). An illustration of sinuous rilles within the Aristarchus plateau is shown in Fig. 3.68. Their apparent variability may provide information on the chemical variability of the lunar lavas, and depending on the source material depth, rilles may also provide information on crustal and even mantle thickness and variability. However, even though the Apollo 15 mission was directed to Hadley Rille, no materials from the rilles themselves have been sampled by any missions.

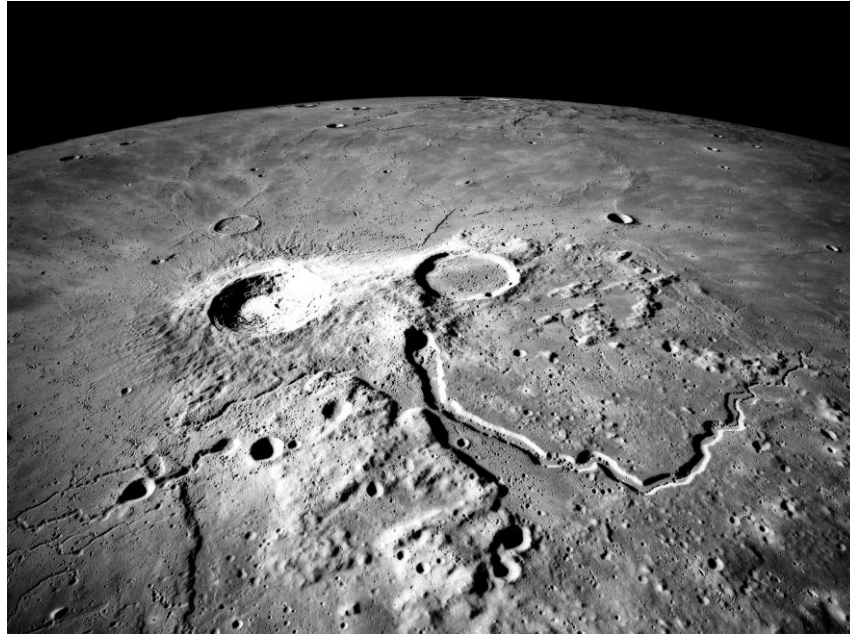


FIGURE 3.68 The Aristarchus plateau (about 200 km across) contains numerous sinuous rilles, the most important being Schröter's Valley (center right), a rille that is about 160 km long, up to 11 km wide and 1 km deep (Apollo 15 photo AS15-M-2610).

Requirements

Here are outlined three main requirements to ensure adequate site selections for Science Goal 3d:

- I. Target sites that demonstrate the small-scale diversity of crustal materials both laterally and vertically.
- II. Target young exposures and outcrops which may provide a window into the complex crustal lithology of a particular locale (*e.g.*, young crater walls, scarps, massifs, etc.).
- III. Target sites where instruments (*e.g.*, heat flow sensors, seismometers, etc.) can be placed to provide constraints on geophysical models.

Methodology

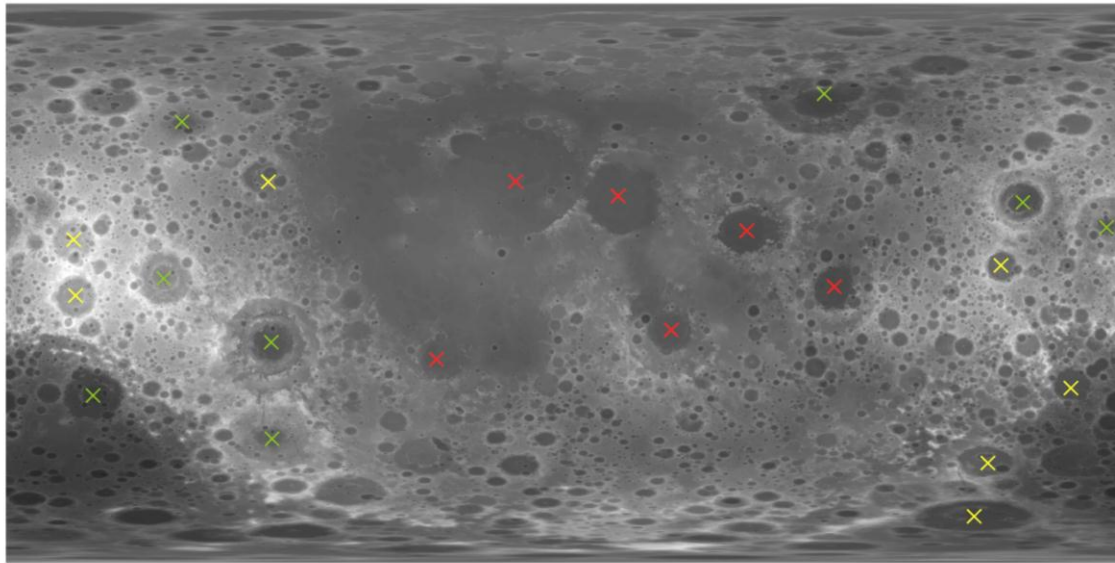
1. Locate areas of gravity anomalies as possible locations where we could set a geophysical experiment.
2. Locate areas of possible exposure of intrusive material to determine the size and extent of local features (plutons, laccolith, etc.).
3. Compile maps of young features, including young crater walls, and young central peaks.
4. Analyze high resolution spectral maps (Clementine RGB) to locate areas where craters have uncovered distinct lithology.
5. Utilize massifs, plateaus and sinuous rilles (and other tectonic cliffs) maps to observe complex region for areas of visible layering and outcropping.

Suggested landing sites

Suggested landing sites for geophysical experiments

In terms of crustal thickness and gravity mapping, setting geophysical apparatus at the extreme points of crustal thickness could yield precious data about the interior of the lunar crust, as well as sampling and subsequent analysis of materials that are present at these sites. Sampling, mapping, and setting up geophysical measurements (*e.g.*, heat flow, seismic reflection) on the surface of the different types of gravity anomalies (Type I and II, primary mascons; *cf.* Fig. 3.69 and Table 3.11) appears necessary to provide further constraints on models and hypotheses that have been made by remote sensing means only. Additionally, comparison of the possibly visible stratigraphy on walls of similar size but different types of anomalies (*e.g.*, primary mascon Humorum, Type I Mendeleev, Type II Mendel-Rydberg) could show layering differences that would better constrain crustal models.

Recent work by Kiefer (2009, and personal comm.) shows that small-scale gravity anomalies can also be used to infer geologically complex regions. For instance, two positive anomalies approximately 100 in size, located in the Marius Hill region, were interpreted as volcanic infiltration in the empty pore-space of the highland breccias. Small-scale positive anomalies were also identified on the edge of the Aristarchus plateau, and may indicate major displacement along multiple faults. These small-scale anomalies could be one of the best tools to assess the local complexity of the crust.



Legend

× primary mascon × basin with type I gravity anomaly × basin with type II gravity anomaly

FIGURE 3.69 Locations of the different types of gravity anomalies (from Namiki *et al.*, 2009 and Matsumoto *et al.*, 2010). Background: LOLA topography.

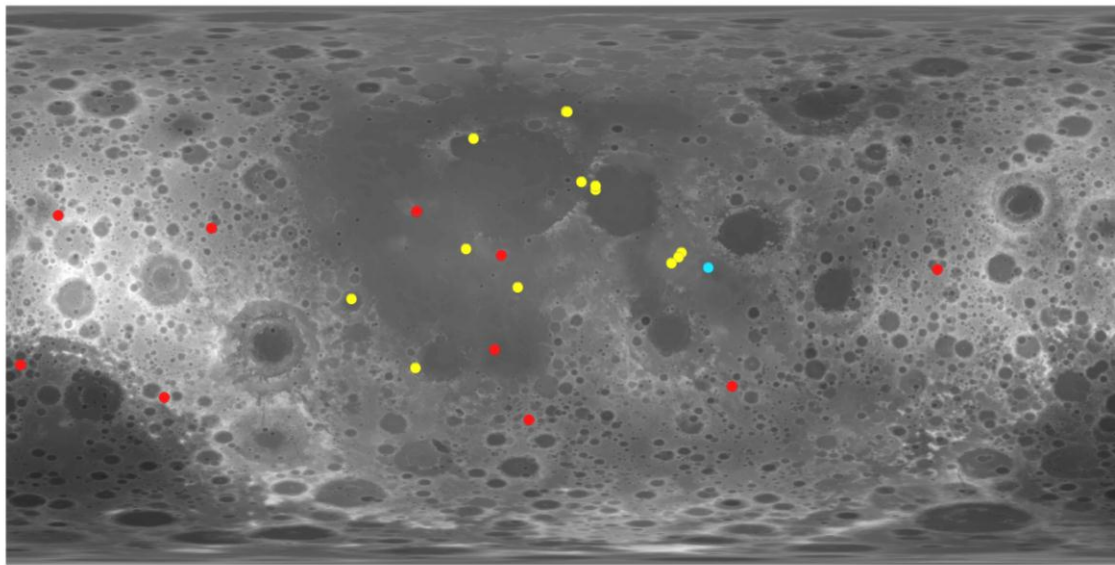
TABLE 3.11 Classifications of major impact basins. PN, N, and I indicate Pre-Nectarian, Nectarian, and Imbrian, respectively; PM, I, II, and NM indicate primary mascon, Type I, Type II, and nonmascon basins, respectively (from Namiki *et al.*, 2009 and Matsumoto *et al.*, 2010).

ID	Basin name	Center latitude	Center longitude	Diameter (km)	Age	Type
--	Crisium	17.0	59.1	418	N	PM
--	Humorum	-24.4	-38.6	389	N	PM
--	Imbrium	32.8	-15.6	1123	I	PM
--	Nectaris	-15.2	35.5	333	N	PM
--	Serenitatis	28.0	17.5	707	N	PM

--	Smythii	1.3	87.5	373	PN	PM
1	Planck	-57.5	135.5	325	PN	I
2	Ingenii	-34	163	325	PN	I
3	Lorentz	34	-97	365	PN	I
4	Dirichlet-Jackson	14	-158	470	PN	I
5	Mendeleev	6	141	365	N	I
6	Korolev	-4.5	-157	440	N	I
7	Schrodinger	-75	134	320	I	I
8	Apollo	-36	-151	480	PN	II
9	Coulomb-Sarton	52	-123	530	PN	II
10	Freundlich-Sharanov	18	175	600	PN	II
11	Moscovience	26	148	420	N	II
12	Mendel-Rydberg	-50	-94	420	N	II
13	Hertzprung	1.5	-128.5	570	N	II
14	Humboldtianum	61	84	700	N	II
15	Orientale	-20	-95	930	I	II
16	Birkoff	59	-147	330	PN	NM
17	Poincare	-57.5	162	340	PN	NM
18	Keeler-Heaviside	-10	162	780	PN	NM
19	Australe	-51.5	94.5	880	PN	NM

Suggested landing sites for intrusive features

Intrusive features are difficult to locate with remote sensing data, especially since high resolution gravity and spectroscopy data (which could be used to spot small scale features) have not yet been publicly released. Figure 3.70 presents probable locations of intrusive material exposures, namely plutons, laccoliths, and intrusive domes that have been reported in the literature.



Legend

● pluton ● laccolith ● intrusive dome

FIGURE 3.70 Map of the locations where intrusive features have been proposed in the literature. These are listed in associated Table 3.12. Background: LOLA topography.

Wohler *et al.* (2009, 2010) studied 13 candidate lunar intrusive domes (Table 3.12 and associated Fig. 3.70), which have been divided into three distinct morphometric classes, using a laccolith model to estimate the intrusion depth and the magma pressure. In-situ measurements of the internal geometric and magma properties of lunar laccoliths would provide very strong constraints on these models.

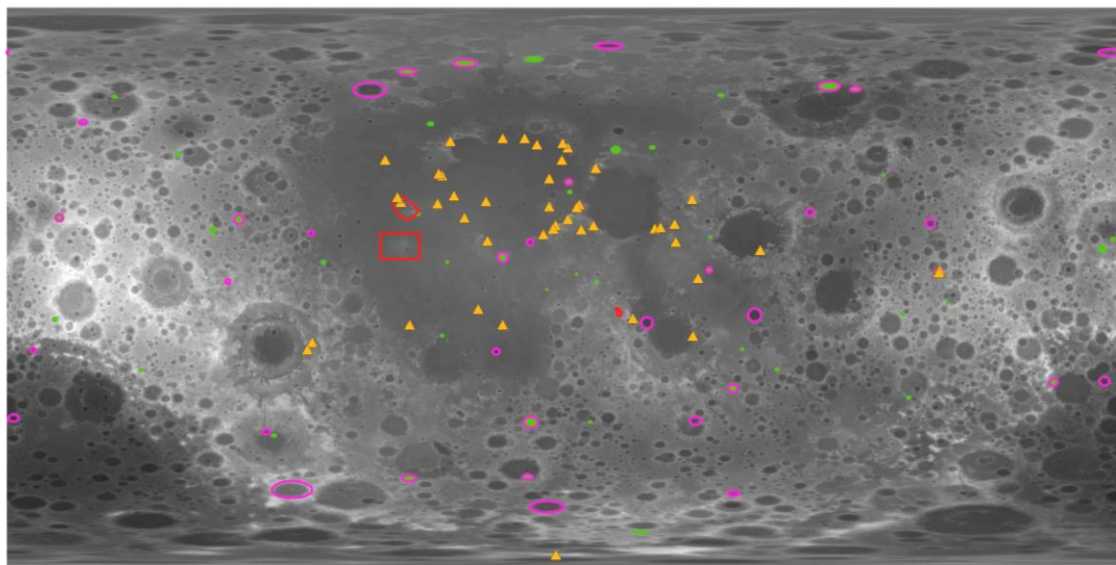
TABLE 3.12 List of the intrusive features that have been proposed in the literature.

Feature name	Feature type	Latitude	Longitude	Diameter (km)	References
Bulliadus	pluton	-20.70	-22.20	60	Pieters <i>et al.</i> , 1991
Copernicus	pluton	9.70	-20.10	93	Pieters <i>et al.</i> , 1991
Tycho	pluton	-43.40	-11.10	102	Pieters <i>et al.</i> , 1991; Tompkins, 1998
Aristarchus	pluton	23.70	-47.40	40	Pieters <i>et al.</i> , 1991
Jackson	pluton	22.40	-163.10	71	Tompkins, 1998
King	pluton	5.00	120.50	76	Tompkins, 1998
Langmuir	pluton	-36.20	-128.73	91	Tompkins, 1998
Orlov	pluton	-26.13	-175.37	81	Tompkins, 1998
Ohm	pluton	18.40	-11.50	64	Tompkins, 1998
Stevinus	pluton	-32.5	54.20	74	Tompkins, 1998
Taruntius	laccolith	5.60	46.50	56	Wichman and Schultz, 1996
Grimaldi 1	intrusive dome	-4.45	-68.62	36x24	Wohler <i>et al.</i> , 2010
Aristillus 1	intrusive dome	33.28	5.67	54x35	Wohler <i>et al.</i> , 2010
Gambert	intrusive dome	-0.75	-14.84	30	Wohler <i>et al.</i> , 2009

Feature name	Feature type	Latitude	Longitude	Diameter (km)	References
Valentine dome	intrusive dome	30.7	10.2	30	Wohler <i>et al.</i> , 2009
Milichius	intrusive dome	11.68	-31.53	27.8	Wohler <i>et al.</i> , 2009
Archytas	intrusive dome	55.71	0.71	33	Wohler <i>et al.</i> , 2009
Archytas	intrusive dome	55.71	1.05	16	Wohler <i>et al.</i> , 2009
Rima Cauchy	intrusive dome	11.06	36.75	12.2	Wohler <i>et al.</i> , 2009
Palmieri	intrusive dome	-26.63	-47.88	13.5	Wohler <i>et al.</i> , 2009
Promontorium Laplace in Sinus Iridum	intrusive dome	47.08	-29.16	10	Wohler <i>et al.</i> , 2009
Smaller dome close to Valentine dome	intrusive dome	31.89	10.26	11	Wohler <i>et al.</i> , 2009
Central Mare Tranquillitatis plains	intrusive dome	7.06	34.66	13.3	Wohler <i>et al.</i> , 2009
Rupes Cauchy	intrusive dome	10	35.19	19.2	Wohler <i>et al.</i> , 2009

Suggested landing sites for fresh outcrops

Sites that contain scarps or large massifs could reveal lithological layering, possibly exposing bedrock. Similarly, fresh crater walls or fresh crater central peaks in particular may provide an insight into the depth and extent of such features, as they have not been altered or covered by layers of regolith. Using the Lunar Impact Crater Database, Copernican and Eratosthenian craters with well-preserved central peaks and Copernican craters walls have been mapped as potential interesting sites. Figure 3.71 provides a combined map of all these young features with the plateaus and massif identified in the literature (*cf.* Fig. 3.67).



Legend

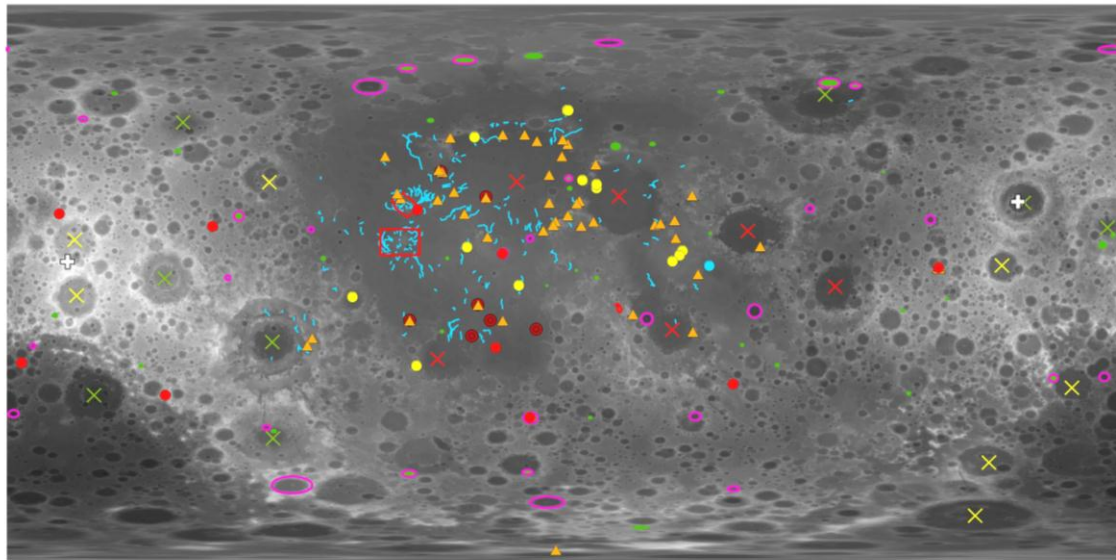
- ▲ massif
- ▭ plateau
- Copernican and Eratosthenian craters with central peak
- Copernican craters

FIGURE 3.71 Locations of fresh outcrops (central peaks or walls of craters) and other complex outcrops (plateaus and massifs) where the crustal material should be exposed on a certain height, and allow estimates of the upper crust complexity on a layer scale. Background: LOLA topography.

Suggested landing sites for the entire Science Goal 3d

Figure 3.72 presents all the features of interest for addressing Science Goal 3d. Sites that present large vertical exposures and show diversity in the Clementine RGB maps are prioritized (*e.g.*, Copernicus, Aristarchus [Fig. 3.73], etc.). Plutonic intrusions are of great interest, but since their detection are based on Clementine low-resolution multispectral mode data, these detections should be confirmed with new high-resolution spectral imagers, such as M³ on Chandrayaan 1, or SP on Kaguya.

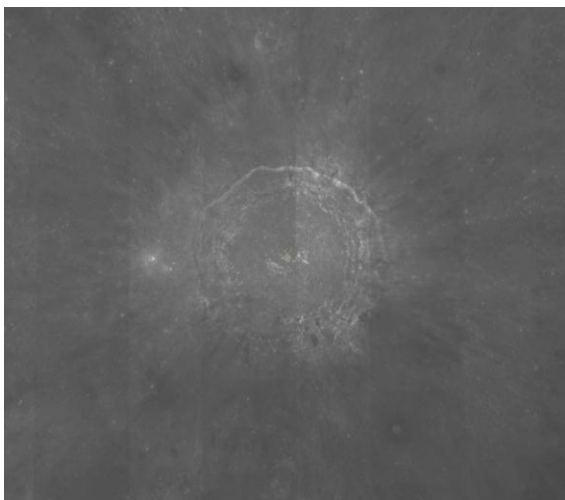
A compiled list of all the suggested landing sites to address Science Goal 3d can be found in Table A3.10.



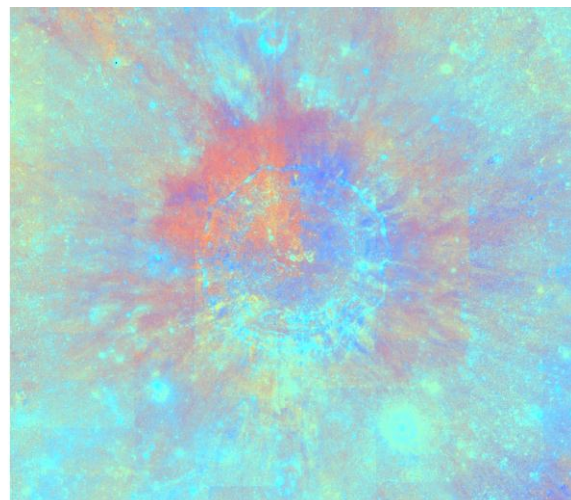
Legend

- | | |
|------------------|--|
| ● pluton | + crustal thickness extreme |
| ● laccolith | × primary mascon |
| ● intrusive dome | × basin with type I gravity anomaly |
| ▲ massif | × basin with type II gravity anomaly |
| □ plateau | □ Copernican and Eratosthenian craters with central peak |
| ● red spot | ■ Copernican craters |
| — sinuous rilles | |

FIGURE 3.72 Integrated map of all the features of interest for addressing Science Goal 3d. Background: LOLA topography.



Clementine 750 nm grayscale basemap



Clementine RGB composite, global mosaic

FIGURE 3.73 Clementine observations of Copernicus Crater (diameter = 93 km). Left: 750 nm filter grayscale image, right: Clementine RGB composite, showing composition variations between the northwestern wall of Copernicus and the other walls (note that they appear similar on the grayscale image). Copernicus is therefore a good example of the complexity of the lunar crust at a local scale.

SCIENCE GOAL 3E: DETERMINE THE VERTICAL EXTENT AND STRUCTURE OF THE MEGAREGOLITH

Introduction

The lunar megaregolith is thought to be the product of the relatively short-lived Late Heavy Bombardment (LHB), or lunar cataclysm, early on in the moon's geological history (Hartmann, 1973). The large impacts responsible for the formation of the lunar basins would have excavated, mixed and fractured the lunar surface to a potential depth of several kilometers. This layer of the crust has been defined by several researchers as the highly fragmented layer, composed of basin ejecta, that is directly above the fractured bedrock (Figs. 3.74 and 3.61). Later, smaller meteoroid impacts (post-LHB) would have pulverized and mixed the very top layer of the crust (the regolith) but would have had a negligible effect on the overall structure of the megaregolith (Hartmann, 1973; Head, 1976). The evolution of surface regolith is addressed in Science Concept 7.

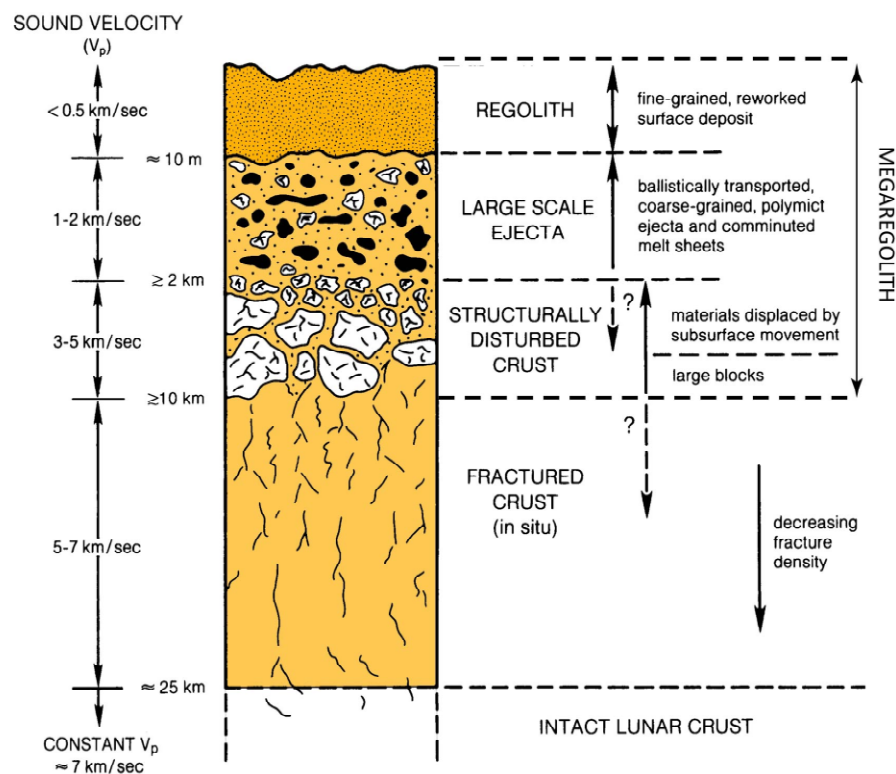


FIGURE 3.74 Schematic cross-section illustrating the effects of large-scale cratering on the upper lunar crust. The megaregolith layer extends from the upper finer-grained regolith downward to the top of the fractured, in-situ crust, with an estimated thickness of tens of kilometers. Seismic velocities are from Tököz *et al.*, (1973). Figure modified slightly from Hörz *et al.*, (1991; Lunar Surface Processes, in The Lunar Sourcebook, pp.62-120).

A more thorough understanding of the megaregolith is critical for various reasons:

It will provide information about the existence and extent of the Late Heavy Bombardment. The megaregolith is thought to be a direct consequence of the basin formation impact events. Measurements of its absolute thickness at various locations on the Moon could provide key information on the occurrence and intensity of the LHB. Also, understanding megaregolith evolution as a process that can bias sampling could indicate if the spike of ages seen in the Apollo and meteorite samples corresponds to the LHB or is simply a result of sampling bias (Chapman, 2007). The notion of the LHB is in part derived from that age spike (Tera *et al.*, 1974).

It will allow better understanding of megaregolith formation and evolution on other terrestrial bodies and on the early Earth. Megaregolith formation and evolution is not a process unique to the Moon. A highly fractured top surface layer will occur on any planetary object subjected to impact cratering, as long as no other geologic processes recycle the top layer (as plate tectonics on Earth). However, the lunar megaregolith is unique in the sense that it has been preserved intact for most of the Moon's geological history.

It will provide means to better analyze the current (and potentially, future) seismic data and, in turn, provide a better understanding of the subsurface structure of the Moon. The seismic data collected by the four Apollo seismometers is significantly affected by the megaregolith layer. The large number of 'seismic boundaries' in the layer (e.g., contacts between different ejecta components) act as seismic refractors and reflectors and are responsible for noise in the resulting signal (Latham, 1972). A better understanding of the megaregolith and its effects on seismic waves is essential to fully comprehend and benefit from the Apollo and future seismic data.

It will provide important constraints on the thermal evolution of the Moon. The porous megaregolith layer acts as a thick insulating blanket and could have significantly slowed down the Moon's cooling. The variable thickness of the megaregolith could potentially explain the difference in heat flow between Apollo station 15 and 17 (Warren, 1987). Also, the presence of the megaregolith layer could have kept the Moon's interior hot enough to explain very young volcanism on the Near Side basins (e.g., Ziethe, 2009). Absolute values of vertical extent and information on the structure of the megaregolith would provide important constraints for thermal evolution models.

Background

The first evidence of a highly fractured surface layer came from seismic data collected during the Apollo Passive Seismic Experiment (1969–1977). The data showed intense scattering that is not characteristic of coherent crystalline rock in the upper 2–3 km, and especially in the upper 100 m or so (Latham, 1972). This intense scattering is represented in the seismic data by a very long-lived quake signal that is atypical of terrestrial earthquake recordings (Fig. 3.75). However, the quality of the seismic dataset has not yet allowed for a precise measurement of the megaregolith thickness.

Short and Forman (1972) used an empirical model estimating ejecta blanket thickness as a function of the distance to the center of an impact crater to estimate an average thickness of the megaregolith. Their results suggest a thickness ranging between 0.74 and 8.00 km, with best estimate values between 1.36 and 2.39 km. Hartmann (1973) used models of the rate of pre-mare regolith production to calculate that the thickness of the megaregolith under the oldest highlands regions should be of the order 2 km, while the mare could have hundreds of meters of regolith between the surface and the bottom of the mare. He estimated that the thickness of the sub-surface regolith in the maria probably depends on the timing of the last flow (e.g., Oceanus Procellarum has a larger mean megaregolith thickness than Imbrium, which has a younger surface). Other researchers have also attempted to constrain the thickness of the megaregolith, with results ranging between a few hundred meters to around 11 km (McGetchin, 1973; Pike, 1974; Hörz *et al.*, 1976; Housen, 1983; Petro and Pieters, 2004; Petro and Pieters 2008).

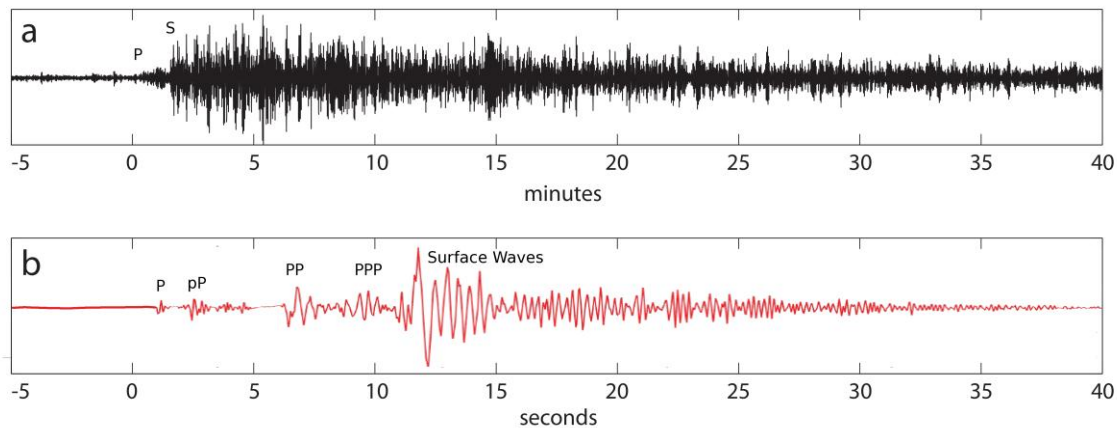


FIGURE 3.75 Comparison between a good quality moonquake (a) and a typical earthquake signal (b), with phase arrival examples. Note how only the P- and S-phases are visible on the moonquake signal. All other phases are lost in the noisy coda. Also, the duration of the moonquake signal is much longer (>40 minutes) than the duration of the typical earthquake (~40 seconds). This long coda is suggested to be a consequence of a thick, fractured surface layer.

Another approach is to estimate upper and lower boundaries of megaregolith thickness by analyzing radar and optical data (*e.g.*, Shkuratov, 2001; Thomson, 2009). Thomson *et al.*, (1974, 1979, 1980) calculated a megaregolith thickness of 1.2 km in the highlands directly south of the major near side basins based on radar and infrared temperature maps. Such images can differentiate between ejecta made up of large-sized boulders (radar-bright, where the large blocks are assumed to come from the underlying bedrock) from ejecta made up of the more fine-grained material component of the megaregolith (less bright; see Fig. 3.76 for an example). The transition between the two types of ejecta occurs at a crater diameter of approximately 12 km (which is equivalent to 1.2 km excavation depth based on Pike 1977, 1980). Thomson *et al.*, 2009 used 70-cm-wavelength radar images of the Moon to detect an increase in the megaregolith thickness of about 1 km from directly south of Mare Humorum to close to the South Pole (Fig. 3.76).

All available estimates on the thickness of the megaregolith layer are based either on models of cratering processes or on orbital data. Current estimates are 1-2 km for the near side mare region, 5-10 km for the highlands and 1-2 km for the South Pole-Aitken region. The thickest megaregolith should be found at the margins of the major basins, because this is where most ejecta was deposited (Mcgetchin, 1973). High-quality absolute thickness measurements at several locations on the lunar surface is essential to validate, previous estimates and to constrain geophysical models of the Moon's evolution. The next sections outline target sites requirements for such measurements and suggest landing sites based on those requirements and on the currently available lunar datasets.

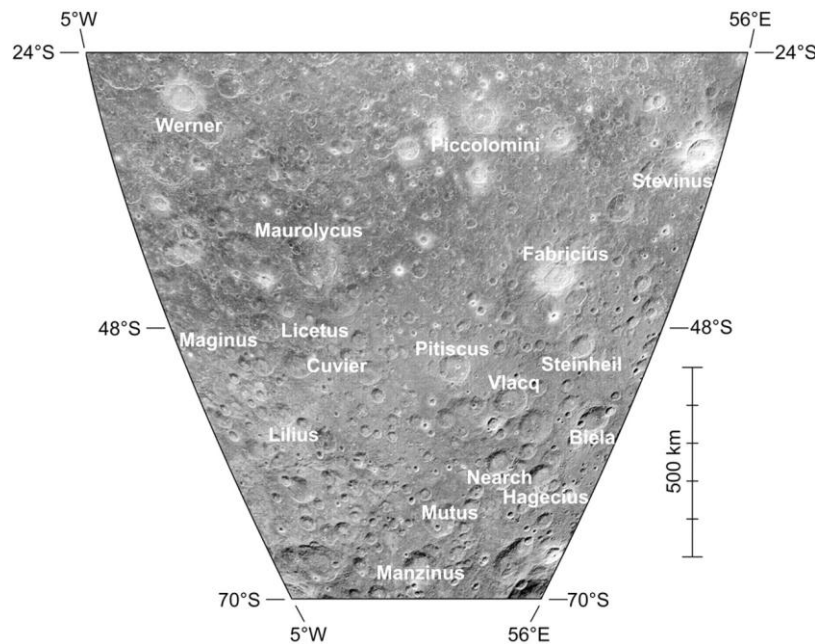


FIGURE 3.76 Southern highlands, 70 cm radar view. Image area is 5°W-56°E, 24-70°S in sinusoidal equal-area map projection. This is an example of a potentially increasing megaregolith thickness toward the south of the image. There is a lack of bright haloes centered on around larger craters in the South, contrarily to the North. This is explained by the fact that same-sized impacts in the North extruded coarser material (bedrock) than in the South (finer grained megaregolith material). (From Thomson *et al.*, 2009).

Requirements

Two requirements were identified in order to achieve Science Goal 3e:

- I. Target sites that will allow for in situ visual and/or geophysical measurement of the extent and structure of the megaregolith.
- II. Target enough sites to collect measurements from the three main regions of the Moon (Nearside Mare, Highlands, South Pole-Aitken).

Methodology

Four different approaches to identify landing sites that satisfy the above requirements have been identified, and are described below.

Installation of a seismometer network on the lunar surface

It is suggested to install a global network of seismometers in order to get precise measurements of the absolute thickness of the megaregolith layer at various locations on the Moon.

However, even with good seismic data, it might be difficult to differentiate between the thickness of the megaregolith layer and the extent of the thicker layer that includes the megaregolith and the fractured crust (refer to Fig. 3.74) as both layers act as strongly scattering structures.

We will not identify the best locations for those geophysical stations here; other missions that are currently under study deal specifically with those issues (e.g., NASA's International Lunar Network¹). However, we recommended installing seismometers over at least the three main geochemical regions of the Moon: the nearside mare region, the highlands, and the South Pole-Aitken.

¹ For more information: <http://science.nasa.gov/missions/iln/>.

Investigation of the central peaks of young and fresh complex craters that have an estimated stratigraphic uplift greater than the estimated megaregolith thickness

The central peak of complex craters is composed of material that comes from deep below the center of the crater (Fig. 3.77). The magnitude of the structural uplift can be estimated using the empirical relation derived by Cintala and Grieve (1998):

$$u_s = 0.022D^{1.45} \quad (3.7)$$

where D is the rim diameter in kilometers and u_s is the estimated structural uplift beneath the central peak in kilometers. By targeting deep craters for which the estimated structural uplift is greater than the estimated megaregolith thickness (1–2 km for maria, 5–10 km for highlands, 1–2 km for SPA), it should be possible to investigate and characterize the structure and composition of deeper levels of the megaregolith. This information could be used along with other measurements (*e.g.*, seismic data) to obtain a more accurate megaregolith thickness.

To be selected, a complex crater has to fit several criteria:

1. Its age has to be either Copernican, Eratosthenian or Upper Imbrian.
 - The megaregolith is a product of basin forming impacts. Only craters that formed *after* the last basin (Orientale) can constrain the layer's overall thickness.
 - The younger the crater, the fresher the central peak and the thinner the surficial regolith layer (this might matter for central peaks with gentler slopes).
2. Its estimated central peak structural uplift must be at least 5 km more than the maximum estimated megaregolith thickness in a given region. This is approximately 7 km in the Nearside Mare region and SPA (equivalent to a crater diameter of approximately 53 km), and at least 15 km in the highlands (equivalent to a crater diameter of approximately 90 km).
 - Only craters with the potential to uplift material from below the base of the megaregolith layer should be targeted.
 - The value of +5 km is somewhat arbitrary, based on both the uncertainty of the thickness estimates and on the uncertainty of the stratigraphic uplift equation.
3. The central peak must be visible on an elevation profile made with the LOLA altimetry data (64 pixels per degree resolution).

Only craters from the Lunar Impact Crater Database were examined here, although other craters that satisfy the criteria above could also be targeted.

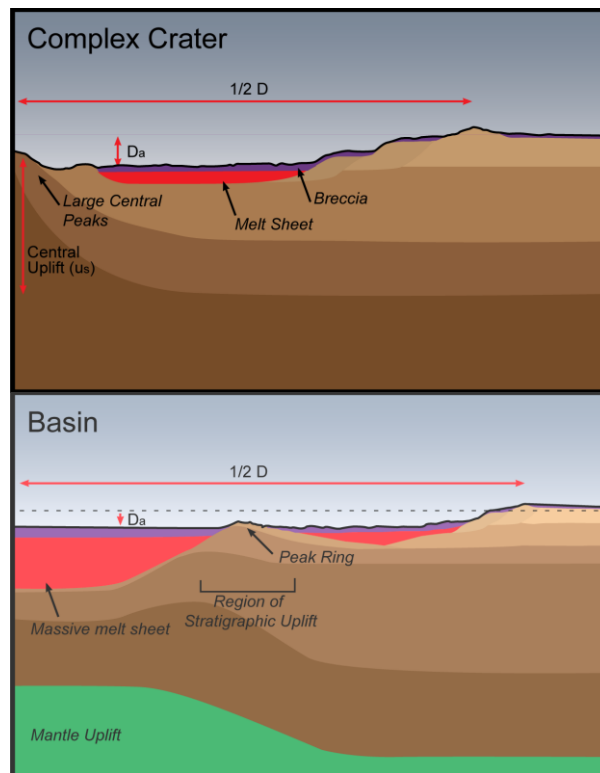


FIGURE 3.77 Schematic cross-section of complex and basin impact structures. u_s corresponds to the structural uplift, which is in the central peak for the complex crater and in the peak ring for the basin. (Image is modified from Fig. 3.10)

Geological mapping of the walls or peak rings of the youngest multi-ring basins

Multi-ring basins are the largest structures on the Moon. The mechanisms of basin formation, as well as their final lateral and vertical structures are poorly understood. However, analysis of seismic and gravity data from the Chicxulub crater on Earth (best terrestrial multi-ring basin analog) suggests that the peak rings are made of brecciated and altered central peak material (Morgan *et al.*, 2000). Also, spectral analysis of the peak rings of Orientale, the youngest lunar basin, suggests they are composed of material coming from deep (Bussey and Spudis, 2000), hinting to a structural uplift similar to the one occurring in the central peak of complex craters (Fig. 3.77). Thus, an investigation of the peak ring composition and structure of multi-ring basins might yield information concerning the megaregolith properties, as would an investigation of the central peaks of large craters. Also, the final depth of some the largest basins could actually be deep enough to penetrate through the megaregolith layer and show the total extent of the layer, along with the top of the fractured crust layer, on the basin walls.

It is suggested that a geological map of the basins' walls and peak rings would be a useful way to determine the thickness and structure of the megaregolith. However, because the megaregolith is a product of the basin forming impact events, only the youngest basins in a particular region should be targeted.

To be selected, a multi-ring basin must fit the following criteria:

1. It has to be relatively young.
 - Because most of the megaregolith material is thought to be ejecta from the basin forming events, only the latest basin will have impacted a mature megaregolith.
 - Young basins will be less likely to be covered in ejecta from other impact events.
2. It has to have well-defined features that have undergone minimal erosion due to subsequent impacts.

- Even the youngest basins are more than 3.8 Ga (Wilhelms, 1987). However, walls and rings of some basins are large and prominent and have not been altered to a great extent with time (*e.g.* Orientale basin).

Geological mapping of the walls of deep Copernican craters

The final depth of some very young craters (Copernican, with well-preserved features) is larger than the minimum estimate of megaregolith thickness over a particular region. Those sites are of interest as the craters' walls might directly show the transition between the megaregolith and the in-situ fractured crust.

The apparent depth of all craters in the Lunar Impact Crater Database was calculated using the LOLA 64 ppd grid. The depth was simply the difference between the highest and the lowest points in a circle centered on the crater and with a radius of 1.25 times the radius of the crater.

To be selected, a young and deep crater has to fit several criteria:

1. It has to be Copernican in age.
2. Its apparent depth need to be larger then the minimum megaregolith thickness estimate for the region where it is located (1 km for the mare region and SPAT and 5 km for the highlands).

Suggested landing sites

Investigation of the central peaks of young and fresh complex craters that have an estimated stratigraphic uplift greater than the estimated megaregolith thickness

Twenty six complex craters satisfied all the criteria and requirements from the above sections. These are presented in Fig. 3.78 below. The figure also shows non-labeled craters for which the uplift is more than the estimated megaregolith thickness, but not within the uncertainty of +5 km that we use as a requirement.

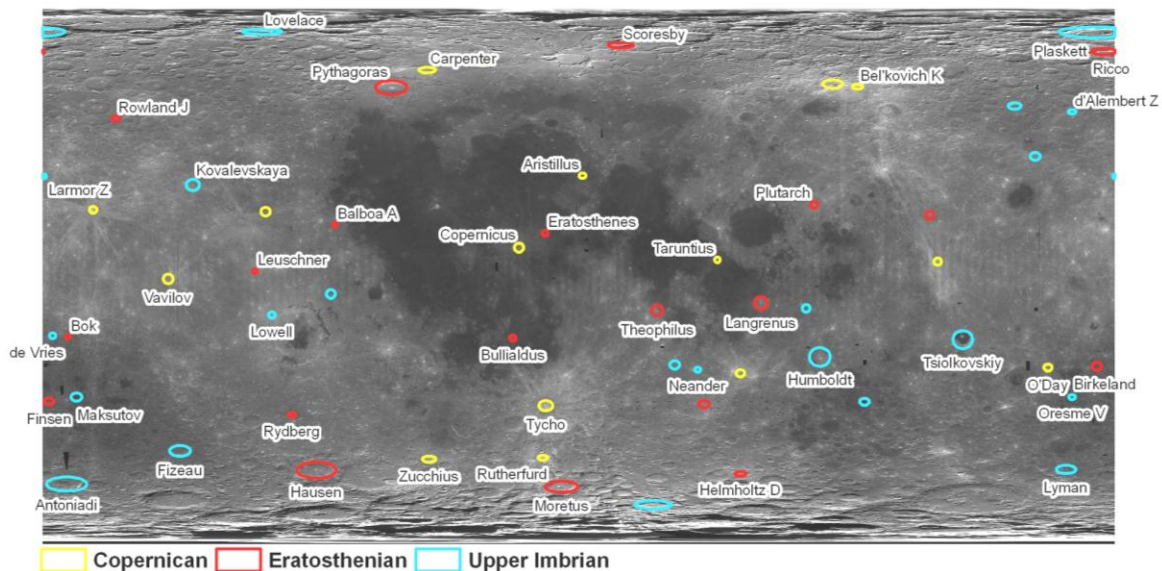


FIGURE 3.78 Spatial distribution of all 26 complex craters selected for Science Goal 3e. The yellow craters are Copernican in age, the red ones are Eratosthenian and the blue ones are Upper Imbrian. The non-labeled features are craters for which the structural uplift is more than the estimated megaregolith thickness, but not more than the +5km uncertainty. A table listing the coordinates, diameter, age and magnitude of stratigraphic uplift for all these craters can be found in Table A3.11. Background is global 750 nm albedo Clementine map.

Geological mapping of the walls or peak rings of the youngest multi-ring basins

We select only well-defined basins that are younger than the large Imbrium impact structure. Imbrium is the second largest impact basin, after South Pole-Aitken, and near side ejecta originating from the Imbrium impact has been estimated to be hundreds of meters thick (McGetchin 1973; Petro and Pieters, 2008). Figure 3.79 shows the location of all major basin structures identified by Wilhelms (1987). The number in brackets below the basin names indicate the relative ages (0 is oldest, 42 is youngest). Other large surface features have been proposed to be basins, but those features are ill defined and would not be part of our selection even if they become confirmed basins. Only two basins are younger than Imbrium: Schrödinger and Orientale. Those two basins have well-defined walls and peak rings and are thus selected among our final recommended landing sites.

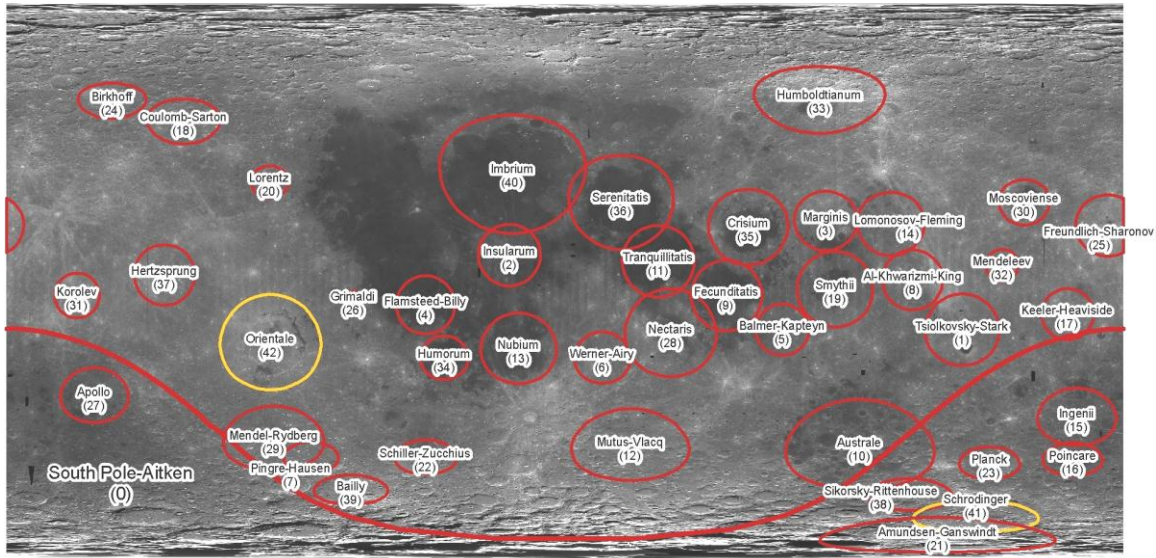


FIGURE 3.79 Spatial distribution of the large impact structures identified as basin by Wilhelms (1987). The numbers in brackets indicate their relative ages, with 0 being the oldest, and 42 the youngest. Orientale and Schrödinger basins are identified in yellow. Those two are the suggested landing sites where geological mapping of the walls and peak rings might yield information about the megaregolith properties. Background is global 750 nm albedo Clementine map.

Geological mapping of the walls of deep Copernican craters

Figure 3.80 shows the craters that satisfy the criteria detailed in the previous section. Interestingly, some of those craters were also selected as craters for which the stratigraphic uplift in the central peak was greater than the estimated megaregolith thickness (Aristillus, Copernicus and Taruntius in the nearside mare region; Bel'kovich K, Carpenter, Rutherford, Tycho and Zucchi in the highlands; O'Day in the South Pole-Aitken Region).

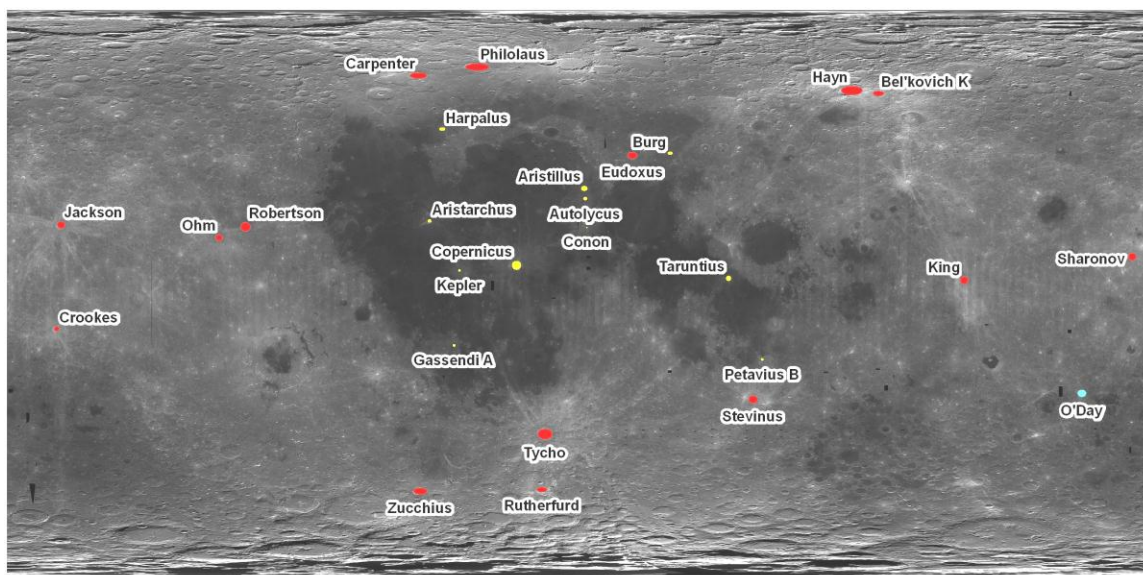


FIGURE 3.80 Spatial distribution of young craters that potentially show the transition between the megaregolith layer and the underlying fractured crust. It is proposed that a geological map of the walls of those craters will yield information of the megaregolith properties. All the craters are Copernican in age. The yellow and blue ones have a final depth greater than 1 km (minimum estimate for megaregolith thickness in the nearside mare and South Pole-Aitken regions). The red ones have depth greater than 5 km (minimum estimate for megaregolith thickness in the highlands). The craters coordinates and apparent depths are listed in Table A3.12. Background is global 750 nm albedo Clementine map.

SUGGESTED LANDING SITES AND CASE STUDIES

This section focuses on some specific landing sites which would maximize the science return relevant to multiple goals within Science Concept 3.

Landing Site Database

After thorough analysis of Science Concept 3 Science Goals, we have assembled an extensive list of possible lunar landing sites where those goals can be achieved. The preferred locations are listed in Table 3.13, outlining the top fourteen choices for sample return, along with the latitude, longitude, diameter, and geochemical terrane. These areas were chosen to obtain a wide array of samples, adhering to the following criteria:

- *Geochemical Diversity:* Select representative sites from each of the three geochemical terranes; *i.e.* the Procellarum KREEP Terrane (PKT), the South Pole-Aitken Terrane (SPAT), and the Feldspathic Highlands Terrane (FHT).
- *Geographical Diversity:* Select sites that are geographically distributed on the lunar surface, as many crustal features vary from the nearside to farside (*e.g.*, crustal thickness, mare flooding).
- *Chronological Diversity:* Select sites of various chronologic and stratigraphic ages.
- *Lithological Diversity:* Select sites that may sample a large variety of rock types, to help complete the lunar sample collection.

A comprehensive list of landing sites from each Science Goal is presented in Table A3.13.

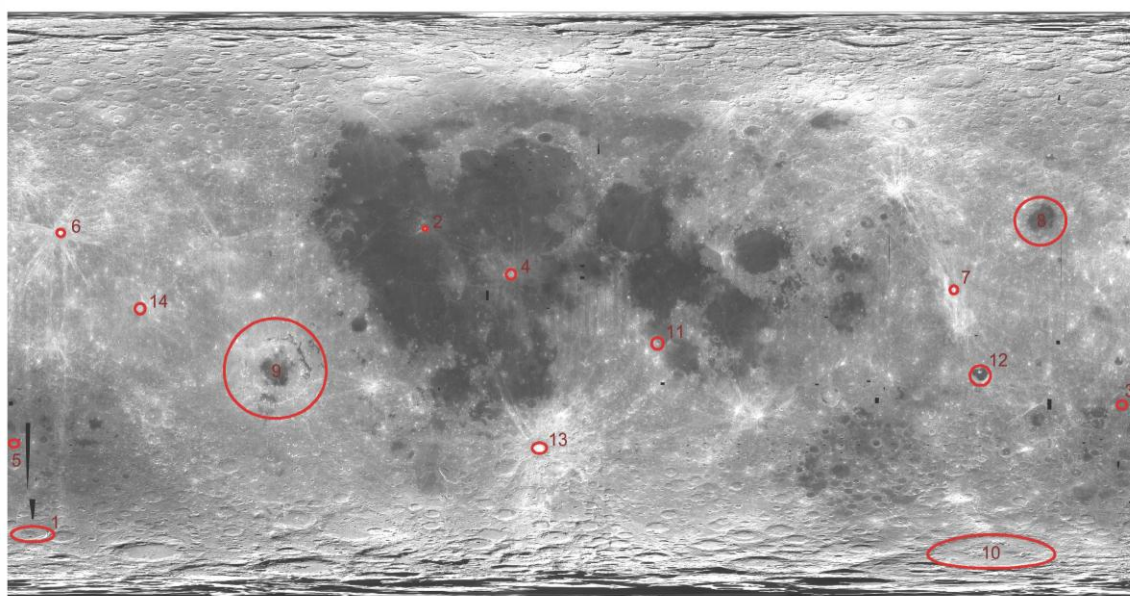


FIGURE 3.81 Map depicting the preferred 14 landing sites for Science Concept 3. Craters are numbered in alphabetical order, corresponding to Table 3.13. Background image: Clementine albedo map.

TABLE 3.13 List of some preferred landing sites, providing a diverse range of samples.

ID	Crater Name	Lat (°)	Long (°)	Diameter (km)	Region
1	Antoniadi	-69.7	-172.0	143.0	SPAT
2	Aristarchus	23.70	-47.40	40.00	PKT
3	Birkeland	-30.20	173.90	82.00	SPAT
4	Copernicus	9.70	-20.10	93.00	PKT
5	Finsen	-42.00	-177.90	72.00	SPAT
6	Jackson	22.4	-163.1	71.0	FHTa
7	King	5.00	120.50	76.00	FHTa
8	Moscoviense	26.0	148.0	445.0	FHTa
9	Oriente	-19.0	-95.0	930.0	FHTo
10	Schrödinger	-75.00	132.40	312.00	SPAT
11	Theophilus	-11.40	26.40	110.00	FHTo
12	Tsiolkovsky	-21.2	128.9	185.0	FHTa
13	Tycho	-43.4	-11.1	102.0	FHTo
14	Vavilov	-0.80	-137.90	98.00	FHTa

Outlined below are the preferred 14 landing sites that could help in achieving three or more of the science Goals within Science Concept 3. Science Goal 3b can be assessed in any of these sites as they expose different rock types, and are all craters where different types of breccias could be sampled. But Science Goal 3b might be more completed in sites containing pyroclastics or mare materials. Within the brackets following the feature name are listed in order the center latitude, center longitude, final rim-to-rim diameter in km, the age described in terms of chronostratigraphy, and the geochemical terrane encompassing the feature; the sites are listed in alphabetical order.

Antoniadi (69.7°S, 172°W, 143km, Upper Imbrian, SPAT)

Landing at Antoniadi crater and collecting samples would satisfy Science Goals 3a, b, c, and e. For Science Goal 3a, this site could be used for sampling the urKREEP layer and possibly mantle material (the crater's proximity to the crust-mantle boundary is within the -5km error bar). Considering Science Goal 3c, the lower crust can be sampled in the ejecta blanket and the lower crust and mantle can be sampled in central peak. For Science Goal 3e, the structural uplift in central peak might show the transition between megaregolith and fractured crustal bedrock.

Aristarchus crater (23.7°N, 47.4°W, 40km, Copernican, PKT)

Landing at Aristarchus crater and collecting samples would satisfy Science Goals 3a, b, d, and e. For 3a and 3b, it might be possible to sample pure anorthosite (PAN), H5 highland type material and KREEP-rich material at this site. In terms of Science Goal 3b specifically, it may be possible to sample M2, M3, the youngest mare type materials, and pyroclastic deposits on and around the plateau, but not inside the crater. The location of this crater on the edge of the geologically diverse Aristarchus plateau and the presence of a young central peak make it an interesting target to study regional and local complexity of the crust relevant to Science Goal 3d. In addition, there might be possible exposures of plutons/intrusive material in the central peak of Aristarchus crater. For Science Goal 3e, the transition between megaregolith and fractured crustal bedrock might be visible in the walls of this young crater. Please refer to the Aristarchus case study in section 3.9.2 for a more detailed overview.

Birkeland (30.2°S, 173.9°E, 82km, Eratosthenian, SPAT)

Landing at Birkeland crater and collecting samples would satisfy Science Goals 3a, b, c, d, and e. This site would be useful for Science Goal 3b since we might be able to sample M5 mare type here. For Science Goal 3a and c, lower crustal material can be sampled in the central peak of this crater. Birkeland has a young central peak which is a good landing site for 3d. For Science Goal 3e, the structural uplift in the central peak might show the transition between megaregolith and fractured crustal bedrock. Birkeland would be a representative crater of the SPAT.

Copernicus (9.7°N, 20.1°W, 93km, Copernican, PKT)

Landing at Copernicus crater and collecting samples would satisfy Science Goals 3a, b, d, and e. It would be useful for Science Goal 3a since we could sample KREEP-rich material and H4 highland-type material here. For Science Goal 3b, there may be cryptomare in the ejecta blanket that could be sampled. The possible exposures of plutons/intrusive material in the young central peak and the spectral complexity based on Clementine UVVIS ratio maps and recent olivine detections make the Copernicus crater a very attractive target for Science Goal 3d. For 3e, the structural uplift in central peak might show the transition between megaregolith and fractured crustal bedrock.

Finsen (42°S, 177.9°W, 72km, Eratosthenian, SPAT)

Landing at Finsen crater and collecting samples would satisfy Science Goals b, c, d, and e. For Science Goal 3b, M5 mare type might be sampled at this site. The site is good for fulfilling Science Goal 3c since it might be possible to sample lower crust material in the central peak of the crater. Finsen has a young central peak which is a good landing site for 3d. Considering Science Goal 3e, structural uplift in the central peak might show the transition between megaregolith and fractured crustal bedrock. In addition, Finsen would also be a representative crater from the SPAT.

Jackson (22.4°N, 163.1°W, 71km, Copernican, FHTa)

Landing at Jackson crater and collecting samples would satisfy Science Goals 3a, b, d, and e. The site is good for Science Goal 3a since it might be possible to sample primary feldspathic crust here. Pure anorthosite (PAN) can also be sampled at this site, which is relevant for both Science Goals 3a and 3b. For Science Goal 3d, there might be possible exposures of plutons/intrusive material in the young central peak. For Science Goal 3e, the structural uplift in central peak might show the transition between megaregolith and fractured crustal bedrock. Please refer to the Jackson case study in section 3.9.2 for a more detailed overview.

King (5°N, 120.5°E, 76km, Copernican, FHTa)

Landing at King crater and collecting samples would satisfy Science Goals 3a, b, d, and e. The site satisfies Science Goals 3a and 3b since it might be possible to sample pure anorthosite (PAN) here. In terms of Science Goal 3d, there might be possible exposures of plutons/intrusive material in the young central peak and/or in the walls of the surrounding massifs. For Science Goal 3e, the structural uplift in central peak might show the transition between megaregolith and fractured crustal bedrock.

Moscoviense (26°N, 148°E, 445km, Nectarian, FHTa)

Landing at Moscoviense and collecting samples would satisfy Science Goals 3a, b, c, and d. The site would be useful for fulfilling Science Goal 3a since mantle material can be sampled in the peak rings and the region shows a weaker Th signature than expected and could thus be used to test the global nature of the KREEP layer. Considering Science Goal 3b, the site is interesting since it could be used for sampling M4 mare type, mare of different ages, pyroclastic deposits, and the newly detected spinel lithology. For Science Goal 3c, lower crust and mantle material can be sampled in the peak rings. Multiple olivine detections in and around the peak rings of Moscoviense could confirm that mantle material is exposed there. In terms of Science Goal 3d, the region is a Type II gravity anomaly and is close to an area with the thinnest crust according to the recent Kaguya results. Thus, this location could be one of the potential sites for setting up geophysical instruments like seismometers.

Orientale (19°S, 95°W, 930km, Lower Imbrian, FHTo)

Landing at Orientale and collecting samples would satisfy Science Goals 3a, b, c, d, and e. The site would be useful for fulfilling Science Goal 3a since it might be possible to sample pure anorthosite (PAN) here and mantle material in the peak rings. Another factor that makes the site relevant for Science Goal 3a is that the region shows a weaker Th signature than expected and could thus be used to test the global nature of the KREEP layer. For Science Goal 3b, pyroclastic deposits, and the old mare within the basin might be sampled. The presence of dark-haloed craters may also be indicative of the presence of cryptomare. Considering Science Goal 3c, lower crust can be sampled in the ejecta blanket and lower crust and mantle should be present in the peak rings of the crater. In terms of Science Goal 3d, the region is a Type II gravity anomaly and could thus be one of the potential sites for setting up geophysical instruments like seismometers. For Science Goal 3e, since Orientale is a young basin, its walls and peak rings might yield some information about the extent and structure of the megaregolith.

Schrödinger (75°S, 132.4°E, 312km, Lower Imbrian, SPAT)

Landing at Schrödinger crater and collecting samples would satisfy Science Goals 3a, b, c, d, and e. For Science Goal 3a, pure anorthosite (PAN) and mantle material can be sampled, and the region shows a weaker Th signature than expected and could thus be used to test the global nature of the KREEP layer. The site would be useful for fulfilling Science Goal 3b since it could be used for sampling pyroclastic deposits. Considering the relevance of the site for Science Goal 3c, lower crust and mantle material can be sampled in the peak rings, recent olivine detections there should be a good indicator of their presence. In terms of Science Goal 3d, the region is a Type I gravity anomaly and could thus be one of the potential sites for setting up geophysical instruments like seismometers. For Science Goal 3e, since Schrödinger is a young basin, its walls and peak rings might yield some information about the extent and structure of the megaregolith. Please refer to the Schrödinger case study in section 3.9.2 for a more detailed overview.

Theophilus (11.4°S, 26.4°E, 110km, Eratosthenian, FHTo)

Landing at Theophilus crater and collecting samples would satisfy Science Goals 3a, b, d, and e. For Goals 3A and 3B, pure anorthosite (PAN) can be sampled here. Theophilus could also potentially fulfill Science Goal 3c: lower crust might or might not be sampled in the central peak of the crater, as the proximity value for Theophilus is in the error bar. Recent olivine detections by Yamamoto et al. (2010) might also indicate the presence of a pluton in the young central peak, what could be interesting for Science Goal 3d. In terms of Science Goal 3e, the structural uplift in central peak might show the transition between megaregolith and fractured crustal bedrock.

Tsiolkovsky (21.2°S, 128.9°E, 185km, Upper Imbrian, FHTa)

Landing at Tsiolkovsky crater and collecting samples would satisfy Science Goals 3a, b, and e. Considering Science Goal 3a, pure anorthosite (PAN) can be sampled in the crater. The site will be useful for fulfilling Science Goal 3b since it might be possible to sample cryptomare in the ejecta blanket. For Science Goal 3e, the structural uplift in central peak might show the transition between megaregolith and fractured crustal bedrock.

Tycho (43.4°S, 11.1°W, 102km, Copernican, FHTo):

Landing at Tycho crater and collecting samples would satisfy Science Goals 3a, b, d, and e. The site will be useful for fulfilling both Science Goals 3a and 3b since it might be possible to sample pure anorthosite (PAN) here. The possible exposures of plutons/intrusive material in the young central peak make it an attractive target for fulfilling Science Goal 3d. For Science Goal 3e, the structural uplift in central peak might show the transition between megaregolith and fractured crustal bedrock.

Vavilov (0.8°S, 137.9°W, 98km, Copernican, FHTa)

Landing at Vavilov crater (on the margin of Hertzprung basin) and collecting samples would satisfy Science Goals 3a, b, d, and e. The site is good for fulfilling both Science Goals 3a and 3b since it might be possible to sample representative highland rocks (H1 type), and PAN (pure anorthosite). Considering Science Goal 3d, the crater is on the rim of a Type II gravity anomaly and could thus be one of the potential sites for setting up geophysical instruments like seismometers. This is also a young crater with fresh exposures in its central peaks and walls. For Science Goal 3e, the structural uplift in central peak might show the transition between megaregolith and fractured crustal bedrock.

Case Studies

Aristarchus crater (23.7°N, 47.4°W, 40 km, Copernican, PKT)

The Aristarchus crater and nearby plateau are interesting sites for investigating the diversity of crustal rocks, showing an incredibly complex mixture of features and lithologies. The Aristarchus region has been studied in much detail in previous literature (*e.g.*, McEwen *et al.*, 1994; Le Mouélic *et al.*, 2000; Chevrel *et al.*, 2009). Being a young Copernican crater, the morphologic features of Aristarchus such as its walls, central peak and ejecta blanket have undergone very little erosion and the crater thus provides a fresh glimpse into the surrounding PKT region. The preserved details are apparent in recent LROC imagery, displaying vivid layered stratigraphy within the central peak.

The location within the nearside mare allows for sampling of a diversity of crustal rocks, including key highland and mare types. Specifically, Aristarchus penetrates into H5 highland type terrain, and is surrounded by a variety of mare types, including M2, M3 and youngest mare. These layers could potentially all be viewed in the central peak, provided there is no substantial erosion or weathering. Figure 3.82 shows a true color image of the central peak of Aristarchus crater from the Lunar Reconnaissance Orbiter Camera. This image distinctly shows layering of multiple rock types. If landing within the crater, samples of the different rock types from debris that have eroded out of the central peak could be collected. In addition, Ohtake *et al.*, 2009 have claimed evidence of pure anorthosite (PAN) within the central peak of Aristarchus. Collecting samples of the bright material from the central peak would provide ground truth to test the results of the spectral analysis.

Olivine-rich exposures were recently detected in a concentric region around Aristarchus crater (Yamamoto *et al.*, 2010). Analysis of data from the M³ instrument onboard Chandrayaan-1, shows the southern half of the crater to be clearly enriched in olivine and the northern half to be rich in low-Ca pyroxene (Mustard *et al.*, 2010). Figure 3.83 shows an M³ color ratio composite image of Aristarchus crater. Other spectral analysis by Pieters *et al.*, 1991 suggests possible plutonic exposure which may also be observed in the central peak. The walls of Aristarchus crater might show the transition between megaregolith and fractured crustal bedrock. Also, since Aristarchus is a young crater, it should be possible to sample different kinds of breccia at different locations within the crater and its ejecta blanket.

Geochemical analysis suggests that Aristarchus crater penetrates into a KREEP-rich region of the PKT. Though Aristarchus itself is not deep enough to have primordial urKREEP material in its melt or ejecta, the young crater lies on the outskirts of the Imbrium basin, which is large enough to sample the urKREEP

within its ejecta blanket (cf. Section 3.4.5 of this report). Samples from Aristarchus crater will likely yield highly enriched KREEP material, with the possibility of remnant urKREEP material from Imbrium. Any residual urKREEP exposure would occur in the uplift of the central peak or in the crater walls, as the crater would need to penetrate the topmost regolith and mare basalt. However, basalt samples with strong KREEP signature are likely to be found throughout the crater.

In addition, the Aristarchus region is incredibly lithologically diverse. Aristarchus crater lies on the Aristarchus plateau, which is an uplifted block of crustal material, formed likely due to volcanic processes (Fig. 3.84). The scarp of the plateau, that rises more than 2 km above Oceanus Procellarum on the southeastern margin, might be an interesting target for observing outcrops of intrusive material and layering of different lithologies. There is also evidence for pyroclastic deposits which may be sampled on the plateau, as well as a system of sinuous rilles (Rillae Aristarchus) dominated by Vallis Schröteri. Such features all suggest that complex volcanic processes once occurred in this region, creating a very lithologically diverse terrain. Observations of possible layered structuring within the central peak and exposed crater walls may provide insight into this lithology.

As explained above, most of the features of interest within the Aristarchus region can be observed within the central peak and exposed walls of the crater. For this reason, we suggest a landing site on the crater floor, midway between the crater walls and the central peak. However, it should be noted that the entire region outside of the crater is also of interest, and if landing within the crater is not feasible, one should strongly consider a site in the plateau region, especially near the scarp of the plateau. As Science Concept 5 specifically discusses products of volcanism on the Moon, we feel that central peak observations will more directly address the scope of Science Concept 3.

Aristarchus

Lat: 23.7

Lon: -47.4

Diameter: 40 km

LROC IMAGES

a: WAC Color Composite
by LROC team

b: Feature from
NAC M122523410L

c: Feature from
NAC M122523410L

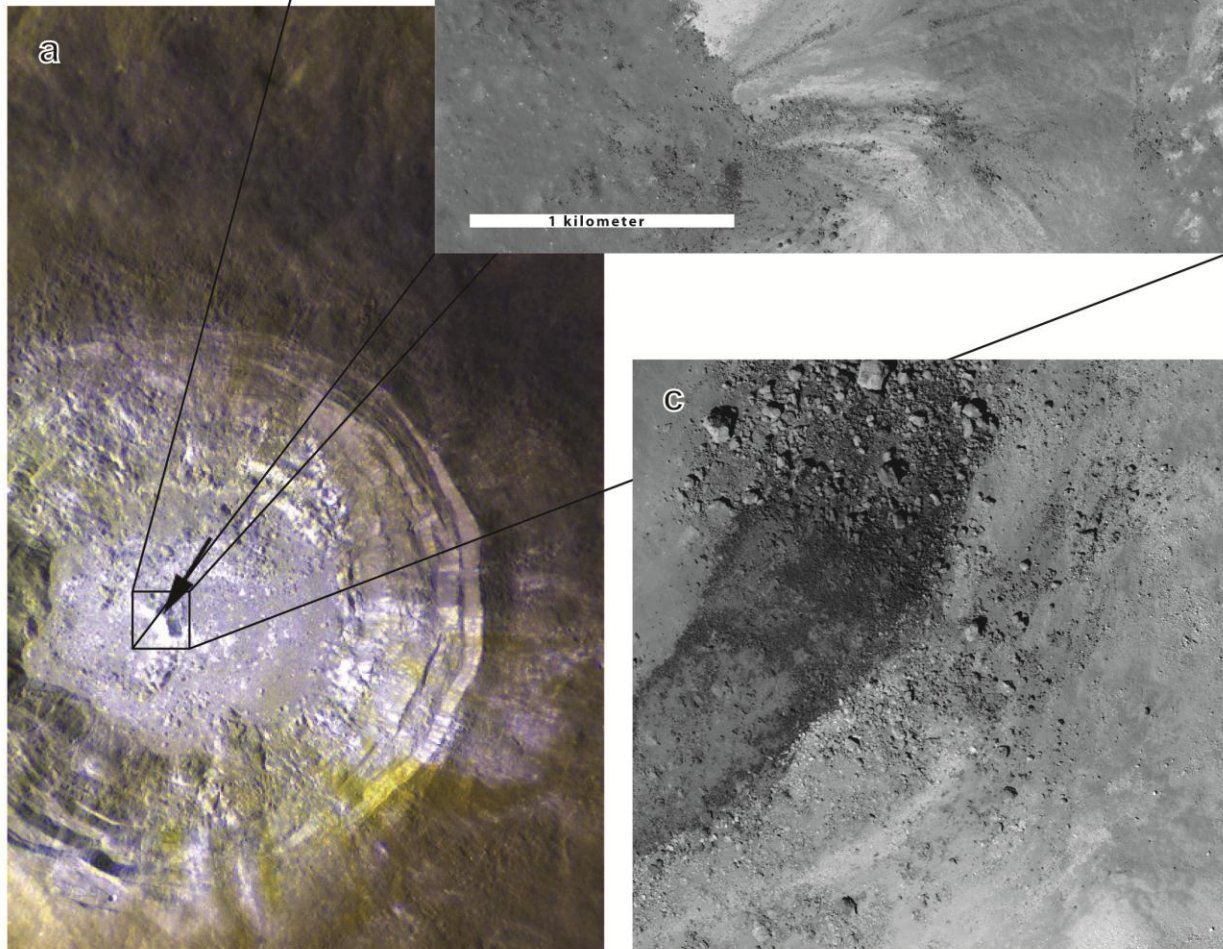


FIGURE 3.84 (a) WAC color composite from featured images on the LROC Image Browser. WAC bands 689 nm, 566 nm, and 321 nm are displayed in red, green, and blue respectively. (b) Image depicting distinct layering features from the central peak of Aristarchus crater. Feature from LROC image M122523410L. (c) Close up view of the layering features from image (b).

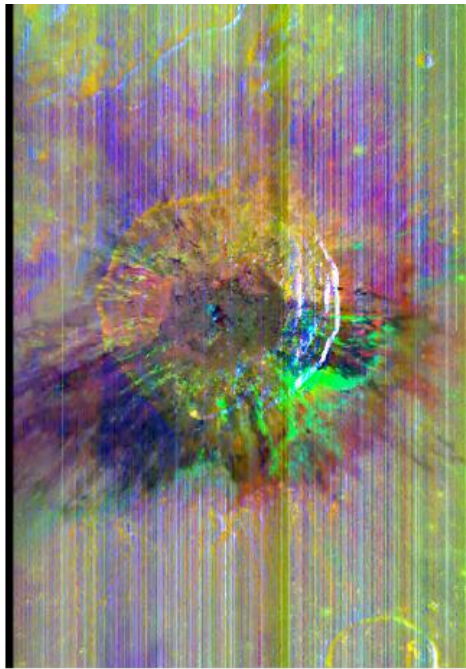


FIGURE 3.83 M³ color ratio composite of Aristarchus crater, showing integrated 2 μm band depth in red, integrated 1 μm band depth in green and UV-VIS ratio in blue (Image from Mustard *et al.*, 2010)

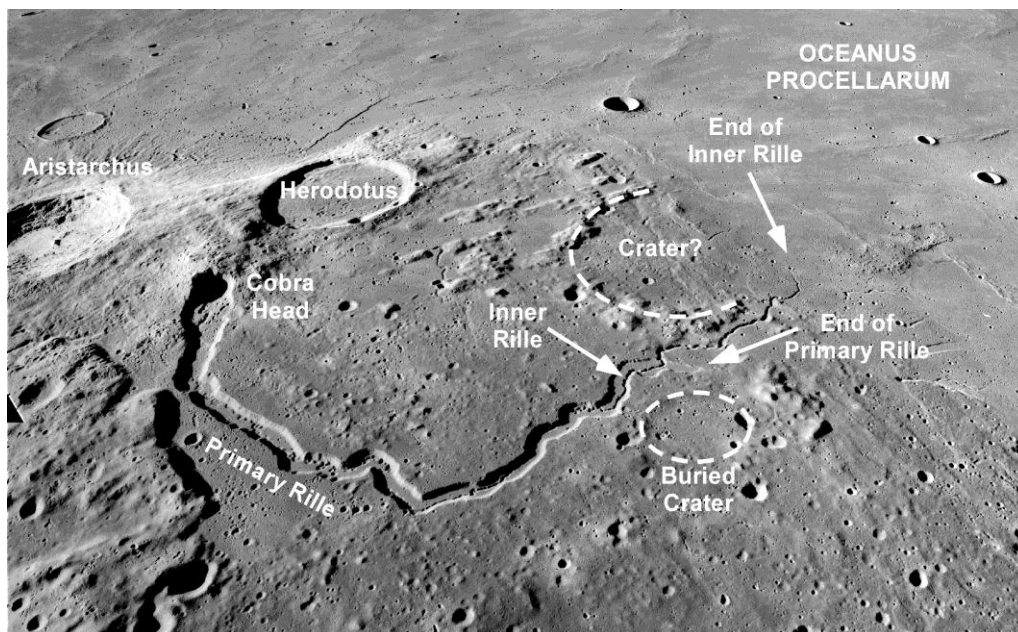


FIGURE 3.84 Apollo 15 Metric Image AS15-M-2612, showing an overview of the geologically diverse Aristarchus plateau.

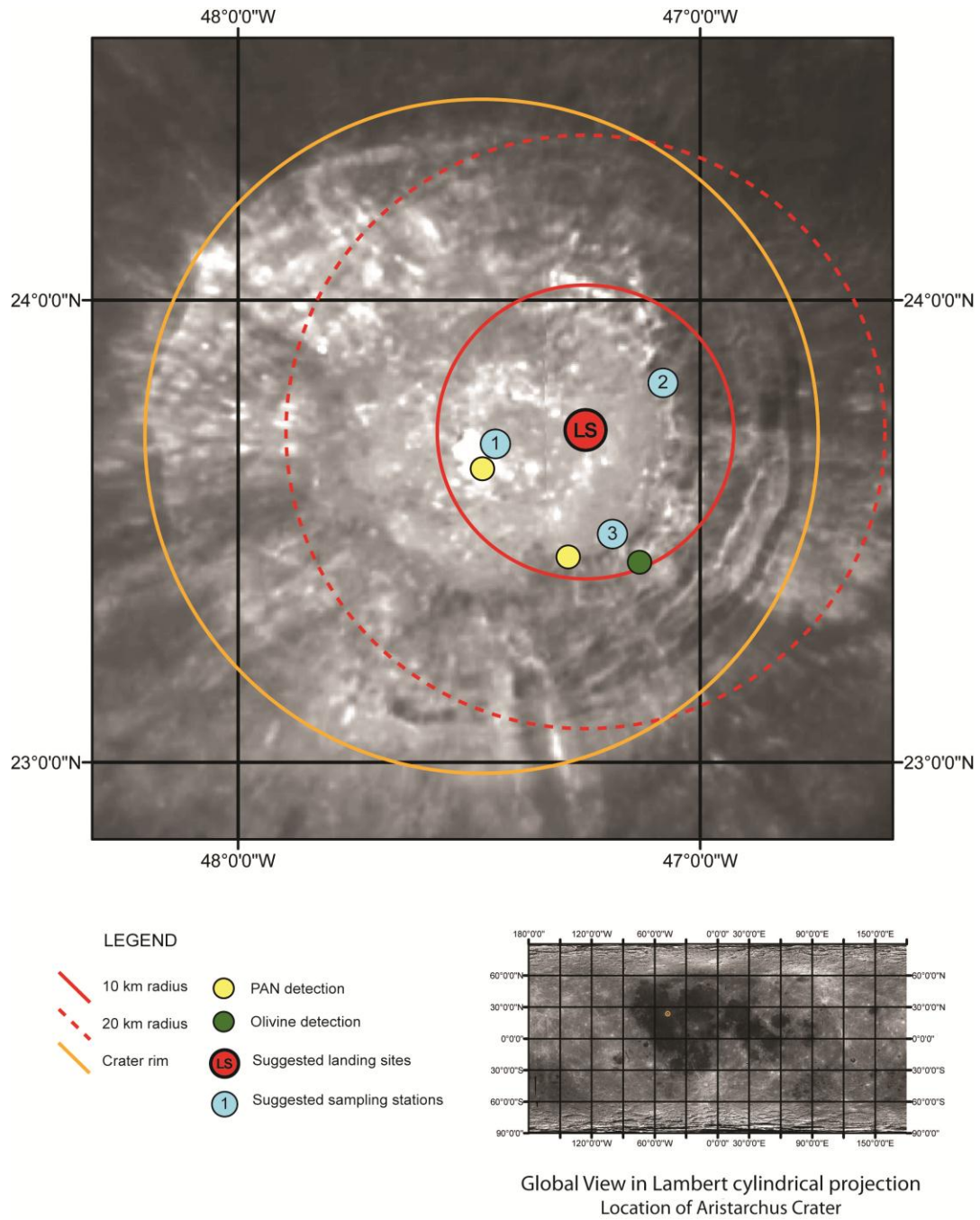


FIGURE 3.85 Diagram of possible landing site for Aristarchus Crater.

Jackson crater (22.4°N, 163.1°W, 71km, Copernican, FHTa)

Lying near the thickest region of the lunar crust, Jackson crater is a prime target area for determining the nature of highlands material. Since the crater lies in the very center of the FHT, landing here would be useful for sampling the primary feldspathic crust. Recent interpretations of spectral data by Ohtake *et al.*, 2009 claim that there may be a clear pure anorthosite (PAN) signature within the central peak of this crater. Jackson's young age would provide an optimum site for sampling material, including different kinds of breccia, as the walls and central peak are well-preserved, and have not been significantly worn from impact debris and space weathering.

Similarly, studies of the highland types by Chevrel *et al.*, 2002 indicate that the surrounding region is very abundant in highland type H1. Representative samples of the highlands (and therefore H1 highland type) are needed, as the Apollo missions mainly sampled material from the nearside mare regions. Currently, most of our knowledge about the highlands is based upon analysis of material from lunar meteorites. Though the entire crater should sample such pure highland material, the optimum location of study may be the central peak and crater walls, as they will show the extent and preserved exposures of rock beneath the regolith.

Studies of Clementine UVVIS spectra by Tompkins *et al.*, 1998 suggest possible pluton exposure within the central peak of Jackson crater, as discussed in Science Goal 3d. This interpretation is reasonable due to the appearance of mafic material within the central peak of the crater as opposed to purely feldspathic highlands material, as may have been expected.

In terms of Science Goal 3e, Jackson crater penetrates deep enough into the surface to sample past the megaregolith and possibly expose areas of crustal bedrock on its walls. Jackson is a particularly exemplary site to sample the extent of the megaregolith, as it lies within center of the farside highlands, and can therefore give a representative measurement of the highlands megaregolith thickness. Being a fresh Copernican age-crater, both the walls and the central peak are likely to retain visible stratigraphical and lithological layering to determine where brecciated rock ends and the exposed crust begins.

In terms of the goals that can be reached at Jackson crater, the site of interest would likely be the central peak since it would expose diverse material from different depths. While the walls may also provide useful information about the extent of the megaregolith, the central peak is also likely to constrain such models. See Fig. 3.86 for recent observations of the central peak at Jackson Crater.

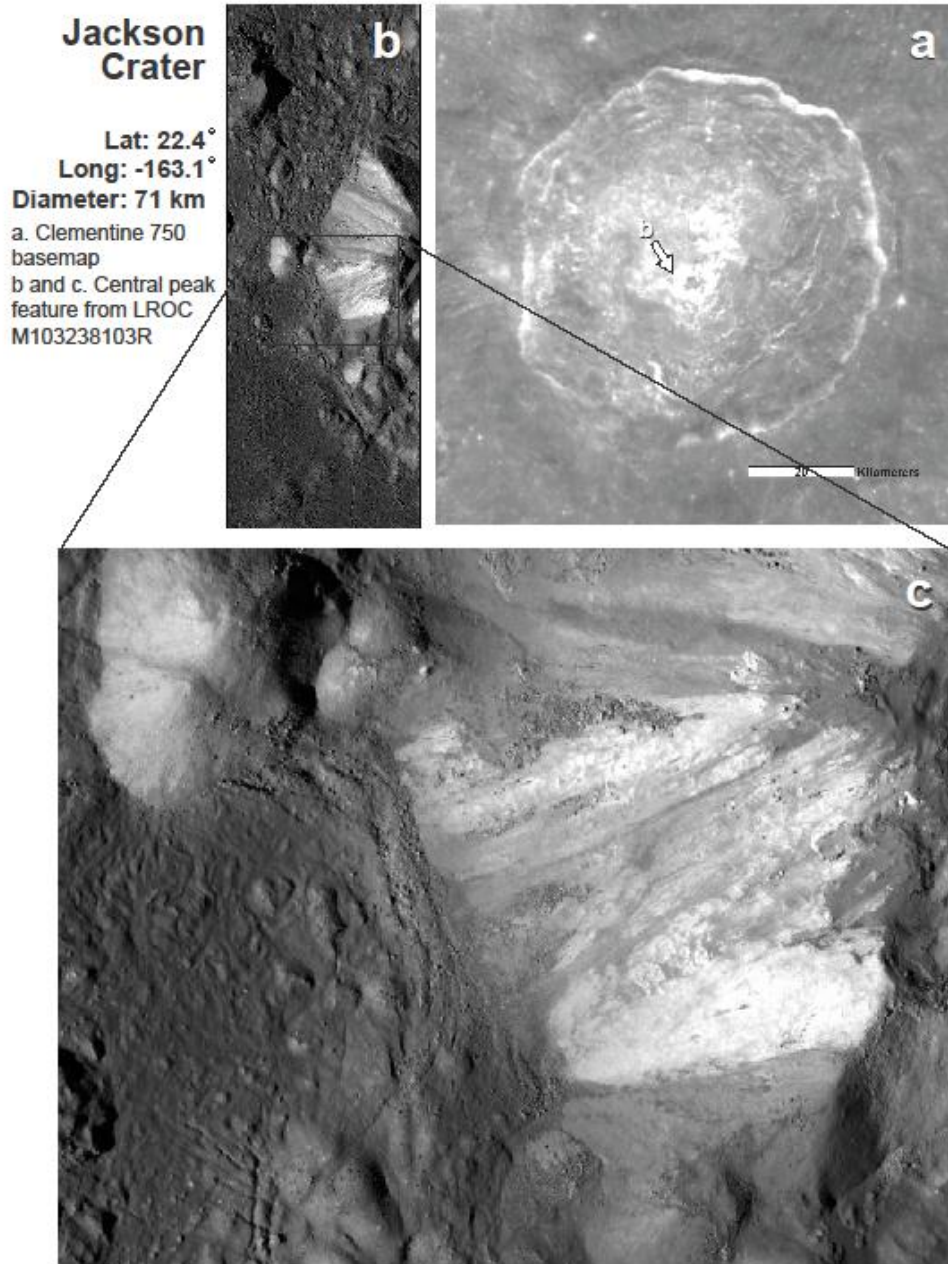


FIGURE 3.86 Features of Jackson Crater's central peak. (a) Taken from Clementine 750 nm baseline spectral map, showing the entire scope of the crater. (b) Feature from LROC image M103238103R, showing the west side of the central peak. (c) Zoom from image b, showing exposed lithologies and rocks with different albedo signatures. Also apparent is the melt sheet on the floor of the crater.

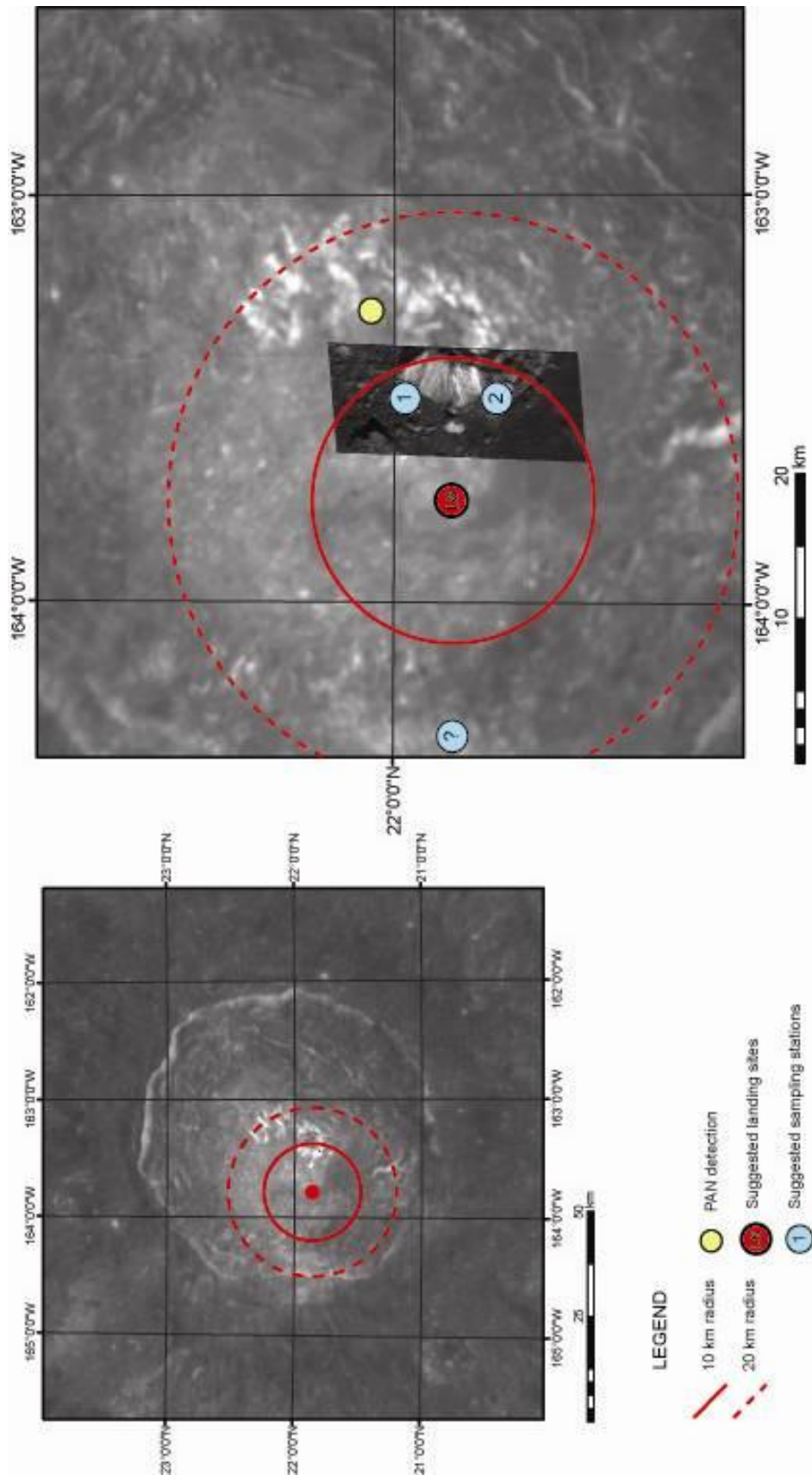


FIGURE 3.89 Potential landing site in Jackson crater. The solid circle represents a radius of 10 km, whereas the dashed circle represents a radius of 20 km from the landing site. The blue dots indicate where interesting sampling or measurement could be made. Stations 1 and 2 are sampling the central peak. It is suggested to make multiple stations along the peak in order to make a geological map of its walls. The station labeled with a question mark is at the rim of the crater. It is beyond the actual mission range (10 km), but it would make an interesting station if the range were extended.

Schrödinger Basin (75°S, 132.4°E, 312 km, Lower Imbrian, SPAT)

Schrödinger Basin is an extremely high priority site for Science Concept 3. Being the second youngest basin (after Orientale), Schrödinger provides some of the best preserved basin features on the lunar surface for scientific study (Kohout *et al.*, 2009). In addition, it is one of only two sites (along with Orientale, again) that can address every Science Goal within Science Concept 3. However, Schrödinger Basin is unique as it provides a glimpse into a region of the Moon that remains enigmatic: the South Pole-Aitken Terrane. This terrane has never been directly sampled, and any meteoritic clasts or samples remain speculative.

In terms of Science Goal 3a, Schrödinger provides access to nearly every layer of planetary differentiation models. The large basin lies within the thin crust of the SPAT, and its large size implies that it would most likely sample mantle material in the melt. In addition, this mantle material may also be exposed within the stratigraphic uplift of the peak rings. Any crater that is thought to sample mantle material from the models outlined in Section 3.3.2 of this report should also sample material at the crust-mantle boundary. In the LMO hypothesis, the early urKREEP layer is thought to be located at this boundary. However, geochemical remote sensing analysis does not provide sufficient evidence for the existence of KREEP-rich material within the confines of Schrödinger basin that would help to confirm the global extent of a primordial urKREEP layer. Thus, investigation into what exists at this boundary would provide insight and constraints onto planetary differentiation models.

Though Schrödinger does not lie within the FHT, it remains a top location to search for pure anorthosite (PAN) material. Detections by Ohtake *et al.* (2009) of PAN material are located within the peak rings of Schrödinger, making these uplifted regions particularly of interest. As such, the peak rings may provide a glimpse into the layered structure of the crust and mantle boundary, if not significantly covered by a layer of regolith.

Other rock types also appear to be pervasive within Schrödinger basin. Pyroclastic deposits are located in the south west region, positioned near a peak ring outcrop. Thus, planning a sampling site near this depository location could also address the prior issues simultaneously. Mg-suite rocks may be sampled as well, as spectral analysis of plutonic rocks (such as gabbro, norite, troctolite, gabbro-norite, anorthositic troctolite, anorthositic gabbro) by Tomkins and Pieters (1999) suggest the possibility of exposure. However, care must be taken in interpreting the results of this analysis, as such findings could suggest the exposure of lower crustal material, which is also expected to be sampled at this site. Yamamoto *et al.*, 2010 has recently detected multiple sources of olivine in the ejecta of craters that penetrate into the peak ring. We use this information and assume that such detections should be pervasive throughout the entirety of the peak ring structures, and locations that can freshly expose parts of the peak ring structure may also sample olivine.

Schrödinger basin is a Type I gravity anomaly, thus categorizing it as a good location for setting up geophysical instruments such as seismometers. In addition, the complex terrain could offer clues into the unique lithology and regional complexity of the SPA region. The placement of seismometers would also address Science Goal 3e, determining the extent of the megaregolith in the region. Being a large young basin in the SPAT, Schrödinger should help constrain models by determining a lower limit on the megaregolith. Fresh exposures and outcrops of bedrock could be key places for placement of these instruments as well as for observations of megaregolith extent.

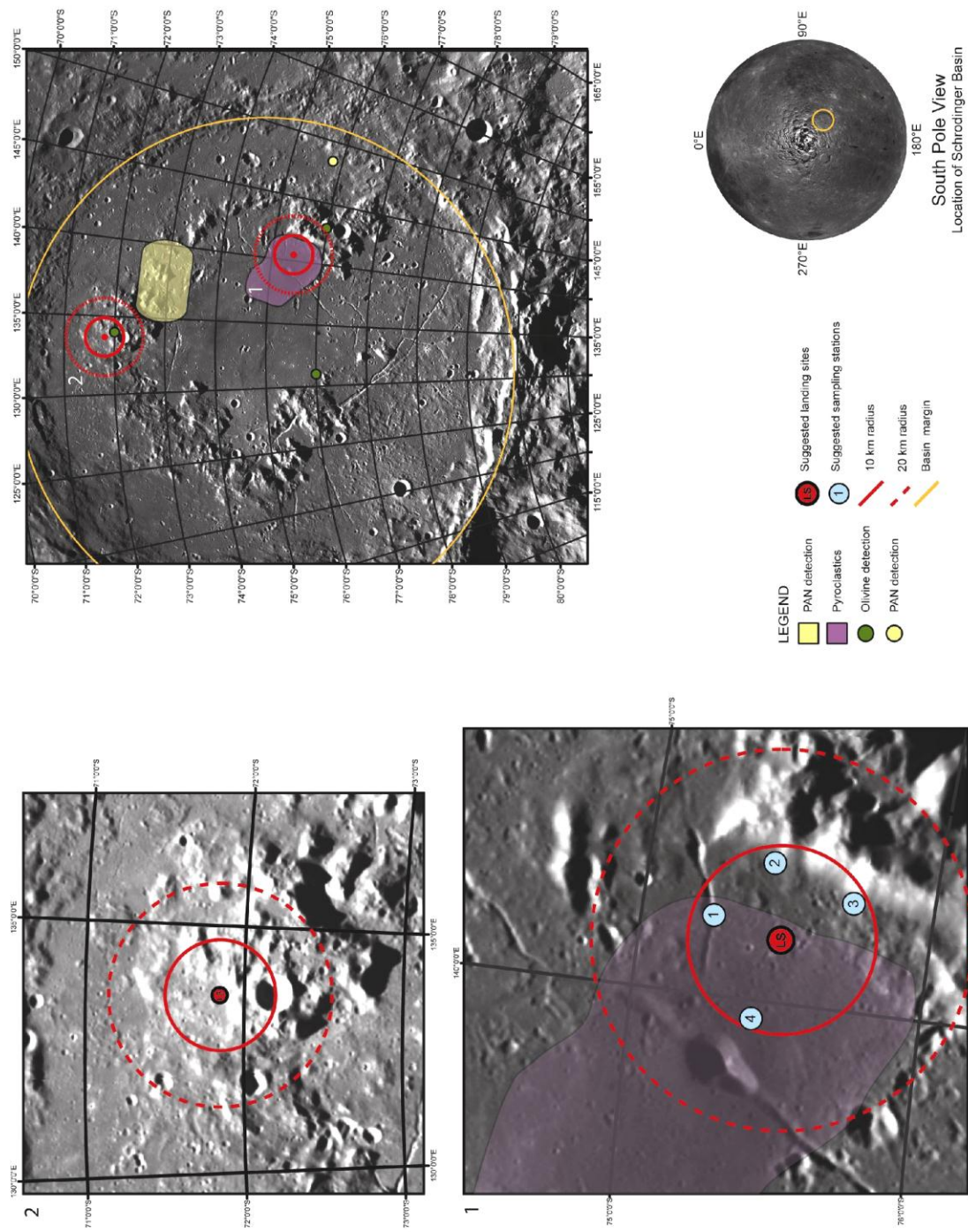


FIGURE 3.90 Diagram of two possible landing sites for Schrodinger Basin, with labeled features.

While Schrödinger's entire peak ring would be of interest as a landing site, it is much too large to traverse without the assistance of a vehicle; therefore, for the purpose of this study, we have identified two particular landing sites of interest (see Fig. 3.88). Landing site 1 is located in the southwest of the basin, near a peak ring outcrop that lies within a field of pyroclastic deposits. This particular site may sample volcanic glass from the deposits, as well as PAN and olivine detected from the nearby crater which has penetrated into the peak ring. There is a possibility of outcropping and bedrock exposure within the walls of the peak rings; however, this region may be covered with a thicker layer of regolith than the second proposed site. The first site designates three stations within the 10 km radius of the landing site. These are chosen as guidelines for the type of studies that we would be interested in. Station 1 is located at a rille, where samples should be taken, and the collapsed rille walls should be analyzed for any exposed layering structures. In addition, as this is a volcanic feature, one should look for unique volcanic lithologies that might occur here. Stations 2 and 3 are located at the base of peak ring massif features. Optimally, samples would be taken on a traverse from one station to the next, to determine how material may differ on a small scale. In particular, outcroppings and possible exposures should explicitly be sampled. Station 4 lies within a large field of pyroclastic deposits. Samples of the volcanic rock and regolith should be taken for comparison to other samples.

Our proposed landing site 2 lies on the peak ring in the north of Schrödinger Basin. Directly on the ring is a fresh crater which appears to expose bedrock and possible layering within the crater walls (*cf.* Fig. 3.89 below). As the peak ring is thought to uplift material from the mantle, possible urKREEP, and both lower and upper crust, this preserved exposure could provide a plethora of useful information with regard to Concept 3. In addition, this crater is the site of olivine detections for Yamamoto *et al.*, 2010, and nearby PAN detections (Ohtake *et al.*, 2009). This site may be much more difficult to traverse, so we would suggest landing just north of the small secondary crater, and exploring the ejecta blanket for overturned materials.

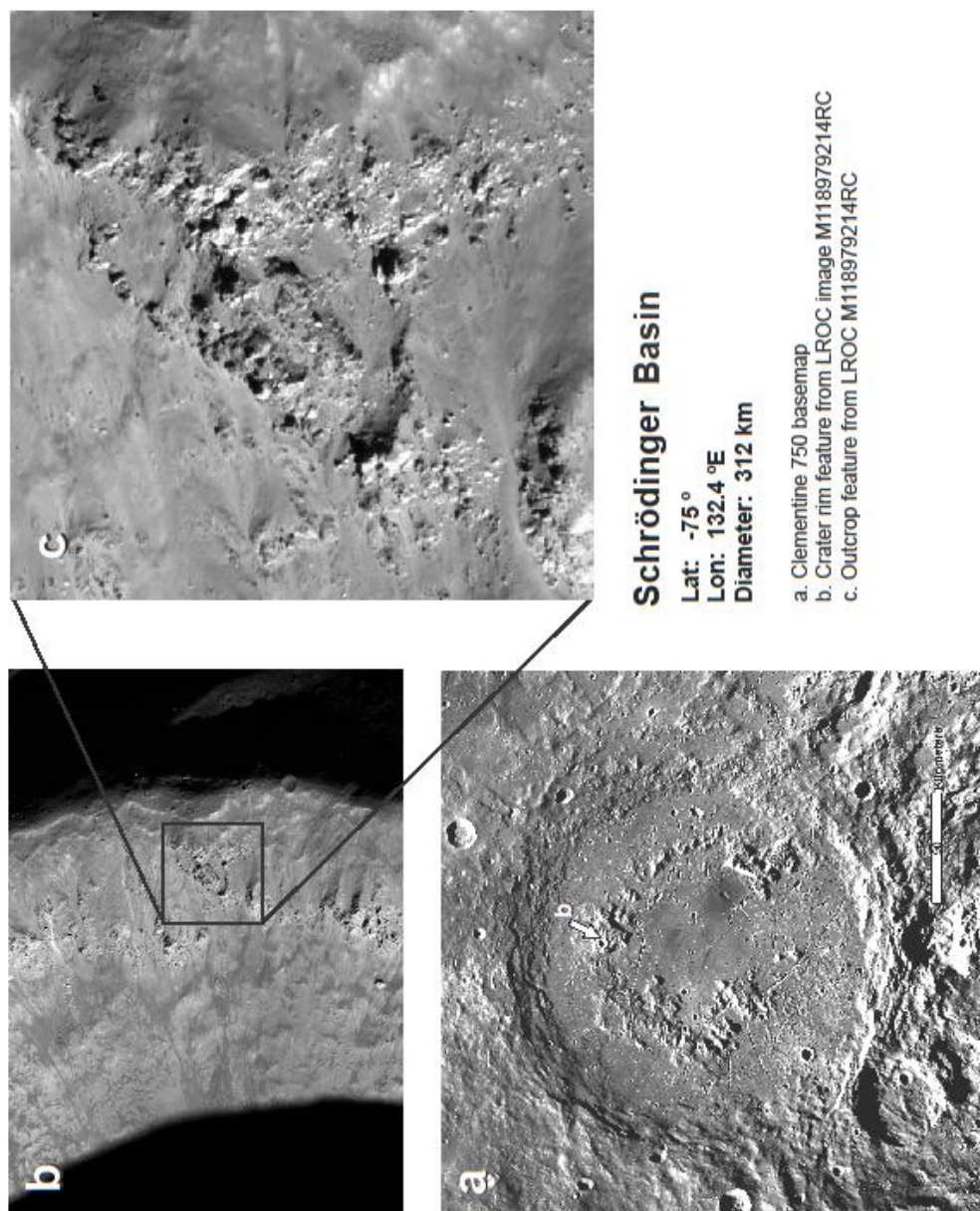


FIGURE 3.91 Features of Schrödinger Basin. (a) Depiction of the entire scope of Schrödinger Basin from Clementine 750 nm basemap. The Arrow points to the crater on the peak ring of interest. This would be the location of landing site 2 within the basin, as it corresponds to olivine and PAN detections. (b) Feature from LROC Image M118979214RC. This image shows interesting outcrops and possible albedo.

CONCLUSION

Multiple landing sites are required to address Science Concept 3 in its entirety. Many locations have been identified as having the potential to address several of the Science Concept 3 Science Goals (refer to Suggested Sites Database in Appendix F2). Only Orientale and Schrödinger were identified as possible locations where all the five Science Goals could be addressed at the same time. Note that Science Goals 3b, d, and e can be addressed virtually everywhere on the surface of the Moon.

Both Science Goals 3a and 3b have been deemed to be “Highest-Priority Science Goals” in the NRC 2007 report, demonstrating the importance of studying the diversity of the lunar crust. Priority should be given to locations where new rock types have the highest chances of being sampled, especially those rock types that may provide a deeper insight into the lunar Magma Ocean hypothesis. As mentioned throughout the report, only a small fraction of the range of rock types that exist on the Moon has been sampled so far, and several lithologies (e.g., mantle and urKREEP layers lithologies, young mare basalts, granites) are crucial in constraining models of the geological history of the Moon.